

Aggregation of Crude Oil-Modified Fine Solids in Aqueous and Non-aqueous Media

by

Juan Darius

A thesis submitted in partial fulfillment of the requirements for the degree of

Master of Science

in

Chemical Engineering

Department of Chemical and Materials Engineering  
University of Alberta

© Juan Darius, 2021

## **ABSTRACT**

At different stages during the extraction of bitumen from the Athabasca oil sands, the removal of unwanted fine solids — whether suspended in aqueous or non-aqueous liquids — continues to present serious challenges to the oil sands industry. These fine solids are unique in that their colloidal properties are altered through adsorption of various bituminous components onto their surfaces. It is imperative to understand how these adsorbed species affect the colloidal stability of the solids in different liquid media.

We report here a systematic investigation on the aggregation of silica particles in both water and organic solvents. The silica particles are either untreated or adsorbed with various fractions of bitumen (a total of six sub-fractions, based on solubility in aliphatic solvents, as well as interfacial activities of the fractions). The organic solvents (in which the solids are suspended) are mixtures of toluene and *n*-heptane at different ratios. The colloidal stability of the solids is examined on both the macroscopic and microscopic scales. On the macroscopic level, “jar tests” are performed to monitor settling rates in relation to the corresponding Stokes velocities. In the case of non-aqueous suspensions, it is revealed that, in terms of the toluene-to-heptane ratio of the solvent, there are clear points of transition between slow and rapid settling. On the microscopic level, direct measurements of adhesion forces are made between pairs of micron-sized glass particles using the microcantilever technique. These force measurements are correlated with the jar test results, revealing the influences that various bituminous fractions have on the colloidal stability of the fine solids.

## **Acknowledgments**

I would like to express my sincerest gratitude to my advisor, Dr. Tony Yeung for his valuable guidance and continuous support throughout my master's degree. Thank you for being a great mentor with a lot of brilliant ideas and constructive feedback. I would like to thank the financial and administrative support from Future Energy Systems (FES) University of Alberta. I appreciated the support, feedback, and time from my defense chair, David Sharp; and the committee members, Dr. Qi Liu and Dr. Hongbo Zeng.

I would also like to give thanks to Dr. Xiaoli Tan, Lisa Brandt, and Brittany Mackinnon for their technical support and meticulous help during the experiments and training in the Institute for Oil Sands Innovation (IOSI) laboratory. I would express special thanks to Dr. Zhenghe Xu, Jim Skwarok, and Rui Li for the laboratory environment and for providing me the knowledge in operating the lab equipment, and my appreciation to Lily Laser and Amy Chow for their assistance in administrative processes.

My milestones will not be achieved without motivation from my loving family. My parents and grandmother deserve a special mention for their trust in my every single decision and for loving me unconditionally throughout my life. I would like to express my gratitude to my fellow friends for their advice for my thesis and motivational encouragement. In particular, I would like to express my greatest gratefulness to ChuuYang Tan, Raymond C.S, WeiChurch Poh, SimYee Chen, and Rachel O.P.H for their help and encouragement throughout the project.

## Table of Contents

<b>ABSTRACT</b>	<b>ii</b>
<b>Acknowledgments</b>	<b>iii</b>
<b>List of Contents</b>	<b>iv</b>
<b>List of Tables</b>	<b>vi</b>
<b>List of Figures</b>	<b>vii</b>
<b>Nomenclature</b>	<b>x</b>
<b>1 Introduction</b> .....	<b>1</b>
<b>2 Literature Review</b> .....	<b>12</b>
2.1 Fractionation of Crude Oils.....	12
2.1.1 SARA Analysis.....	12
2.1.2 Extended-SARA Analysis.....	13
2.1.3 Interfacially Active and Remaining Asphaltenes Subfractions.....	14
2.2 Solvent Selection and Asphaltene Precipitation.....	15
2.2.1 Solvent Selection.....	15
2.2.2 Asphaltene Precipitation.....	16
2.3 Adsorption of Asphaltene Onto Solid and Its Surface Chemistry.....	18
2.3.1 Adsorption of Asphaltene Onto Solid.....	18
2.3.2 Surface Chemistry.....	19
2.4 Aggregation of Particles and Collision Theory.....	20
2.5 Sedimentation and Settling Rate.....	20
2.5.1 Sedimentation.....	21
2.5.2 Free Settling.....	23
2.5.3 Hindered Settling.....	23
2.5.4 Effect of Aggregation in Sedimentation.....	24
2.5.5 Settling Rate Measurement.....	24
2.6 Inter-particle Forces in Colloidal Systems.....	28
2.6.1 Interaction Forces Based on DLVO theory.....	28
2.6.2 Interaction Forces Based on non-DLVO theory.....	30
2.6.3 Inter-particle Forces Measurement Methods.....	33
<b>3 Research Methodology</b> .....	<b>39</b>
3.1 Preparation to Obtain Bituminous Materials.....	39
3.2 Macroscopic Experiments: Jar tests.....	41
3.2.1 Materials.....	41
3.2.2 Sample Preparation for Jar Tests.....	43
3.2.3 Measurement of Settling Rate.....	44
3.3 Microscopic Analysis: Direct Force Measurement.....	45
3.3.1 Materials.....	45
3.3.2 Preparation of Straight Micropipette.....	45
3.3.3 Preparation of Microcantilever.....	46

3.3.4 Force Measurement by Microcantilever Technique.....	47
3.4 Scope of Experiments.....	51
<b>4 Results and Discussion.....</b>	<b>53</b>
4.1 Preliminary Experiments: Colloidal Stability.....	53
4.1.1 Stable Systems.....	54
4.1.2 Unstable System.....	64
4.1.3 Summary for Preliminary Experiments.....	67
4.2 Macroscopic Analysis: Heptol Jar Tests.....	69
4.2.1 Bitumen-treated Silica and Controls.....	71
4.2.2 Silica Surface-Modified by Asphaltenes and Maltenes .....	74
4.2.3 Silica Surface-Modified by Sub-fractions of Asphaltenes.....	76
4.2.4 Silica Surface-Modified by Sub-fractions of Maltenes.....	77
4.2.5 Summary for Heptol Jar Tests.....	79
4.3 Microscopic Analysis: Interparticle Forces Measurement.....	82
4.3.1 Pure Glass Surface and Bitumen-treated Surface .....	82
4.3.2 Glass Surfaces Adsorbed with Bitumen, Asphaltenes, and Maltenes.....	85
4.3.3 Glass Surfaces Adsorbed with Sub-fractions of Asphaltenes and Maltenes	88
<b>5 Summary and Future Works.....</b>	<b>91</b>
<b>References.....</b>	<b>94</b>

## List of Tables

Table 3.1	Sample Size for the Experiments.....	52
Table 4.1	Parameter for Stokes Velocity Calculation.....	54
Table 4.2	The List of Hamaker Constant with Respective References .....	66
Table 4.3	A Summary for Preliminary Experiments .....	68
Table 4.4	Hamaker Constants for Various Materials .....	73
Table 4.5	Summary for Different Solids in Heptol Jar Tests.....	81

## List of Figures

Figure 1.1	(a) The oilsands consist of bitumen, water, and solids in slackened sands form. (b) The morphology and arrangement of components in oil sands deposit.....	2
Figure 1.2	Process flow of the water-based oil sands extraction.....	2
Figure 1.3	Fundamental principles of non-aqueous extraction chart.....	5
Figure 1.4	The best solvent selection is to fulfill the intersection between three main considerations.....	6
Figure 1.5	Stable colloidal system of bituminous solids in NA liquid (left). Destabilizing leads to fines aggregation, follows by sedimentation (right)...	8
Figure 2.1	E-SARA fractionations of crude oils with proposed subfractions on maltenes. ....	14
Figure 2.2	Interfacial tension of the asphaltenes subfractions suggests that IAA is more surface-active .....	15
Figure 2.3	Solvent selection with respect to degree of aromaticity to obtain the desired specifications.....	16
Figure 2.4	Asphaltene precipitation in light n-alkanes in the different solvent to bitumen ratio. ....	16
Figure 2.5	Asphaltene content in the bitumen depends on the type of solvent and ratio. The plot on the left is in a narrower range of the S:B ratio for better visualization.....	17
Figure 2.6	The inclination in aggregation and size is increased with the increment in n-heptane content in the solvent. ....	18
Figure 2.7	Possible configurations that influence the physicochemical properties of the surface.....	19
Figure 2.8	Schematic of the aggregation mechanism.....	21
Figure 2.9	Two types of sedimentation in concentrated suspension systems.....	22
Figure 2.10	Schematic of the optical observation of mudline.....	24
Figure 2.11	Batch Settling curve to study the sedimentation process.....	25
Figure 2.12	Schematic of the novel ashing technique and the typical plot.....	27
Figure 2.13	Graph with settling rate on the y-axis and degree of aromaticity on the x-axis by novel ashing technique.....	27
Figure 2.14	Stern, diffuse and electric double layer of particle.....	29
Figure 2.15	The interactions of the polymer-like material adsorbed on the particle and surface with both good and poor solvents. ....	32
Figure 2.16	Cross-bridging of two particles with long chain macromolecules adsorbed on the surfaces.....	33
Figure 2.17	The SFA with the main components and arrangement of the two mica cylinders.....	34
Figure 2.18	Results by SFA for asphaltenes interactions in both heptane and toluene....	35

Figure 2.19	The main components in AFM with their configuration.....	36
Figure 2.20	AFM imaging and plot for dip-coating asphaltene film surface-interactions in toluene.....	36
Figure 2.21	Standard plot for force measurement with microcantilever technique with respect to the volume of the toluene in heptol. ....	38
Figure 3.1	Fractions of bitumen based on precipitation and adsorption.....	39
Figure 3.2	Schematic of procedures to obtain subfractions based on adsorption onto the oil-water interface. ....	40
Figure 3.3	(a) Bituminous-treated silica appeared as greenish powder, and (b) chemically-treated with white colour. ....	42
Figure 3.4	Jar test preparation procedures.....	43
Figure 3.5	Measurement of settling rate by the optical method. ....	44
Figure 3.6	David Koff Instruments (Pipette puller). The magnified part shows the platinum ribbon where the pipette would be pulled into two parts with tapered ends.....	46
Figure 3.7	Forging and melting equipment associated with a 10x objective lens microscope to observe and control the process. The enlarged picture displays the thick platinum wire (for melting the tips) and a thread-like wire (for shaping the microcantilever). ....	46
Figure 3.8	The geometry of Microcantilever.....	47
Figure 3.9	Configuration of the microcantilever technique to measure the inter-particle forces.....	48
Figure 3.10	The force measurement instrument in real practice.....	49
Figure 3.11	(1)The straight micropipette moved toward the stationary microcantilever on the right, (2) after the surfaces come into contact, the micropipette on the left was gently withdrawn back, (3) the microcantilever was deflected due to the adhesive force, (4) the microcantilever jumped back to the original position and the maximum deflection could be measured.....	50
Figure 4.1	The settling rate of pure silica in water. ....	56
Figure 4.2	Adsorption of methyl-chloro silanes on the surface of silica ....	57
Figure 4.3	The settling rate of hydrophobic silica in toluene.....	58
Figure 4.4	The interaction of bitumen treated silica in toluene (as a good solvent) .....	60
Figure 4.5	The settling rate of bitumen treated silica in toluene.....	60
Figure 4.6	The settling rate of bitumen treated silica in water.....	61
Figure 4.7	Collapsed molecules configuration on bitumen treated silica in water (as poor solvent) ....	62
Figure 4.8	The interaction of bitumen treated silica in water.....	63
Figure 4.9	The interaction of bitumen treated silica in heptane (as poor solvent) .....	65
Figure 4.10	A 3 × 3 matrix for the dispersion of silica in various solvents system.....	69



Figure 4.11	Bitumen-treated silica in heptol jar tests, as the example for the experimental procedure in general.....	70
Figure 4.12	Settling curves of pure silica in heptol.....	71
Figure 4.13	Settling curves of hydrophobic silica in heptol.....	72
Figure 4.14	Settling curves of bitumen treated silica in heptol.....	72
Figure 4.15	Settling curves for asphaltene-modified silica in heptol.....	75
Figure 4.16	Settling curves for maltene-modified silica in heptol. ....	75
Figure 4.17	Settling curve for interfacially active asphaltene-treated silica in heptol....	76
Figure 4.18	Settling curve for remaining asphaltene-treated silica in heptol.....	77
Figure 4.19	Settling curves for interfacially active maltene-treated silica in heptol.....	78
Figure 4.20	Settling curves for remaining maltene-treated silica in heptol.....	79
Figure 4.21	Three models of settling behaviours.....	79
Figure 4.22	Transition ranges for various treated silica particles in heptol.....	80
Figure 4.23	Adhesive forces for pure glasses surface in pure heptane and toluene.....	83
Figure 4.24	Adhesive forces in heptane, for clean and bitumen-treated surfaces.....	84
Figure 4.25	Adhesive forces in heptol, between surfaces treated by bitumen.....	85
Figure 4.26	Adhesive forces in heptane, between surfaces treated by bitumen and its fractions. ....	86
Figure 4.27	Adhesive forces for asphaltene treated surface in heptol. ....	87
Figure 4.28	Adhesive forces for maltene treated surface in heptol. ....	87
Figure 4.29	Adhesive forces for interfacially active asphaltene-treated surfaces in heptol.....	88
Figure 4.30	Adhesive forces for remaining asphaltene-treated surfaces in heptol.....	89
Figure 4.31	Adhesive forces for interfacially active maltene-treated surfaces in heptol.	89
Figure 4.32	Adhesive forces for remaining maltene-treated surfaces in heptol.....	90

## Nomenclature

$t$	time	<i>s or hour</i>
$m$	Mass	<i>kg</i>
$F$	Force	<i>N</i>
$V_{Stokes}$	Particle free settling velocity in Stokes regime	<i>m/s</i>
$V$	Particle hindered settling velocity	<i>m/s</i>
$d$	Hydrodynamic diameter	<i>m</i>
$\mu$	Fluid viscosity	<i>Pa.s</i>
$g$	Gravitational acceleration	<i>m/s<sup>2</sup></i>
$\rho_p$	Particle density	<i>kg/m<sup>3</sup></i>
$\rho_f$	Fluid density	<i>kg/m<sup>3</sup></i>
$K$	Hydrodynamic volume factor	
$n$	Richardson-Zaki index	
$\alpha_p$	volume fraction of the particle in the suspension	
$Q$	Magnitude of electrical charge of particle	<i>C</i>
$E$	Interaction energy between two particles	<i>N/m</i>
$D$	Separation distance between two particles	<i>m</i>
$R$	Radii of particle	<i>m</i>
$A$	Hamaker Constant	<i>J</i>
$1/\kappa$	Debye length	<i>m</i>
$IFT$	Interfacial Tension	<i>mJ/m<sup>2</sup></i>
%	mass fraction	<i>wt %</i>
	volumetric fraction	<i>v %</i>
$S:B$	Solvent-to-bitumen ratio	<i>%</i>
$S:L$	Solid-to-liquid ratio	<i>%</i>
$h$	Mudline/ interface height	<i>mm</i>
$\alpha$	Degree of aromaticity (volumetric fraction of toluene in heptol)	<i>v %</i>
$K_b$	Microcantilever stiffness	<i>N/m</i>
$\delta$	Microcantilever deflection	<i>m</i>

## 1. Introduction

The world's third-largest proven oil reserves are the oil sands in Northern Alberta, with 167 million barrels at the end of 2018; this accounts for 9.7% of the global resources (BP Statistical Review, 2019). The reserves in Canada are estimated to last for the next 88 years, based on its reserves-to-production ratio. In parallel, the International Energy Agency reports that global demand will increase by more than 20% between 2018 and 2050 (Energy Information Agency, 2009). Within Alberta, the demand is projected to reach 400 thousand barrels per day by 2024 (Alberta Energy Regulator, 2015), resulting in prominent prospects in the oil and gas industry. Alberta oilsands comprise approximately 96.7% of the Canadian oil reserves. According to the Alberta Energy Regulator (AER), oil produced from bitumen in Alberta had reached 3 million barrels per day for the first time in 2018. About 20% of Alberta's total bitumen reserves can be recovered through surface mining (J. Masliyah et al., 2011), from deposits mainly distributed in the northern part of Fort McMurray, the Athabasca Basin. The rest are located at Peace River and Cold Lake Basin.

The Alberta oilsands is a complex mixture of extra-heavy crude oil (called bitumen), water, solids, and clays (shown in Figure 1.1). It is extracted from the loose sand deposits in the northern region of the province. Alberta's oil sands operations are the world's largest industrial project, owing to the geological formation of the Rocky Mountains that pushed the hydrocarbon towards the Alberta/Saskatchewan border. The oil sands were formed 50–100 million years ago from the decomposition of mostly marine sea creatures and algae, and followed by the biodegradation of lower molecular weight molecules by microbes, resulting in heavier and complex components that comprise the viscous bitumen (Gray et al., 2009).

The typical Athabasca oil sand deposits are comprised of bitumen 6-14 wt%, water 3-7 wt%, and 80-85 wt% mineral solids (i.e mainly coarse silica sand with the particles size larger than 44  $\mu\text{m}$  and only 15-30 wt% of the solids are fine clays that are less than 2  $\mu\text{m}$  in sizes — such as kaolinite, illite and fractional amounts of smectite, chlorite, and montmorillonite). The micron-sized clays are one of the main challenges in the extraction process as they disrupt the separation process (Oil Sands Discovery Center, 2016; Oil Sands Magazine, 2020b).

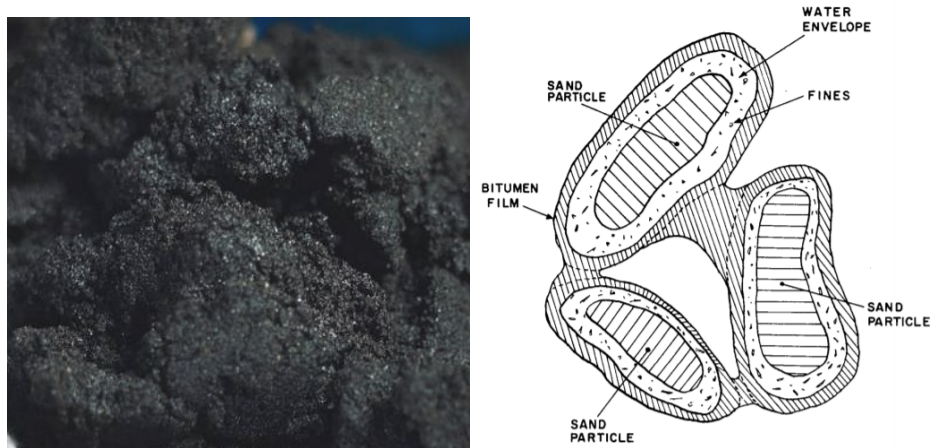


Figure 1.1. (a) The oilsands consist of bitumen, water, and solids in slackened sands form. (b) The morphology and arrangement of components in oil sands deposit (Clark, 1963).

The current commercial trend in bitumen extraction for surface-mined ore is the Clark hot water extraction (CHWE) process, which was invented by Karl Clark in the 1920s (Clark, 1963) and with some modified operating parameters (e.g. lower processing temperature). The overall process for water-based extraction is presented in Figure 1.2.

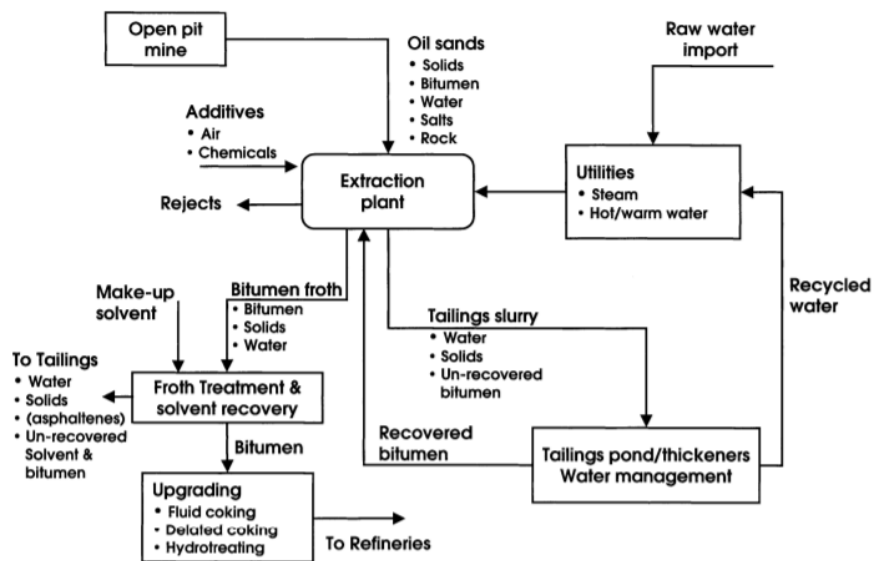


Figure 1.2. Process flow of the water-based oil sands extraction (J. Masliyah et al., 2004).

The two main processes in bitumen recovery are liberation and aeration. The oil sands ores are crushed for lump size reduction and warm water is added to form a slurry. The liberation process mostly occurs during the hydro transport of the slurry in a turbulent flow. In addition, mechanical

agitation and conditioning with chemical additives are implemented to enhance the detachment of bitumen from the sand grains. Subsequently, the liberated bitumen droplets would attach to free air bubbles through an aeration process in a primary separation vessel (i.e. the main component of the process, where up to 90% of bitumen is recovered). The aerated bitumen has a significantly lower density and rises to the top of the vessel and forms a “froth,” which has a typical composition of 60 wt% bitumen, 30 wt% water, and 10 wt% solids (J. . Masliyah et al., 2011). On the other hand, the heavy solid particles would sink to the bottom of the separation vessel. The significant difference in density between aerated bitumen and coarse sands should favour the gravity separation process. Nonetheless, with clays present in the system, their positively-charged edges would attach to the negatively charged bitumen surfaces, thus disrupting the aeration mechanism as bitumen could not attach to the air bubbles due to its surfaces being fully covered by clays.

The air bubbles bounded in the froth could be readily removed by a heating process and/or by gravity drainage, while the remaining water (usually in the form of emulsions) and unwanted fine solids have to be further separated in a mechanism called “froth treatment,” which produces a stream that is conventionally at about 98 – 99.9 wt% bitumen (J. . Masliyah et al., 2011). This is where organic solvents play a significant role in diluting the bitumen to reduce its density and viscosity so that the remaining solids would settle to the bottom with the aid of incline plated settlers and/or centrifuges. Filtration, in general, is not a practical way of removing fine solids as the maintenance costs are prohibitive.

In industrial practices, two main types of hydrocarbons are used as a solvent in froth treatment: naphtha-based and a lighter paraffin-based; both solvents have their advantages and disadvantages (Oil Sands Magazine, 2020a). Naphtha is readily produced in the upgrading plant as a by-product; its integration into the froth treatment process is a natural and economic choice. On the other hand, paraffinic solvent produces a higher bitumen quality (typically 99.9%) as the asphaltenes (fraction of the bitumen with high molecular weight and complex ring structures that is responsible for the high viscosity of bitumen) will precipitate in such a solvent, forming structures which gather and confine the remaining solids and water.

In 2018, a total of 17 refineries in Canada contributed 2 million barrels of crude oil per day (CAPP, 2019). At the same time, the environmental footprints associate with the oil sands industry (due to bitumen extraction, upgrading, transportation, and combustion) provide destructive impacts on the

surroundings that are not negligible. Some acute environmental issues are related to the ‘aqueous-based’ extraction method:

- Energy Consumption and Emission of Green House Gasses (GHGs)

Bitumen extraction from oil sands has a greater carbon footprint than the recovery of conventional light crude oil due to the use of steam and warm water to liquefy the bitumen (thermal energy is generated from the combustion of natural gas); the heavy machinery and vehicles for surface mining, and cracking of heavy hydrocarbons, also add to the total carbon footprint of the operations. GHG emissions from fuel consumption by oil and gas extraction, in general, have increased rapidly since 2005 due to the 158% increment in the extraction of bitumen and related activities; this trend is forecasted to be maintained (Environment and Climate Change Canada, 2019).

- An enormous amount of water consumption

Oil sands extraction facilities are considered to be water-intensive, where three to four barrels of ‘freshwater’ are required to convert a single barrel of bitumen from the ores. All process-affected water is retained on-site and is never allowed to be discharged to the surroundings as Alberta Environment enforces a zero-discharge policy. The main source of freshwater is from the nearby Athabasca River that also supplies water for municipal consumption. Therefore, the water level and quality become the focus in the community. At present, water consumption brings disadvantages to the residents and ecosystem, especially during the low flow season as the river surface would be covered in ice for 5 months during winter (Oil Sands Magazine, 2020c).

- Land disturbance and tailings ponds

A total of 760 km<sup>2</sup> of land was disturbed since the commencement of the oil sands operation, mainly due to surface mining, and about 25% of it is due to the construction of tailings ponds. Tailings ponds are the ‘temporary’ solution to the water that has been contaminated by the extraction process, which is not allowed to be released to the environment before proper treatment. The wastewater contains chemical elements that are harmful to the environment and health, caused by the contamination of the oil through the removal of the solids. The reclamation of tailings ponds is another issue that has been studied for decades, as the clays can take years/decades to be separated naturally from the water. The feasibility is still under questioned as no tailings pond has been totally reclaimed yet (Gosselin et al., 2010).

Another important drawback of the water-based extraction process is its inability to achieve desirable bitumen recovery (e.g. around 60% only) from low-grade ores as clays could disrupt the process (J. Masliyah et al., 2011).

Due to the increasing global demand for fossil fuel, the oil sands industry in Alberta is expected to expand in size. Under these circumstances, the above-mentioned issues must be overcome in order to maintain the industry's sustainability. In one such initiative, alternative extraction technologies have been studied to partially or completely replace water with organic solvents as an effort to circumvent the negative environmental impacts brought by aqueous extraction and transportation (Gosselin et al., 2010). This alternative solvent-based extraction is broadly known as non-aqueous extraction (NAE), with its simple operating principles illustrated by a basic flow diagram in Figure 1.3. The schematic of solvent-based extraction is congruent with the aqueous process, with a large amount of warm water replaced with hydrocarbon solvent and its possibility to be operated at ambient temperature.

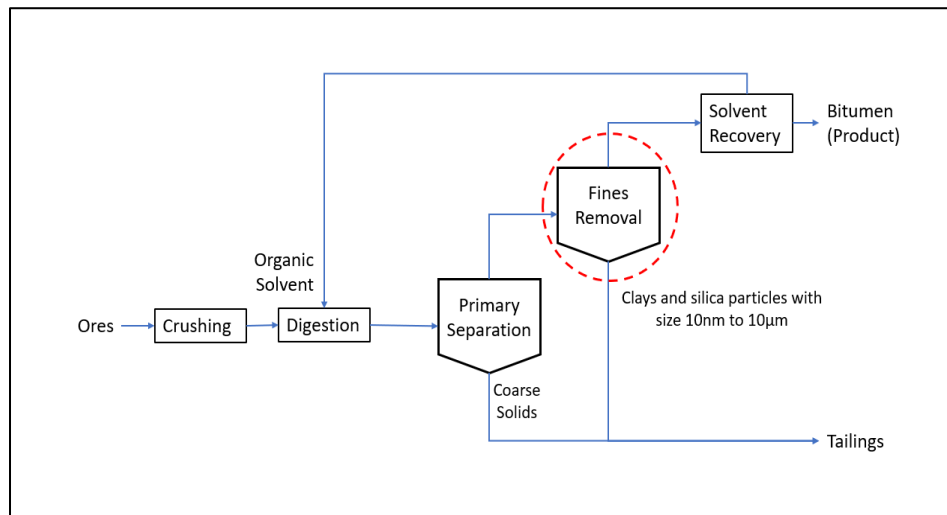


Figure 1.3. Fundamental principles of non-aqueous extraction chart. Adapted from (Fotovati, 2011; Lin et al., 2017) with appropriate adjustment to fit with the study.

Mined oil sand ores are first crushed; they are then mixed with a hydrocarbon solvent in which bitumen is soluble (partially or completely). This process is known as the digestion and dissolution of bitumen into the solvent. Subsequently, the mixture is fed into the primary separation vessel where coarse solids would be eliminated by gravity settling to the tailings. The clays and silica particles that are nanometers to microns in size are the fines that pose major problems since

conventional methods (e.g. centrifuge, hydro cyclone, or filtration) are not efficient in their removal. A *finer removal* process (red circle in Fig 1.3) must therefore be in place to eliminate such particles and prevent fouling problems downstream. After fines removal, the diluted bitumen enters the solvent recovery unit where the solvent would be recovered (through distillation) and recycled to the upstream for ore digestion again. The extracted bitumen would be further upgraded or sold directly in the market.

NAE is not a recently developed concept; its history could be traced back to a few decades ago (Cormack et al., 1977; Sparks et al., 1988). Unfortunately, its progress only reached the bench- and pilot-scale; no process was commercialized. The successful research into this technology could be a breakthrough to reduce the issues brought by oil sands mining operations. Three main questions in all proposed non-aqueous processes must be answered to develop a sustainable solvent-based extraction and commercialization attempt:

### 1. Solvent Selection

Finding an ideal solvent for NAE is a real challenge as three essential requirements have to be considered and satisfied simultaneously (see the intersection of these three features, as illustrated in Figure 1.4). These three essential criteria are extraction performance, economic aspects, and EHS (environmental, health, and safety) concerns.

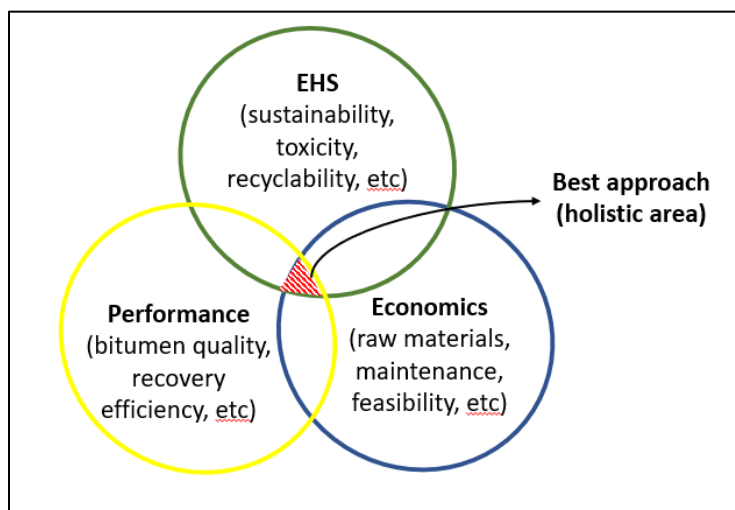


Figure 1.4. The best solvent selection is to fulfill the intersection between three main considerations (Lin et al., 2017).



## 2. Solvent Recovery

Solvent recovery is another major problem to be solved in the NAE process since it involves both economical (one of the costliest parts) and environmental issues. Based on the Alberta Energy Regulator policy, solvent loss in the dry tailing must be controlled to a minimum number lower than 0.4% volume of solvent per unit bitumen produced (Alberta Energy Regulator, 2015). The focus of the recovery is not only during the main NAE process but also on the tailings where the rejection of solids might contain residual bitumen and solvent that are trapped within, causing severe pollution to the environment.

## 3. Fines Removal

Fine solids (e.g. clays, silica particles, asphaltenic aggregates, etc.) in the diluted bitumen would have a detrimental implication on bitumen quality, leading to catalyst poisoning and fouling of unit operations or even in the pipelines. The fines have been in contact with bitumen for a very long period, and this leads to a surface-modified solid that is stable in diluted bitumen (i.e. form a stable colloidal system and the dispersed materials are difficult to separate). The rejection of fines to the tailings also creates a sedimentation problem because emulsions of water and bitumen are inordinately stable due to the clays and the natural surfactants.

The focus of this MSc research is on the last challenge, namely, fines removal. In terms of the process flow diagram, it is the operation that is circled in red in Figure 1.3. The fine solids that must be removed are in the size range of nanometers to microns, and they are known to be stable when dispersed in organic solvents (this colloidal stability can be asserted almost by definition, since particles that are unstable in non-aqueous liquids, even if very small in size, will aggregate and be eliminated by gravity settling).

We hypothesize that the surfaces of the fines are altered by being in contact with bitumen for long periods, making them resistant to aggregation in non-aqueous solvents; this, in turn, renders gravity settling in NAE an ineffective means of eliminating such particles. Investigating the colloidal stability of bitumen-modified solids in non-aqueous liquids may shed light on the conditions under which fine particles could be destabilized in the suspensions, resulting in the formation of large clusters (i.e. aggregation) and their removal by sedimentation (i.e. gravity settling). The issue and proposed solution are summarized in Figure 1.5

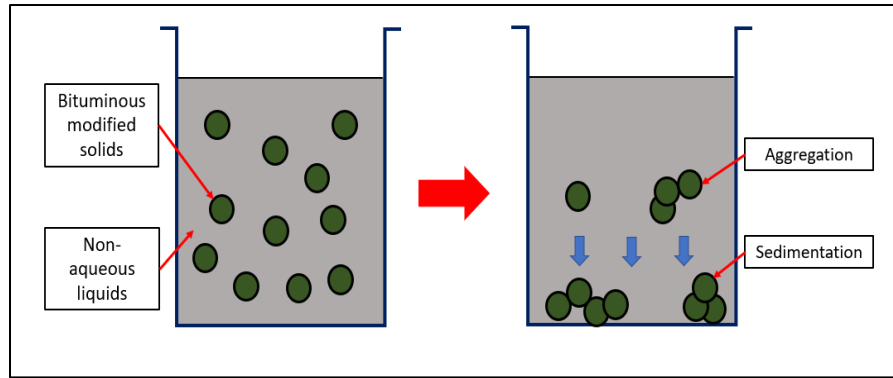


Figure 1.5. Stable colloidal system of bituminous solids in NA liquid (left). Destabilizing leads to fines aggregation, follows by sedimentation (right).

In many respects, non-aqueous extraction is similar to froth treatment operations in water-based extraction; the main difference between these two processes is the presence of emulsified water in froth treatment that is not seen in NAE (other than the minute amount of connate water in oil sands). Nevertheless, in NAE, a small amount of water deliberately added to the diluted bitumen (commonly less than 10%) could favor the removal of fines by forming agglomerates of the solids due to the strong capillary forces (Lin et al., 2017). The addition of external water to non-aqueous systems, although a viable means of removing fine solids, will not be the focus of this study. Instead, we will examine the possibility of fines removal by manipulating the composition of the hydrocarbon medium. Previous studies had revealed that the precipitation of asphaltenes (the component of bitumen with high molecular weights and complex structures) was responsible for the removal of emulsified water and fines in diluted bitumen as the asphaltenic “flocs-network” structures could bind and trap these materials. The flocs formed might increase in size in a cascading manner as they collide and aggregate due to the bridging (Farnard et al., 1985) or van der Waals interactions (Fotovati, 2011).

In the oil sands industry, naphthenic and paraffinic solvents are the two types of diluents used in froth treatment to attain a high quality of diluted bitumen with small amounts of solids and water. Naphthenic froth treatment (NFT) is normally adopted in plants that are linked directly to the upgrading facilities (it is implemented by Syncrude and Suncor for more than 30 years), while paraffinic froth treatment (PFT), which was developed in the 1990s, is a newer technology that can lead to much cleaner diluted bitumen, but at the expense of hydrocarbon loss (Kosior et al., 2018; Rao & Liu, 2013).

Naphthenic and paraffinic solvents have been proved to facilitate the removal of fines by simple gravity settling under certain conditions; these are, however, only two “data points.” In this work, the main goal is to determine more precisely those conditions that would favour fines removal in non-aqueous media. This can be achieved if the underlying mechanism responsible for the aggregation of fines (e.g. whether due to precipitation of asphaltene, or solely by van der Waals forces, or others) is determined. If precipitation of asphaltene is behind the phenomenon, would the sedimentation occur if the asphaltenes were absent (i.e. de-asphalted bitumen) in the system? Is the mechanism limited only to asphaltenes? And what happens if asphaltenes are replaced with maltene or other fractions? On the other hand, could the removal of fines be due purely to the destabilization of the colloidal system at the designated condition, leading to self-aggregation? The determination of the best conditions under which aggregation would occur naturally becomes crucial as the accumulated flocs could be separated by gravity from the hydrocarbon medium. The following are the main concerns:

- Dosage of solvent compared to the bitumen (i.e. in diluted bitumen): normally in terms of solvent to bitumen (S:B) ratio.
- Solids-to-liquids ratio: the amount of dispersed phase (fines) in the continuous phase (non-aqueous solvents), expressed in dispersed phase volume fraction. A higher number of solids leads to more efficient aggregation as the distance between solids is shortened and the solids are packed with higher density, thus making it easier to be in contact and form flocs by adhesive forces.
- Characteristics (i.e. chemistry) of solvents: in this case, the focus is on the degree of aromaticity (i.e. the amount of aromatics in an aliphatic-aromatic solvent mixture).

This study will focus on the last point: to understand the fundamentals of solids removal as a function of the aromaticity in the solvent system. Here, the S:B ratio (mentioned in the first point) is not relevant since bitumen will be absent in the system (focus only on pure solvent and not diluted bitumen — effectively working at infinite S:B ratio), and the dispersed phase volume fraction (mentioned in the second point) will be maintained at a constant value throughout all experiments. In this thesis, the main goal is to reveal the mechanism(s) for the aggregation and sedimentation of fine solids, leading to their removal in non-aqueous media. Objectives of this study are stated as follows:

1. **Macroscopic scale:** To methodically study colloidal stability, as indicated by the aggregation and sedimentation of model solids dispersed in various non-aqueous media. Firstly, the settling behaviour of bitumen-treated particles was examined and compared with the controls (pure silica that was hydrophilic, and chemically-treated silica that behaved hydrophobically) in hydrocarbon media (pure toluene and *n*-heptane) and aqueous medium (water) in order to provide a baseline idea on the stabilizing mechanisms. Subsequently, the study is continued with bitumen-treated silica particles (the empirical model for solids that were treated with different fractions of bitumen with only single layer adsorption) in hydrocarbon media, namely heptol — a model solvent mixture of *n*-heptane and toluene — with various degrees of aromaticity (i.e. different volume fractions of toluene in the mixtures). All experiments were designed in a simplified clean system (i.e. in pure solvents only, without any liquid bitumen or emulsified water that might complicate the interactions) to reveal the most fundamental mechanism(s).
2. **Microscopic scale:** To investigate the interparticle forces between two individual model solids in various media by utilizing the microcantilever technique. The interactions of these *two* particles could represent the mechanism that governs billions of particles in the macroscopic analysis; hence, it can reflect the underlying physics of settling behaviours.

This thesis is arranged in the sequence of the following chapters:

Chapter 1 is an introduction to the overall oil sands extraction operation (i.e. the recovery process from raw oil sands ore to bitumen) and its economic feasibility. Non-aqueous extraction (NAE) is discussed as an alternative to the current water-based method that leads to serious environmental issues. A major challenge in NAE, namely, the removal of unwanted solids in non-aqueous media, has provided a strong motivation for this thesis. Lastly, the research objectives are stated in this chapter. Chapter 2 examines the relations between key process parameters through a literature review of previous research results. It also provides the background information for understanding the fundamentals and the underlying physics in aggregation, sedimentation, and interparticle forces in colloidal systems. Chapter 3 describes the framework on how the experiments are conducted and the materials used. Two experimental approaches to study the colloidal behaviour of the system, namely, the macroscopic analysis (i.e. “jar tests”) to study the settling rates of bitumen-modified silica particles in various solvents, and the microscopic analysis to measure the adhesive

forces between two particles with a novel microcantilever technique. Lastly, the experimental scopes are summarized in tabular form. Chapter 4 covers the experimental results with a detailed discussion of the settling behaviour of bituminous particles in hydrocarbon media. The stability of the colloidal system is phenomenologically categorized by a binary approach and further associated with the degree of aromaticity (toluene content in the solvent) in non-aqueous liquids. The correlation between the adhesive forces with the settling rate is established in this chapter. Finally, a conclusion and recommendation for future work are given in Chapter 5.

## **2. Literature Review**

Chapter 2 provides a general review of the mechanisms that are related to the main objective in this research, namely, the elimination of fines in non-aqueous media. Froth treatment and non-aqueous extraction are two major processes in the oil sands industry that involve the dispersion of fine solids in non-aqueous liquids, forming a stable colloidal system. An understanding of the stabilizing mechanism(s) could offer crucial information on how dispersed particles can be removed through destabilization, aggregation, and sedimentation. Asphaltenes, the complex macromolecules in bitumen, may be responsible for the colloidal stability as they adsorb onto the surfaces of particles and create repulsive forces in hydrocarbon at certain levels of aromaticity. In addition to asphaltenes, bitumen can be further separated into other components (e.g. maltenes). It may not wise to attribute the entirety of asphaltenes to colloidal stability, as only a small component of it is considered interfacially active; further fractionation of asphaltenes was proposed to provide a deeper understanding of the underlying mechanism of stability. Mechanisms related to bitumen behaviours, mainly asphaltenes in various solvents (e.g. precipitation, adsorption, aggregation, and sedimentation), would be further investigated regarding the main principles and the governing equations. Interactions between “contaminated” particles in organic liquids were thoroughly studied to determine the dominant forces between them and how such forces lead to various settling behaviours. Methods to study settling behaviours and interparticle interactions (i.e. in terms of forces) will also be discussed.

### **2.1 Fractionation of Crude Oils**

#### **2.1.1 SARA Analysis**

Analysis of the chemical composition of crude oils is an arduous process due to the material's complexity and strong dependence on the methodology. The most commonly accepted process is known as SARA fractionation, which was first introduced by Jewell et al. (1972) based on ion-exchange, coordination, and adsorption chromatographic separation. A few years after, a standard method known as ASTM D2007-93 had been developed by using *n*-hexane to separate the asphaltenes (A), then further divided the maltenes in chromatographic separation of non-asphaltic oils into three components, namely saturates (S), aromatics (A) and resins (R) (ASTM D2007-93, 1993). The SARA analysis is explained in the first part of Figure 2.1, which indicates that the fractionation utilized a simple combination of solubility and chromatographic adsorption. Further

studies in this area led to a modification in the technique (e.g. NH<sub>2</sub> materials columns HPLC or thin layer chromatography) and the solvent used (e.g pentane or heptane instead of n-hexane) (Fan & Buckley, 2002).

Overall, the SARA analysis often leads to erroneous results, especially on the chromatographic separation part, as the boundaries between fractions are not sharp; each fraction strongly depends on the eluent (solvent) and adsorbent (column materials). The results from SARA can display distinctive differences in measurement by variant laboratories or even different techniques (Fan et al., 2002; Kharrat et al., 2007). Therefore, recent researches focused neither on the actual molecules nor chemical compositions, but rather on separation depending upon their solubility and interfacial activities. This newly developed concept is known as ‘Extended-SARA (E-SARA)’.

### **2.1.2 Extended-SARA Analysis**

The traditional SARA analysis emphasizes characterizing asphaltenes based on their solubility by precipitation in varying mixtures of aliphatic-aromatic solvents and reduced interfacial tension (Fossen et al., 2007). This method, however, is unable to relate the key functional groups in the sub-fractionations to the phenomena shown in asphaltene aggregation, precipitation, and adsorption. As a next step, the extended-SARA (or E-SARA) analysis is proposed as the complement to the existing fractionation (i.e. SARA) with the extension in asphaltenes based on adsorption characteristics and interfacial activities. In the past, the entire asphaltene fraction was believed to be responsible for the formation of stable W/O emulsions. However, more recent studies had shown that only a small subfraction of the asphaltenes was attributed to emulsion stabilization. Such a subfraction is called “interfacially active asphaltenes” or IAA; its identification is based on preferential partitioning to the oil-water interface (i.e. propensity to adsorb at the surfaces of emulsified water droplets). The asphaltenes that do not migrate to the oil-water interface, and instead remain in bulk solution, are collectively referred to as “remaining asphaltenes” or RA (Qiao et al., 2017). The extended-SARA subfractions are depicted in Figure 2.1. The complete fractionation procedures were published by Yang et al. (2014) and would be further discussed in Section 3.1. Preparation to Obtain Bituminous Materials. Based on this concept, maltenes might be able to be separated into interfacially active and remaining subfractions instead of the chromatographic adsorption subfractions with unclear boundaries.

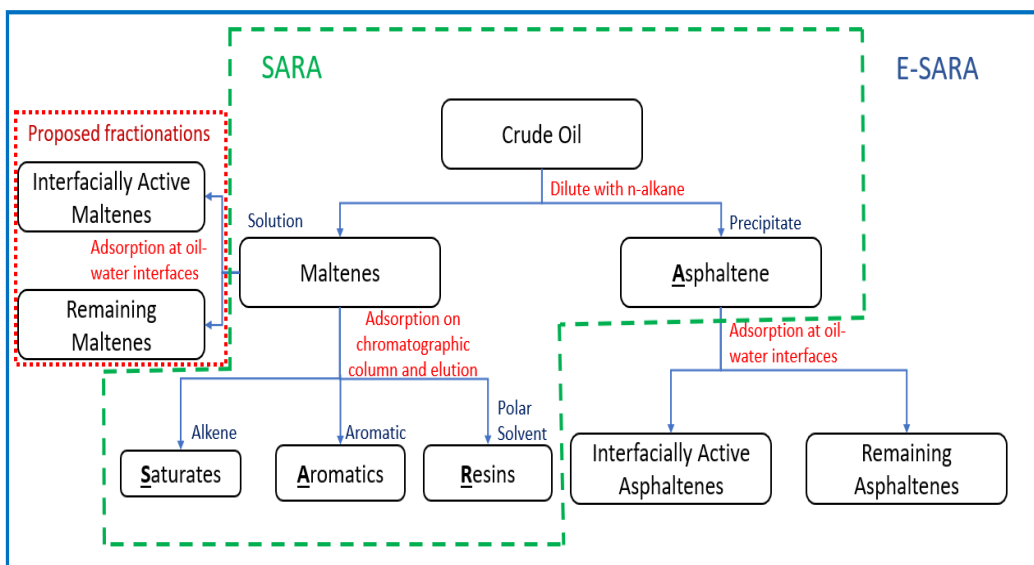


Figure 2.1. E-SARA fractionations of crude oils with proposed subfractions on maltenes.

Adapted from (Qiao, 2019) with some adjustments.

### 2.1.3 Interfacially Active and Remaining Asphaltenes Subfractions

Interfacially active asphaltenes (IAA) account for less than 2 wt% of whole asphaltenes (WA); yet, this subfraction is responsible for the stabilization of W/O emulsions. The remaining asphaltenes (RA) were observed to behave similarly to WA. This is not surprising since WA comprises primarily this subfraction (i.e. more than 98%).

The main differences in IAA and RA are briefly summarized in the following:

- IAA is more surface active than RA (i.e. at the oil-water interface) as suggested by interfacial tension and film rupture tests. On the other hand, WA and RA exhibited similar results in interfacial tension measurement as shown in Figure 2.2 (F. Yang et al., 2014).
- The highest concentration of sulfoxide groups was found in IAA molecules. These functional groups play a crucial role in enhancing interfacial activity (i.e. adsorption at oil-water interfaces, the formation of rigid interfacial films, and stabilization of W/O emulsions) (Qiao et al., 2018). The sulfoxide functional group has high polarity as a consequence of the electronegativity difference between oxygen and sulfur in the S=O bond, causing it to be a strong hydrogen bond acceptor (Qiao et al., 2017).
- The sulfoxide groups also induce hydrogen bonding between the IAA molecules (i.e. self-assembly), resulting in the formation of supramolecular structures in the solvent and porous



networks at the O/W interfaces (F. Yang et al., 2015). This self-assembled structure and combination of various weak associations of IAA with water interfaces result in irreversible adsorption at the interface, with fewer freedom arrangements.

- In general, IAA molecules have higher paraffinic content (either straight-chain or cyclo-paraffinic) but lower aromatic content compared to RA.

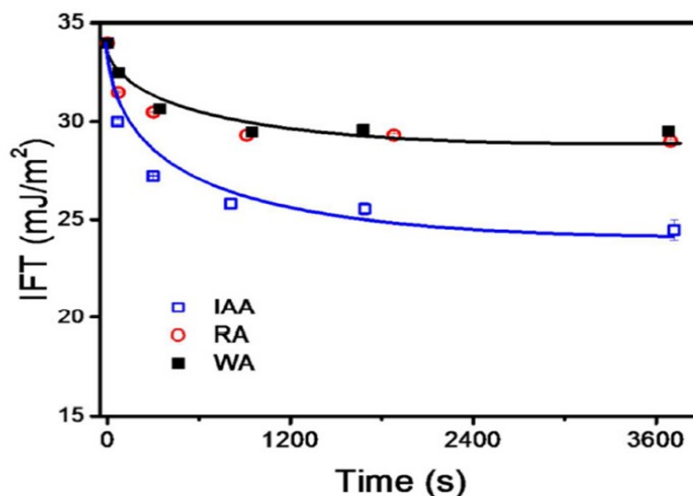


Figure 2.2. Interfacial tension of the asphaltenes subfractions suggests that IAA is more surface-active (F. Yang et al., 2014)

## 2.2 Solvent Selection and Asphaltene Precipitation

### 2.2.1 Solvent Selection

During the digestion step in the NAE process, a solvent is introduced as the diluent to dissolve bitumen from the oil sand ores. Some considerations on the solvent selection criteria were discussed in Chapter 1. Here, we will further examine the correlation of solvent chemistry with the occurrence of self-aggregation (i.e. asphaltene precipitation) that leads to sedimentation in solution. The solvent used for the process is commonly a complex mixture of hydrocarbons, primarily the aliphatics (i.e. saturated straight, branched, or even cyclic chains) and aromatics (i.e. unsaturated ring-type compounds with a minimum of one benzene ring). Figure 2.3 provides a better illustration for choosing an appropriate solvent in the system based on the desired conditions that favor certain mechanisms. Paraffinic is basically part of aliphatic by excluding the saturated closed ring (cyclic) compounds.

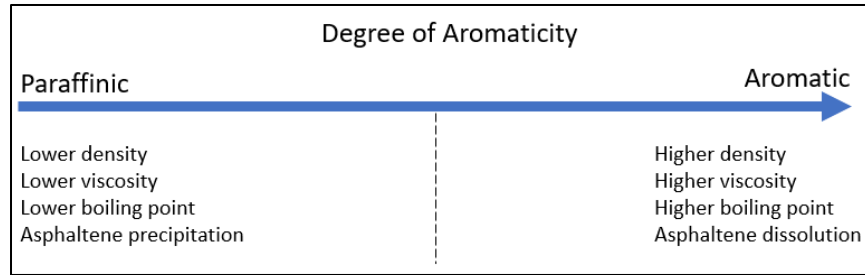


Figure 2.3. Solvent selection with respect to the degree of aromaticity to obtain the desired specifications. Adapted from (Oil Sands Magazine, 2020a).

Nikakhtari et al. (2013) reported that the solubility parameter of solvents was directly correlated with the amount of fine solids in the bitumen product. Another study describes mixtures of *n*-heptane and toluene were able to produce desirable bitumen with solids and water contents less than 0.5 wt% at room temperature; yet, the ratio between these two solvents was crucial, as an inappropriate ratio might cause the reverse effect (i.e. mitigation of fines to the bitumen) (Hooshari et al., 2012).

### 2.2.2 Asphaltene Precipitation

Asphaltene itself is another controversial subject that receives attention from researchers as the fractionation boundaries are not clear and are often mixed up with resins, which are polar compounds as well. To minimize ambiguity, asphaltenes, in this case, are defined as the fraction that is precipitated by *n*-alkane, and the soluble part is maltene (no further fractionations). Studies on the precipitation of asphaltenes by light alkanes normally were conducted in various S:B ratios with the application in paraffinic froth treatment (PFT), shown in Figure 2.4.

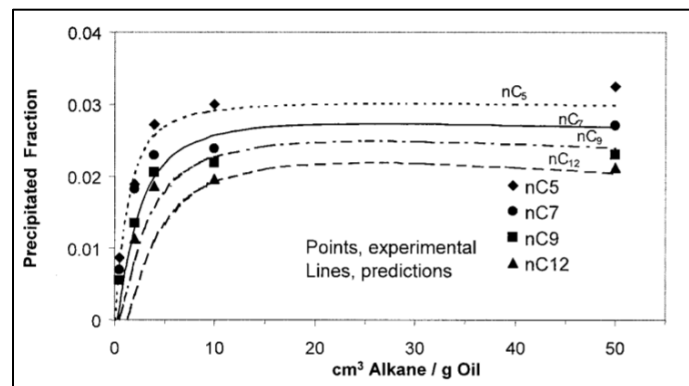


Figure 2.4. Asphaltene precipitation in light *n*-alkanes in the different solvent to bitumen ratio.

Sourced from Buenrostro-Gonzalez et al. (2004).

A recent study by Xu (2018) with a different arrangement in a graphical presentation is shown in Figure 2.5. The asphaltene content in the bitumen product drops significantly with increasing S:B ratio for all types of *n*-alkanes. It was proposed that solubility parameters are behind the phenomena.

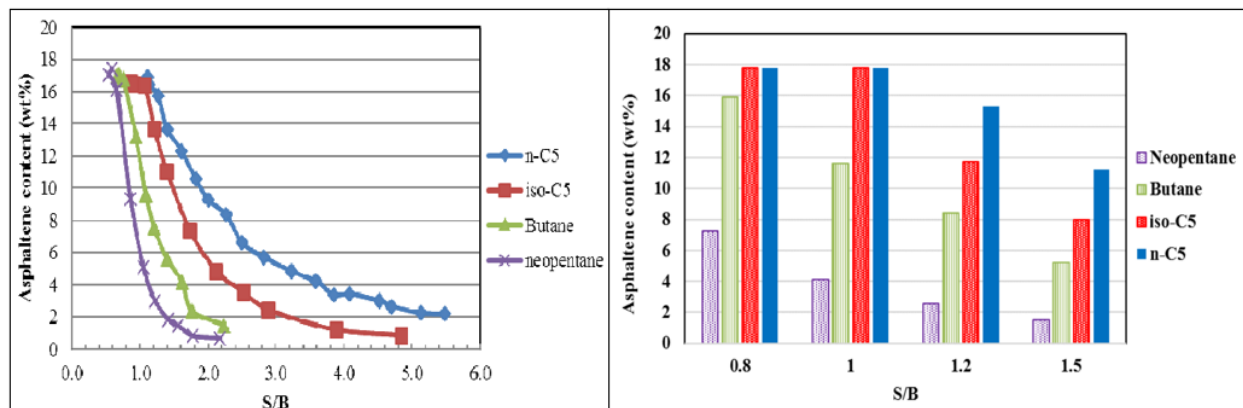


Figure 2.5. Asphaltene content in the bitumen depends on the type of solvent and ratio. The plot on the left is in a narrower range of the S:B ratio for better visualization (Xu, 2018).

The aromaticity of the solvent is strongly related to precipitation, with decreasing aromaticity favoring asphaltene precipitation (Zhang et al., 2016). As the aromaticity of a solvent increases, the interaction between asphaltene molecules or aggregates gradually shifted from weak attractive force (in paraffinic) to repulsion (in aromatic). The underlying physics for the forces (i.e. repulsion in good solvent and attractive forces in poor solvent) would be further discussed in Section 2.6.

The aggregation behaviour of asphaltenes is not proportionally related to the ring system; it has more to do with the associations of polar functional groups (carboxylic acid, carbonyl, sulfoxide, and derivative groups), especially between the sulfoxide groups. Higher concentrations of the polar functional groups (in asphaltene subfractions) lead to a higher probability of aggregation as the sulfoxides allow more binding sites; this explains why IAA has a significantly higher aggregation tendency than RA (Subramanian et al., 2017). In addition, the sizes of IAA aggregates are larger since the nearby IAA molecules or small clusters would bind together through hydrogen/polar bonding (Qiao, 2019). The sizes of the aggregates in the solvent also determine the interaction behaviours, with the denser and smaller aggregates having a lower probability of repelling each other when in contact. The repulsive force (either in magnitude or range) is expected to decrease with the decrement in the degree of aromaticity in the solvent. Figure 2.6 shows the tendency to

form aggregates, with the aggregate sizes strongly related to the amount of aromatics in the mixture; the modifiers ‘T’ and ‘HT’ for the subfractions specify the solvent that was used in the fractionation procedure: T for toluene, and HT for a 50:50 heptol mixture.

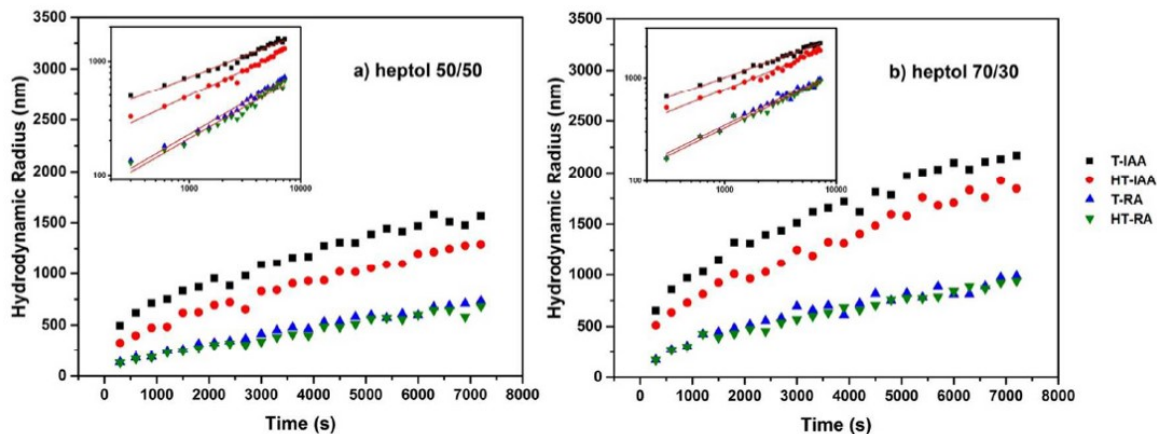


Figure 2.6. The inclination in aggregation and size is increased with the increment in n-heptane content in the solvent. Adapted from Qiao et al. (2018).

## 2.3 Adsorption of Asphaltenes onto Solids and Its Surface Chemistry

### 2.3 Adsorption of Asphaltenes onto Solids

Adsorption of asphaltenes onto a solid surface is generally in the form of a single thin layer (molecular level); it is often irreversible as the process is more likely one of chemisorption (i.e. chemical adsorption) instead of deposition onto a surface (i.e. physical adsorption) (López-Linares et al., 2011). The mechanism depends significantly on the chemical and structural characteristics inherited from the source of asphaltenes or the method of fractionation. Besides, it is also strongly correlated with the physical and chemical properties of the sorbent/ solid surfaces (Adams, 2014).

Both clay minerals (e.g. kaolinite, illite, montmorillonite) and silica are hydrophilic with Si-O-Si and Al-OH (in the case of clay minerals) or hydroxyl silanol Si-OH (for silica surface). The adsorption of asphaltenes is mainly mediated by the polar groups as active sites since the outer layer is terminated by hydroxyls (Tombácz & Szekeres, 2006). The only difference between the two sorbents is the swelling ability of clay minerals (mostly montmorillonite). The swelling of clay minerals is noticed when water or other solvents are present; yet its effect on the adsorption

is negligible because the adsorption of asphaltenes is at the surface only and does not permeate into the inner interlamellar layer (Cosultchi et al., 2005).

The surface properties of mineral clays and silica could be altered by the adsorption of asphaltenes, shifting from hydrophilic (water-wet) to becoming more hydrophobic (oil-wet); the amount of surface modification depends on the packing density and conformations of the adsorbed molecules. This allowed the ‘contaminated’ solids to remain at the oil-water interfaces, as their surface properties are intermediate between being purely hydrophilic or hydrophobic (Jiang et al., 2011).

### **2.3.2 Surface Chemistry**

The physicochemical properties of surfaces are mainly affected by the nature of the long-chain compounds on the outer layer (Butt et al., 2003). In general, the interaction between a surface and the solvent is significantly governed by the type and length of the chain, chain packing density, and charge distribution. In addition, the impact of solvent type on the interaction is a non-negligible factor: a good solvent could further extend the chain length and mobility (further discussed in Section 2.6.2.1).

As alkyl chains are hydrophobic by nature, their adsorption onto a solid surface would render the surface more hydrophobic when the coverage exceeds a critical packing. Since asphaltenes are macromolecules with complex structures and long chains, the surfaces on which they adsorb would behave similarly as the asphaltenes (i.e. hydrophobic). However, the chain density must be sufficiently packed for the modified surface to be hydrophobic; otherwise, the sparse arrangement might cause the surface to become partially hydrophilic or hydrophobic. Among the subfractions of asphaltenes, IAA molecules pack most densely on a hydrophilic silica surface, leading to the closest packing arrangement with the least surface mobility (Qiao et al., 2018).

Figure 2.7 depicts the possibilities for an adsorbed surface to be hydrophilic or hydrophobic, depending on the charge, chain length, and density of the adsorbate: (a) The surfaces are charged negatively by various processes (e.g. hydroxyls dissociation in alumina and silica or preferential solubility in AgI case). The surface charges convey hydrophilicity behaviour. (b) Long alkyl chains with hydrophobic nature adsorbed onto the surface with a close-packed configuration which formed a new outer surface that behaved hydrophobically. (c) Excessive cations contributed a positive net charge to the outer layer, leading to hydrophilic behaviour. The hydrophobic

behaviour of the alkyl chains as the outer layer shifted to hydrophilic when the concentration of the chains was increased and engaged more counterions to stabilize the system. (d) The short alkyl chains with sparse packed arrangement would retain the hydrophilicity. (e) The densely packed configuration of short alkyl chains could induce hydrophobicity to the surface. (f) Long alkyl chains attached to the surface with loose-packing may be able to alter it to hydrophobic (only limit to the condition where coverage must transcend the critical packing density).

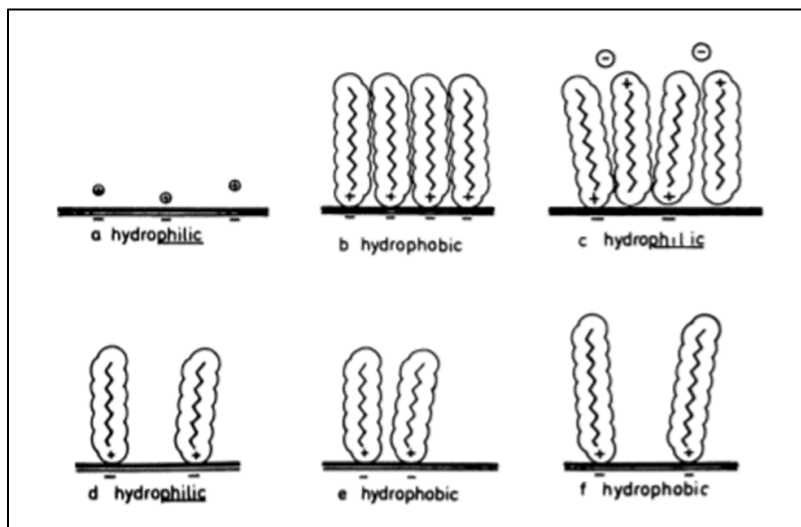


Figure 2.7. Possible configurations that influence the physicochemical properties of the surface.

(Source: Lagaly, 1987)

## 2.4 Aggregation of Particles and Collision Theory

Particle aggregation refers to the assembly of neighbouring dispersed particles into larger aggregates (or flocs) due to the net attractive force between particles (often referred to as flocculation) or cross-bridging between them with the aid of ‘third party’ molecules (often called coagulation). This process is an indicator of the functional destabilization of the colloidal system (Bratby, 2016). Destabilization can be attained simply by changing the properties of the solution (e.g. pH, salinity, temperature, or degree of aromaticity) or by the addition of coagulant/ flocculant. The difference in density between the aggregates and liquid would lead to a solid-liquid separation process by sedimentation. Colloidal instability in the suspension to form heavier clusters is widely exploited in the industry (e.g. wastewater treatment, mineral processing, oilsands tailing, etc.) as solid-liquid separation could be achieved easily by gravity settling, which is the most straightforward and economical method.

Aggregation is illustrated as a three-step mechanism in Figure 2.8: (1) A stable colloidal system contains particles that remain dispersed in suspension for extended periods (i.e. days, years, or beyond). (2) The colloidal particles require destabilization to promote aggregation by various methods, such as chemical addition or properties adjustment. (3) With the particles in the liquid suspension sufficiently destabilized, they would collide with each other via two mechanisms: Brownian motion (perikinetic aggregation) and/or driven by the motion of the suspending fluid (orthokinetic aggregation). The rate of aggregation is mainly controlled by the collision efficiency (or inversely, the stability ratio) and frequency (Gregory, 2009).

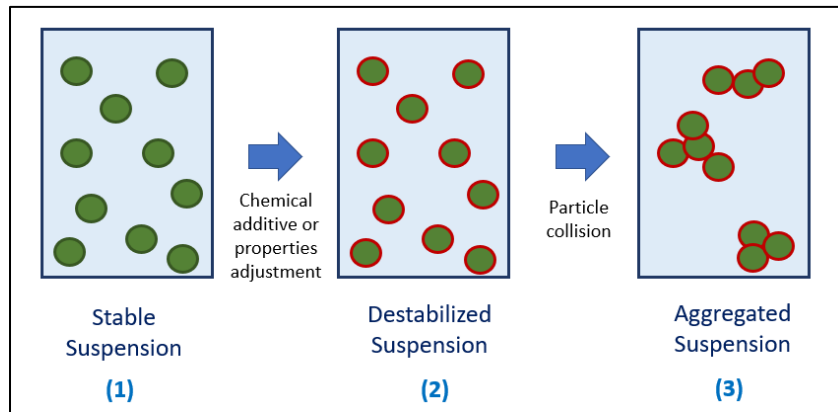


Figure 2.8. Schematic of the aggregation mechanism. Redrawn based on Gregory (2009).

When two particles are sufficiently close to one another, the interparticle forces would come into play, causing the interaction to be attractive or repulsive, depending on the properties of the surfaces and the solvent (i.e. liquid media). The main interparticle forces (whether attraction or repulsion)—their origins and dependence on separation distance—will be discussed extensively in Section 2.6.

## 2.5 Sedimentation and Settling Rate

### 2.5.1 Sedimentation

The first experimental study of the sedimentation on concentrated suspension was traced back to (Coe & Clevenger, 1916). In general, sedimentation can be categorized into Type 1 and Type 2, as shown in Figure 2.9. In the figure, portion A is the clear liquid zone; the distinctive line below this zone (i.e. the boundary between the clear liquid layer with the murky suspension) is usually called the ‘mudline.’ Zone B is the portion of the suspension that retains the initial concentration.

Zone C is a region of variable particle concentration, with density increasing with the depth. Finally, Zone D is the bottom portion that contains the packed sediment.

For Type 1 settling (Figure 2.9a), the sedimentation process is initiated when particles in the suspension begin to migrate downward (i.e. fall to the bottom). After a sharp acceleration period that is followed by the formation of clear liquid (zone A), the interface between the transparent liquid and suspension falls at a constant rate in Zone B until the mudline reaches the upper layer of Zone C (i.e. Zone B has disappeared). The rate would diminish when the mudline is close to the layer of sediment until the “critical settling point,” where the clear liquid (Zone A) would be in direct contact with the sediment layer (Zone D) and both Zones B and C disappear. As time progresses, the sediment would consolidate as the liquid is forced upward around the sediments, creating a loose bed of particles at the bottom (Richardson et al., 2013).

Type 2 settling (Figure 2.9b) is less common and occurs in situations where the particle distribution is very broad. The larger particles would settle faster, leaving the smaller ones behind. For this reason, the sedimentation rate consistently drops throughout the entire process, with the formation of a variable composition zone and the absence of the constant composition zone. Type 2 settling is known as differential settling.

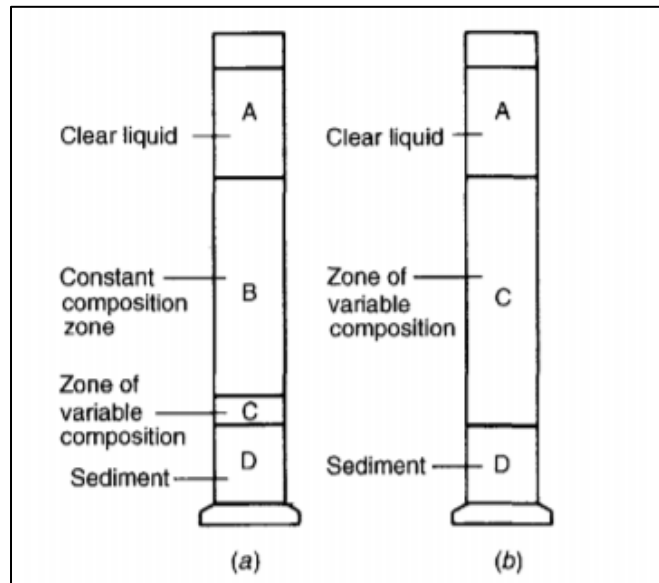


Figure 2.9. Two types of sedimentation in concentrated suspension systems.

Source: (Coe & Clevenger, 1916)



### 2.5.2 Free Settling

Sedimentation and settling rate of particles is significantly influenced by the concentration of particles in the suspension, which relates to the distance between particles and hence their interactions. A single particle with an adequate distance from the walls would encounter free settling in which the settling rate is not interfered with by the retarding wall effect. In low concentration suspensions, the space between particles is sufficiently large to avoid interparticle hydrodynamic effects (i.e. the crossing of streamlines around the particles). The settling velocity of this single-particle situation is described by the well-known Stokes's law, which is valid for Reynolds numbers less than 1.0 (i.e. the laminar flow regime):

$$V_{\text{Stokes}} = \frac{2}{9} \frac{\Delta\rho g d^2}{\mu} \quad (2.1)$$

Where,  $V_{\text{Stokes}}$  (m/s) is the particle's free settling velocity in the Stokes regime,  $\Delta\rho$  ( $\text{kg/m}^3$ ) is the density difference between particle and fluid,  $g$  ( $\text{m/s}^2$ ) is the gravitational acceleration,  $d$  (m) is the hydrodynamic diameter of the particle, and  $\mu$  (Pa. s) is the fluid viscosity (J. . Masliyah et al., 2011).

### 2.5.3 Hindered Settling

In real situations, a suspension often contains a high concentration of solids which alters (hinders) the overall settling velocity as the streamlines of a settling particle affect the settling rate of nearby particles. In addition to these hydrodynamic effects, interparticle forces and changes in the effective fluid density and viscosity will also influence the overall particle settling rate (Davies, 1968; Steinour, 1944). Therefore, the sedimentation rate of particles in this system (namely hindered settling) is lower than that of a single particle (of the same size) that falls in an infinite medium. The mathematical correlation developed from experiments by Richardson & Zaki (1954) is widely used in chemical engineering:

$$\frac{V}{V_{\text{Stokes}}} = (1 - K\alpha_p)^n \quad (2.2)$$

Here,  $V$  (m/s) is the hindered settling velocity, which normally is expressed as a ratio with the Stokes settling velocity;  $K$  is the hydrodynamic volume factor (which depends on the shape and

size of the particle),  $\alpha_p$  is the volume fraction of the particle in the suspension, and  $n$  is the Richardson-Zaki index that is a function of the Reynolds number.

### 2.5.4 Effect of Aggregation in Sedimentation

The sizes of the aggregates increase by collision and decrease as the aggregates break up due to shear (i.e. hydrodynamic) forces. Combined with the formation of substantial cluster networks during aggregation, this mechanism could affect the sedimentation structural properties (e.g. settling rate, sediment size, etc.) which are functions of the aggregated particle volumetric concentration and their interparticle interaction (Michaels & Bolger, 1962). Consequently, whenever sedimentation occurs as a result of aggregation, the settling behaviour of the suspension depends on the initial concentration of the particle and the optimum conditions for the inter-particle forces to be exerted (either repulsion or attraction).

### 2.5.5 Settling Rate Measurement

#### 2.5.5.1 Optical Observation on Batch Settling Experiment

Optical observation is the most direct way of estimating the settling rate of particles/aggregates by monitoring the mudline (i.e. the interface between the clear liquid and murky suspension). A typical experimental setup is shown in Figure 2.10. Behind its simplicity, two major requirements must first be met for this method to be applicable: a clear liquid on the top and a sharp interface line.

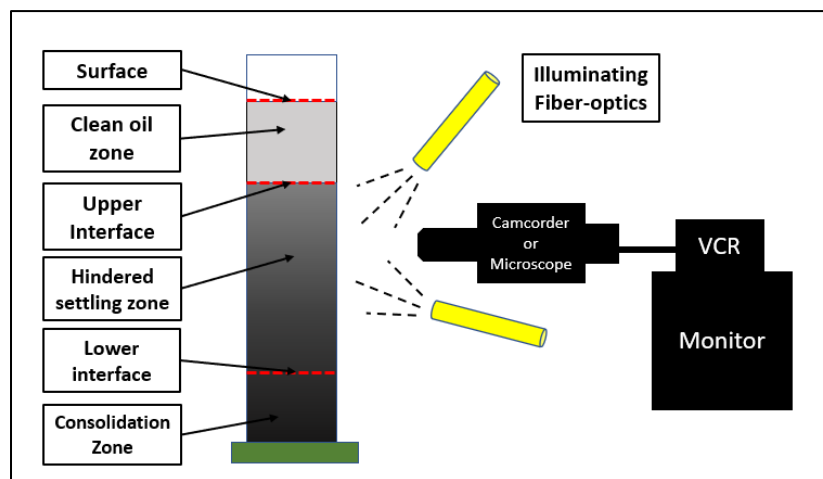


Figure 2.10. Schematic of the optical observation of mudline.

(Redraw from source: Long et al., 2002)

This test is normally conducted using a graduated glass cylinder which contains the dispersion of interest. Illumination is often provided by fiber-optic cables; if a lamp is used, care should be taken that there is no heat transfer to the liquid. The suspension is initially mixed and quickly transferred to the glass cylinder for monitoring. The height of the interface should be recorded with a camcorder that can be replayed in movie clips to obtain more accurate data (especially when settling is rapid). The data would be simply plotted with the positions of interface versus time in a settling chart as displayed in Figure 2.11.

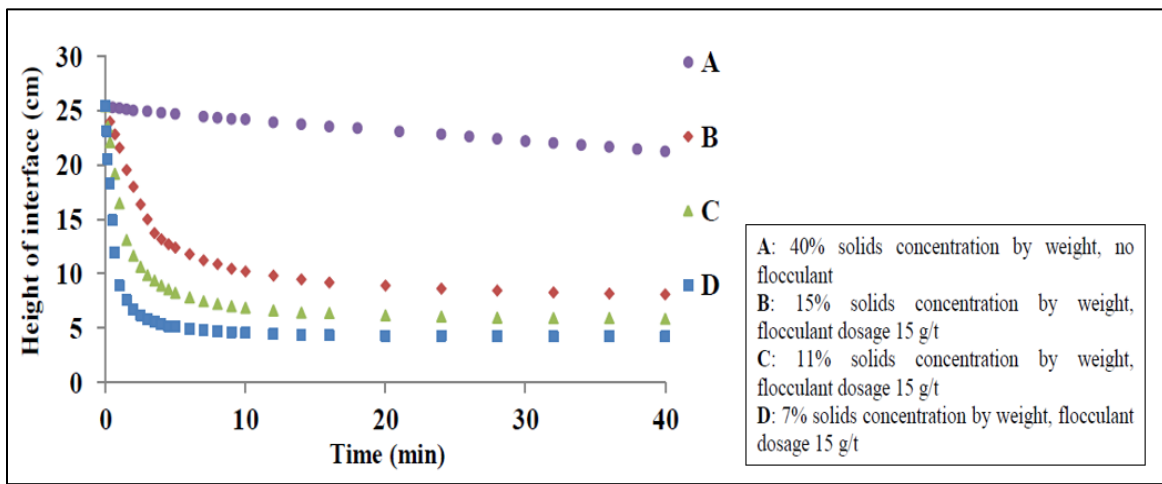


Figure 2.11. Batch Settling curve to study the sedimentation process.

Adapted from: Garmsiri & Shirazi (2012).

The batch settling curve was the sedimentation result by optical observation. The data, reproduced from Garmsiri & Shirazi (2012), was a study on the settling behaviour as the function of solids concentrations and flocculant dosages. This is also a good example to show the two common models of batch settling curve in an aggregation associated sedimentation process. At the low initial concentration of the aggregates, the system could be considered as a discrete unit of particles and non-moving fluids (i.e. without hindered settling). The aggregates migrated downward at a consistent settling rate and subsequently gathered at the bottom to form a sedimentation bed. When the concentration became higher, the maximum settling rate is not determined at the initial time, but as the increasing of the initial height of mudline. This behaviour serves as the characteristic of structural aggregation correlated with the continuous network of the flocs (Richardson et al., 2013).

The first model of settling behaviour would see an accelerated settling rate as aggregation occurred (the nearby particles would collide and form aggregates). Quantitatively, the aggregates formed

would increase in size as they drop to the bottom as a function of distance in the z-axis (i.e. depth) due to contact (i.e. in the range of interaction) with other particles. Therefore, the aggregates consisting of original particles and occluded fluids are substantially larger with the density intermediate between those of the particle and the fluid. Subsequently, the rate would decrease when the interface is close to the layer of sediment. This behaviour is reflected in cases B to D in Figure 2.11, where the aggregation is encountered with the addition of flocculant.

The second model behaviour indicates the solids fall to the bottom at a constant rate that is consistent with case A in Figure 2.11. It suggested that the particles experience free settling without aggregation, or the aggregates assembled are uniform in size (at least narrow particle size distribution). This sedimentation system could be considered as fully dispersed uniform size aggregates that correlated with the free settling velocity of individual aggregate as a constant composition zone (Michaels & Bolger, 1962).

#### **2.5.5.2 Novel Ashing Technique**

A semi-empirical analysis was first published by Jin et al. (2011) to be applied to the sedimentation of modified silica particles in hydrocarbon suspensions where the system is very opaque (i.e. dark bitumen liquid), making visual observation impossible. This novel ashing method measures the solids concentration at a fixed point over time (as seen in Figure 2.12a) instead of tracking the location of the mudline. The moment when sedimentation started was denoted as  $t = 0$ . Quantification of the sedimentation rate was by collecting small samples of the suspension at a fixed location in the container at various times. The solid content would be examined by the “ashing” method – vaporizing all the organic materials in a high-temperature muffle furnace, leaving only the inorganic matters (i.e. the particles). The mass of the inorganic materials ( $m$ ) was weighted using a microbalance. The solids collected would decrease over time as sedimentation progressed. A standard plot (Figure 2.12b) of solids mass ( $m$ ) versus settling time ( $t$ ) is used to obtain the initial slope,  $dm/dt$ , as an indicator of the settling rate.

The settling rate of bitumen-treated silica in terms of  $dm/dt$  in pure heptol systems (i.e. different volumetric ratio of *n*-heptane and toluene; without dissolved bitumen in the liquid) was plotted in Figure 2.13a. The results show a strong dependency between the settling rate of bitumen-treated particles with the degree of aromaticity of the solvent: the settling rate decreases as the graph moves toward the right (as the toluene content in the solvent increases), suggesting greater

colloidal stability. This phenomenon suggests that, in liquids of higher aromatic contents, the particles would repel each other due to steric barriers created by bituminous molecules there were irreversibly adsorbed onto the particle surfaces during particle pre-treatment. These high molecular weight components of bitumen would extend their structures in aromatic environments, forming “swollen brushes” around the particle which induces repulsive forces when two particles come into the range. These steric repulsion forces are responsible for the low or undetectable settling rate as the system is colloidally stable (Fotovati, 2011).

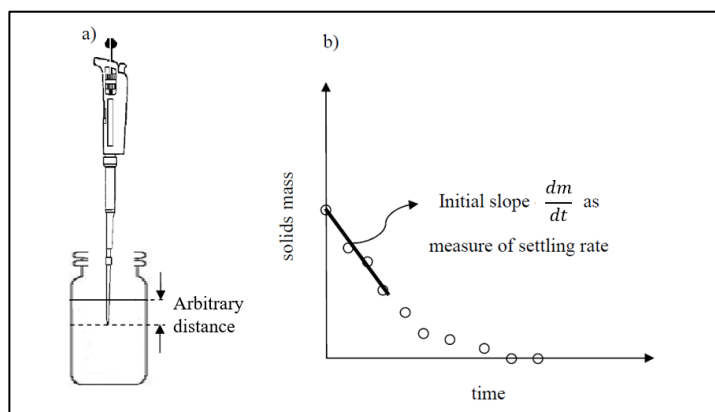


Figure 2.12. Schematic of the novel ashing technique and the typical plot (Fotovati, 2011).

Figure 2.13b show similar results from another investigation (Jin et al., 2011) that conducted the experiments on sedimentation rate in different degrees of aromaticity and coupled with the adhesive forces in respective toluene volume fractions in the solvent to correlate between these two important parameters in colloidal stability.

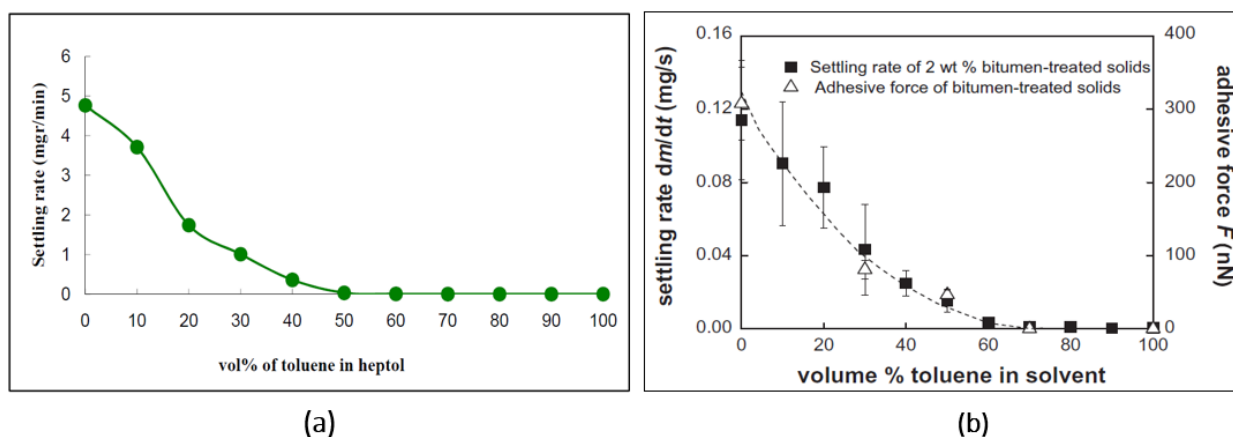


Figure 2.13. Graph with settling rate on the y-axis and degree of aromaticity on the x-axis by novel ashing technique (Fotovati, 2011; Jin et al., 2011).

## 2.6 Inter-particle Forces in Colloidal Systems

Interaction forces between colloidal particles in suspension are generally related to their stability as to aggregation. If the attractive forces are dominant, the system would be destabilized, triggering aggregation, and followed by sedimentation. Attractive forces are almost similar in all types of suspensions (i.e. mainly the van der Waals forces). While the repulsive forces could be due to electrostatic (in aqueous solvent) or steric (in either aqueous or non-aqueous solvent).

### 2.6.1 Interaction Forces Based on DLVO theory

The DLVO theory is named after Derjaguin, Landau, Verwey, and Overbeek, who initiated the theory that explains the forces between charged surfaces in aqueous media and the resulting colloidal stability. Two main forces are attributed to the control of stability in a colloidal system, namely van der Waals and electrostatic. When two colloidal particles approach each other in an aqueous/polar solvent, electrostatic repulsion is felt as the electric double layers around the two particles overlap. In parallel, van der Waals attraction increases as the separation between the particles decreases. According to the DLVO theory, the interaction energy between two colloidal particles depends on:

- Attractive interaction,  $E_{vdw}$  as the consequence of van der Waals forces to destabilize the dispersion through aggregation
- Repulsive interaction,  $E_R$  as they overlap the electric double layers to maintain the dispersion of the particles in suspension

These two interaction energies are of fundamentally different origins and do not interfere with one another; the total energy can therefore be obtained from a simple summation:

$$E_T = E_{vdw} + E_R \quad (2.3)$$

#### 2.6.1.1 Coulombic Interaction

The interaction between two electrically charged particles is attractive if they are oppositely charged, and repulsive if otherwise. The Coulombic force  $F$  is a function of the magnitude of the two charges  $Q_1$  and  $Q_2$  (in coulombs) and the separation  $D$  (m) between them:

$$F \propto \frac{Q_1 Q_2}{D^2} \quad (2.4)$$

### 2.6.1.2 Electric Double Layer (EDL) Repulsion

Double layer forces generally occur between charged particles in a polar medium (i.e. typically water, electrolyte, or liquid with high dielectric constant). The charged particles would attract counterions from the solvent via Coulombic interaction, forming an ion cloud or electric double layer around the particle (Liang et al., 2007). The charging of a particle's surface in an aqueous medium may originate from various mechanisms, including the ionization/dissociation of surface groups and binding/adsorption of ions from solution (Israelachvili, 2011).

An electric double layer (EDL) surrounds the charged particle in an aqueous solution, comprising the Stern and diffuse layers. The first layer (i.e. the Stern layer) corresponds to immobile ions at the charged surface. The second layer, called the diffuse layer, consists of free accumulated counterions and depleted co-ions which form a loose structure that surrounds the particle but are not firmly adsorbed onto the surface. When two charged surfaces are sufficiently close, the concentration of counterions within the gap would be higher than that in the bulk solution, generating an osmotic pressure in the gap that pushes the two surfaces apart. This is the origin of the electric double layer repulsion, as illustrated in Figure 2.14. The concentration of counterions decreases exponentially with increasing distance from the charged surface; the characteristic length of this exponential decay is called the Debye length that is denoted as  $1/\kappa$  in all references.

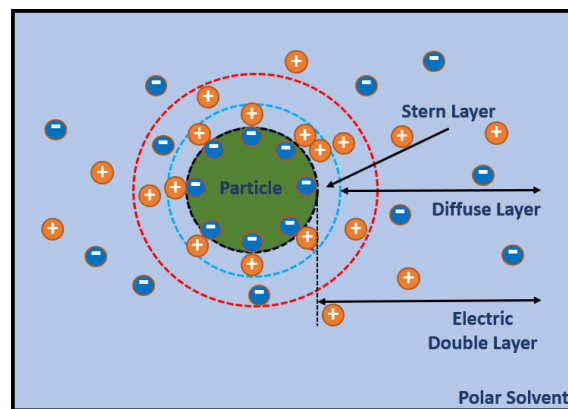


Figure 2.14. Stern diffuse and electric double layer of particle. Redrawn from Lai et al. (2018)

### 2.6.1.3 Van der Waals Attraction

The van der Waals force, a collective long-range attractive interaction between polar molecules, has three basic origins: Keesom orientation forces (permanent dipole-permanent dipole

interactions), Debye induction forces (permanent dipole-induced dipole), and London dispersion forces (induced dipole-induced dipole interactions). Although the total van der Waals force is the sum of these three contributions, the dispersion forces are the most important since the other two may or may not be present, depending on whether there are permanent dipoles (Israelachvili, 2011).

In a colloidal system, the attraction between two particles is dependent on their sizes, shapes, separation distance, and the composition of the particles and the medium. For instance, the van der Waals interaction between two spheres of radii  $R_1$  and  $R_2$  that are separated by a distance  $D$  (the shortest distance between the surfaces) is given by

$$E_{\text{vdW}} = -\frac{A}{6D} \frac{R_1 R_2}{(R_1 + R_2)} \quad (2.5)$$

where  $A$  is the Hamaker constant, a central parameter to understanding particle interactions, including aggregation, dispersion, flotation, and self-assembly of nanoparticles. Its magnitude depends on the properties of the two particles and the medium. The Hamaker constant for the interaction of two particles submerged in a solvent (i.e. particle 1 and 2 in medium 3) is

$$A_{132} = (\sqrt{A_{11} - A_{33}})(\sqrt{A_{22} - A_{33}}) \quad (2.6)$$

In contrast with EDL repulsion, van der Waals attraction is almost insensitive to charge-related properties (e.g. electrolyte strength, pH as correlated to point of zero charges, etc.). It is important to note that van der Waals interactions between macroscopic objects, regardless of their shapes, are always dependent on the separation distance through some form of the power law. The EDL interaction, on the other hand, is one that decays exponentially with distance. The summation of these two types of functional dependencies leads to very interesting predictions on colloidal stability; this is the essence of the DLVO theory. In addition to van der Waals and EDL interactions, other non-DLVO forces have also been proposed.

### 2.6.2 Interaction Forces based on Non-DLVO Interactions

Interactions of colloidal particles based on the DLVO theory (discussed in the last section) are continuum theories that depend on the bulk properties of the solvent and the opposing media (e.g. dielectric constant, refractive index, and density). EDL repulsion only occurs in an aqueous or polar solvent where ions could be solubilized and migrate toward oppositely charged surfaces.



However, particles in non-aqueous environments (e.g. hydrocarbon such as toluene and *n*-heptane in this study) would not be surrounded by electric double layers as ions are not soluble in these liquids (due to their low dielectric constants). As a result, charged particles in non-aqueous solvents can be subjected to very long-range Coulombic interactions (Eqn 2.4). In addition, the DLVO theory does not account for interactions between two surfaces that are within a few angstroms in separation (Liang et al., 2007). These interactions that involve the physical nature of the molecules (e.g discrete size, shape, and surface chemistry) would be further discussed in non-DLVO interactions.

### **2.6.2.1 Steric Repulsion**

The stability of colloidal systems can also be governed by another common type of non-DLVO interaction that involves “macromolecules” with polymer-like structure (Napper & Netschey, 1971). Adsorbed long-chain molecules on particle surfaces can either collapse on the substrate or extend out into the solution, depending on the “quality” of solvent. A good solvent can expand the adsorbed long-chain molecules to maximize contact with the solvent. In a poor solvent, interactions between the chain and the solvent molecules are thermodynamically unfavourable, causing the chain to contract and adopt a tight configuration to minimize contact with the solvent molecules. When two particles, each with adsorbed macromolecules, approach one another in a solvent, the interaction could be repulsive (steric repulsion) or attractive (cross bridging; further discussed in the next section), depending on the adsorption mechanism of macromolecules onto the surfaces, surface coverage of the adsorbed molecules, and interactions with the solvent (Ortega-Vinuesa et al., 1996).

Bitumen comprises, among its many components, complex molecules of high molecular weight, polar heteroatoms, and long-chain molecules. When bitumen comes into contact with a solid surface, some bituminous materials would adsorb irreversibly onto the surface and behave similarly as a polymer with steric behaviour in solution (Wang et al., 2010). Figure 2.15 shows the conformations of adsorbed bituminous materials on particles and flat surfaces. (a) In a good solvent (e.g. toluene), the adsorbed molecules would extend into the solvent and create “brush-like” structures, leading to hydrophobic behaviour (due to the nature of the chains). (b) The adsorbed bituminous materials in a good solvent would behave similarly as on a flat surface, giving rise to steric repulsion when two particles approach one another. (c) The long-chain molecules on

the flat surface would configure themselves in a “compacted structure” when in contact with a poor solvent (e.g. heptane or water); the behaviour of the surface depends on the packing density and the chain length. (d) The chains adsorbed on the particle would collapse onto the surface when submerged in a poor solvent, with the overall property of the surface being partially hydrophilic (inherent property of silica) and partially hydrophobic (due to the adsorbed molecules). Also, in the absence of steric repulsion, other colloidal forces, such as van der Waals attraction, may come into effect.

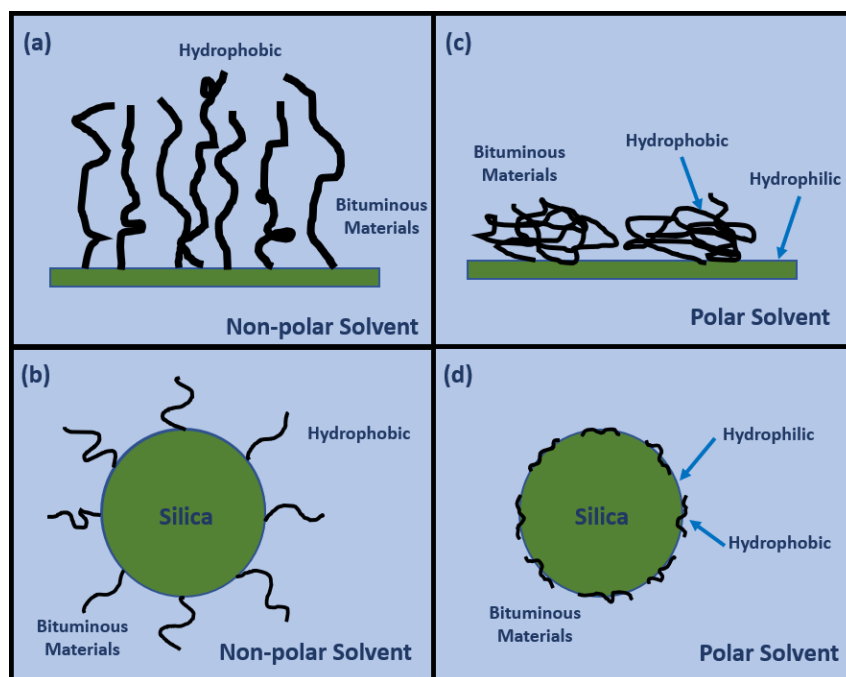


Figure 2.15. The interactions of the polymer-like material adsorbed on the particle and surface with both good and poor solvents.

### 2.6.2.2 Cross-bridging

Polymer-like macromolecules in colloidal suspension promote stability due to steric repulsion. However, under certain conditions, the same molecules can adsorb simultaneously onto more than one particle, causing destabilization and aggregation. This phenomenon is widely known as cross-bridging (Figure 2.16), which could lead to the formation and growth of large flocs (Swenson et al., 1998). Nonetheless, this process is inefficient since a high concentration of polymers is required to build up bridges between the particles. Moreover, the attachment of a polymer on multiple points is not stable, especially in an agitated environment. While agitation may benefit

the bridging mechanism by promoting particle encounters, it can also lead to floc breakage due to hydrodynamic shear (Hogg, 2012). Macromolecules are often used to cause aggregation and subsequent separation of certain colloidal species through cross-bridging; the molecules used for such purposes are called flocculants.

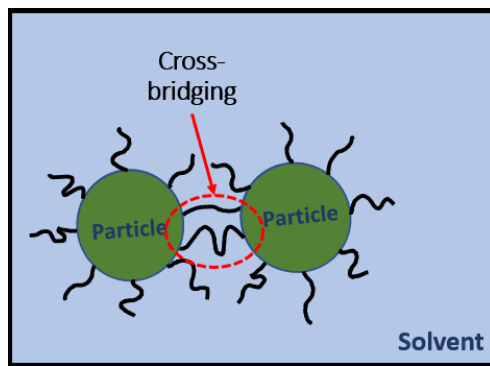


Figure 2.16. Cross-bridging of two particles with long-chain macromolecules adsorbed onto the surfaces. Redrawn from: (Lai et al., 2018).

### 2.6.2.3 Solvation Interactions

When the separation between two surfaces is comparable to the typical size of a solvent molecule (on the order of Ås), the molecular details of the solvent, as well as the interfacial structure, have to be taken into account (Bresme & Oettel, 2007). The manner in which solvent molecules order themselves at the solid-liquid interface is usually different from that in the bulk. When two surfaces approach one another very closely, layers of solvent molecules must be moved to close the gap, thus creating peculiar types of short-range interactions. The approaching surfaces would experience geometric constraining effects with attractive interactions between the surface and the solvent molecules (Liang et al., 2007). Hydration forces are formed in the same mechanism with the water as the solvent. Both forces are correlated to the physical and chemical properties of the surface (discussed before).

## 2.6.3 Inter-particle Forces Measurement Methods

### 2.6.3.1 Surface Forces Apparatus (SFA)

The surface forces apparatus (SFA) was first introduced by Tabor & Winterton (1969) to directly measure van der Waals forces between two surfaces. In recent years, the application of SFA has

been widely extended to measure physical forces between surfaces, such as electrostatic, steric, adhesion, capillary, or even forces due to the structure of surfaces and liquid (e.g. hydration or solvation forces).

Two thin and molecularly smooth mica specimens are formed in a half-cylindrical shape and mounted at the right angle (crossed) as shown in Figure 2.17. The cylindrical surface at the bottom was held fixed and linked to a piezoelectric transducer that could regulate the separation distance between the two surfaces, while the upper specimen was attached to the end of an elastic spring with a well-defined spring constant. As one surface is moved toward the other by the transducer, the separation of the two surfaces could be measured by an optical technique. The interaction force can be calculated based on the known deflection and the spring constant by Tabor & Winterton (1969).

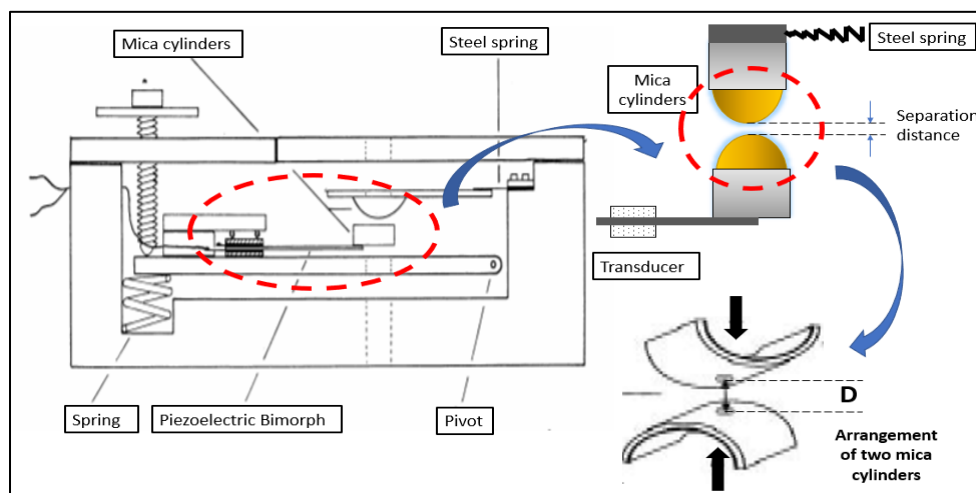


Figure 2.17. The SFA with the main components and arrangement of the two mica cylinders (Tabor & Winterton, 1969).

State-of-the-art SFAs can now be used to measure both lateral and normal forces between two surfaces immersed in a solvent with a spatial resolution of less than 1 Å. The improved version also offers in-situ non-equilibrium (i.e. dynamic) measurements (Israelachvili et al., 2010).

Figure 2.18 shows typical plots of SFA results, where on the y-axis were interparticle forces normalized by the cylinder radius, while the x-axis depicts the separation distance. The SFA was also utilized to measure the forces between asphaltene-coated surfaces in heptane and toluene (Natarajan et al., 2011). The adhesion forces between two asphaltene surfaces were correlated to

van der Waals interactions, which were accountable for asphaltene aggregation in paraffinic solvents (i.e. heptane), while the repulsion observed in the toluene case (with the increment in incubation time) was due to the steric nature of the swollen asphaltenes.

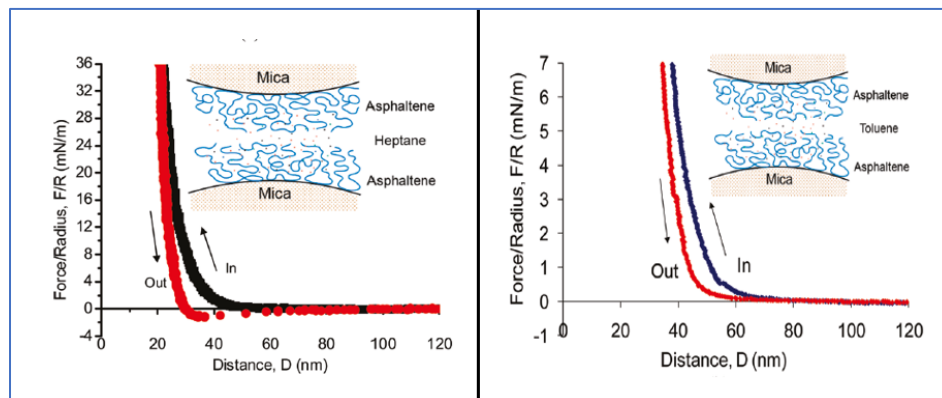


Figure 2.18. Results by SFA for asphaltenes interactions in both heptane and toluene.

Sourced from: (Natarajan et al., 2011)

### 2.6.3.2 Atomic Force Microscope (AFM)

The atomic force microscope (AFM) is another direct force measurement tool, using the “scanning probe microscopy” technique to generate images of a surface with the aid of a physical probe. The force between the probe and the surface can be quantified by the following steps. An individual particle is mounted on the tip of an AFM cantilever, positioned above the specimen surface that is connected to the piezoelectric translation stage (i.e. component that scans the surface for imaging). The entire operation can be arranged in a well-sealed liquid cell with a solvent injected into the cell slowly and the system is held for 15 mins to equilibrate before force measurement begins. When the tip approaches the surface in the vertical direction, the force between the tip and the sample surface causes the cantilever spring to deflect downward or upward, depending on the nature of the force (i.e. either attractive or repulsive). The deflection is detected by aiming a laser beam onto the upper surface of the cantilever spring above the tip and reflected onto a position-sensitive detector (PSD). The signal from the PSD is translated into deflection of the cantilever. Together with the information about displacement from piezoelectric translation, the force between these two surfaces could be calculated as a function of separation distance by applying Hooke’s law (Fotovati, 2011; Wang et al., 2009).

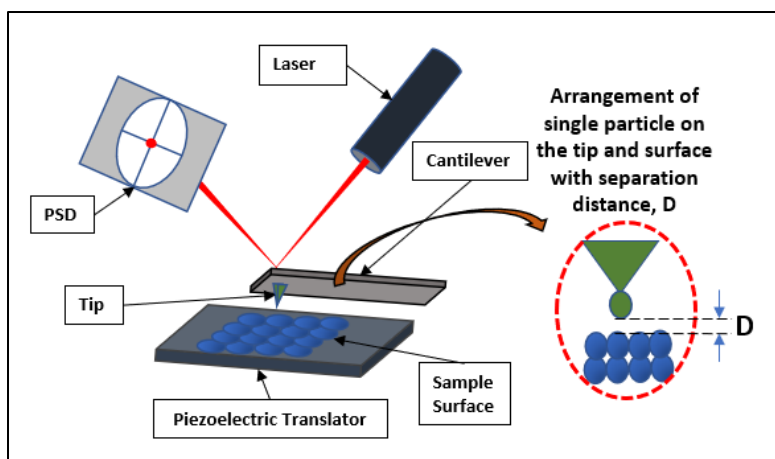


Figure 2.19. The main components in AFM with their configuration. Redrawn from: (Fotovati, 2011) with some adjustments.

The results by AFM could be surface imaging or plot with normalized forces (scaled by effective radius) versus separation distance as seen in Figure 2.20. Asphaltenes were successfully coated on the surface of silica by the dip-coating method, as seen in Figure 2.20. Contact angle measurements suggested that the asphaltenes were adsorbed irreversibly as a monolayer on the hydrophilic silica. The plot in Figure 2.20 (right) showed the repulsive forces in toluene. The observed repulsive forces principally originated from steric interactions when parts of asphaltene molecules extended out into the good solvent to form a swollen brush structure that would repel each other when they are compressed (Wang et al., 2009). The adsorption of asphaltenes onto the hydrophilic silica most likely involved polar groups being anchored onto the silica surface, leaving the other parts (e.g. alkyls that behave hydrophobically) to be exposed to the solvent.

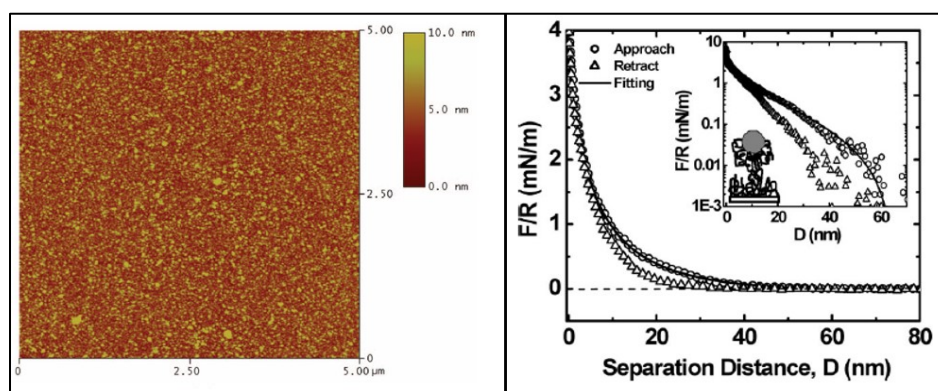


Figure 2.20. AFM imaging and plot for dip-coating asphaltene film surface-interactions in toluene (Wang et al., 2009).

### 2.6.3.3 Microcantilever Technique

Both the SFA and AFM are capable of force measurements in a solvent environment, as demonstrated by previous researchers. However, contamination from toluene as a solvent in the liquid cell is common, which might cause severe damage to the high-priced apparatus. Another consideration in the case of AFM is the delay time of several minutes for the solvent to be injected into the cell. This might be a problem if the experiments had to be conducted immediately after the introduction of solvent in order to obtain real-time measurement and avoid erroneous data due to aging or reaction between the surfaces and solvent.

The micro-cantilever technique was used due to its simplicity and compatibility with experimental requirements. The objective of this present study is to understand the primary features regarding interparticle interactions in solvent environments, without dwelling on secondary details related to force-distance relationships. This novel technique was first introduced by Moran et al. (1999) to measure the interfacial tensions of individual emulsion droplets. And later it was broadly used in oil sands researches to determine simple interparticle forces (Yeung et al., 2000).

The microcantilever measures the adhesive force between two glass spheres (note: the surfaces of the spheres can be modified for different experiments). As in the case of AFM, the stiffness of the microcantilever can be known accurately. If the sphere at the tip of this cantilever is subjected to an adhesive force, its magnitude can be determined from the deflection of the cantilever. Unlike the AFM and SFA, however, the microcantilever is incapable of detecting the magnitude of repulsive forces; it can only report that such a repulsive force exists (which is all the information needed to predict colloidal stability). The whole procedure was conducted under the microscope that is connected to a CCD camera and computer. The force measuring configuration and sequences was explained step-by-step in Figures 3.9 and 3.11.

The adhesive force between two bitumen-treated ‘particles’ in heptol-diluted maltene at approximately 2 wt% is shown in Figure 2.21. This result indicated that the adhesive force between the particles was exactly correlated with the ratio of aromaticity in the solvent, which increased with the rise of heptane content and was absent in higher content of toluene (greater than 60%). Van der Waals forces are believed to be responsible for the adhesion as the asphaltene was absent in the system.

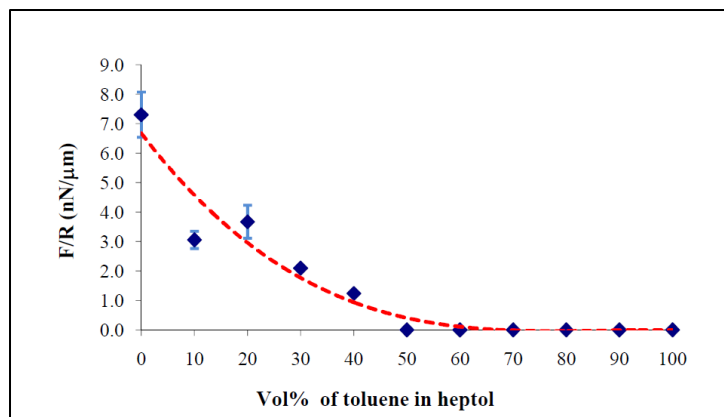


Figure 2.21. Standard plot for force measurement with microcantilever technique with respect to the volume of the toluene in heptol. Source: (Fotovati, 2011).



### 3. Research Methodology

The present study on the aggregation and sedimentation of the modified silica particles was conducted in two parts: starting with macroscopic analysis, then followed by an investigation on the microscopic scale. The macroscopic analysis involved monitoring the settling rates of micron-sized silica particles in different liquid media. On the microscopic scale, a micropipette-cantilever method was used to measure interparticle adhesive forces between two ‘spherical’ surfaces in different solvent environments.

#### 3.1 Preparation to Obtain Bituminous Materials

Bituminous materials were obtained from fractions of bitumen sample (Syncrude Canada Ltd) based on precipitation and adsorption on water-oil interfaces as shown in Figure 3.1.

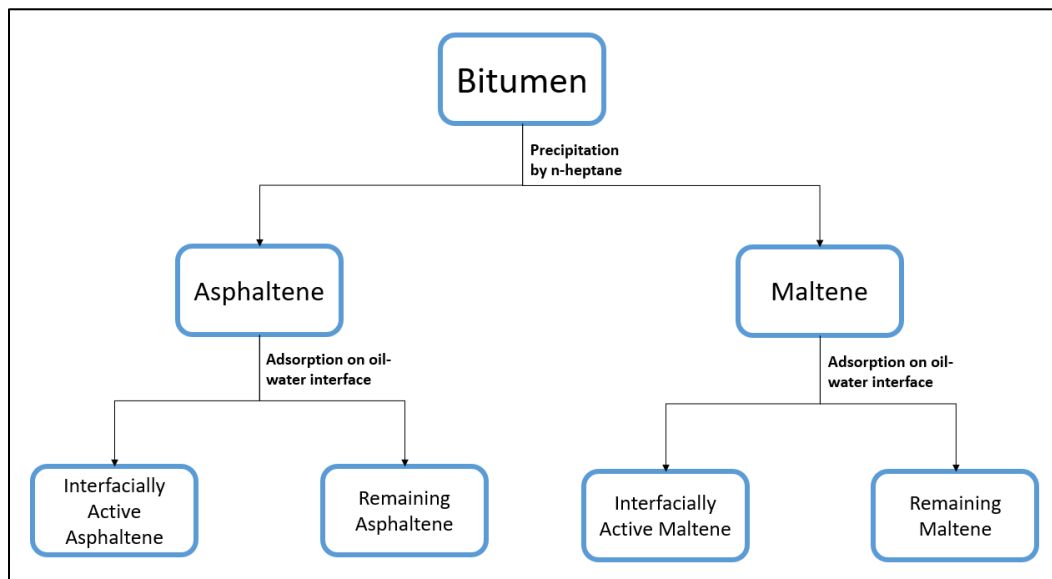


Figure 3.1. Fractions of bitumen based on precipitation and adsorption. Adopted from (Qiao, Harbottle, Tchoukov, Masliyah, et al., 2017) with extension in maltene subfractions.

Asphaltene and Maltene, the two fractions of bitumen were separated by the ASTM recommended procedure (ASTM D2007-80) with the modification of using the *n*-heptane instead of *n*-pentane. Note that these two fractions were based only on solubility and not molecular structures (i.e the amount of each depends on the ratio and type of precipitant). Maltene was the part that was soluble in *n*-heptane, while, asphaltene was the precipitated portion. These two fractions were next further

separated based on interfacial activity (i.e. tendency to adsorb onto the oil-water interface) by a sequence of procedures as shown in Figure 3.2

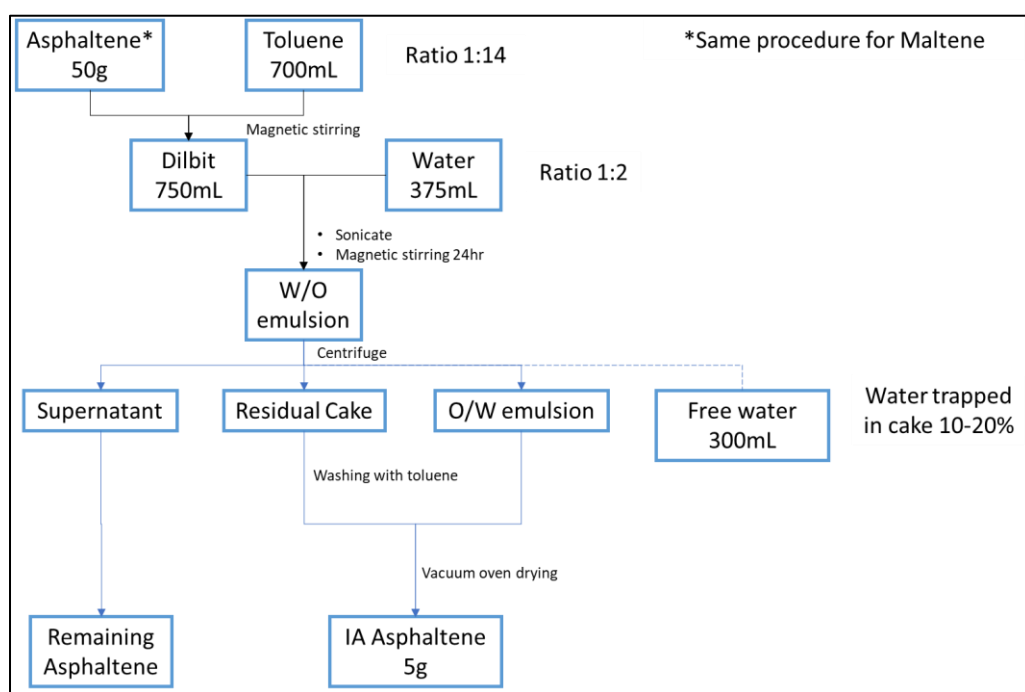


Figure 3.2. Schematic of procedures to obtain subfractions based on adsorption onto the oil-water interface, was referred from (Qiao et al., 2017; F. Yang et al., 2015).

The asphaltenes were dissolved in toluene at a feed-to-solvent volume ratio of 1:14 with the aid of a magnetic stirrer (Fisher Scientific, 11-610-49SH). This is followed by the addition of distilled water at the volume ratio of 2:1. The solution was homogenized in a water bath sonicator for 5 minutes and stirred with a magnetic stirrer for 24 hours to form a water-in-oil emulsion. The emulsion was then centrifuged at 4000 g for 20 minutes, creating the following layers in the centrifuge tube (listed from top to bottom): a supernatant (dark oil phase), an oil-in-water emulsions, free water, and a compacted cake of solids. The supernatant was next exposed to the air under the fume hood to remove the toluene; the asphaltenes that remain after drying was named Remaining Asphaltenes (RA). The oil-in-water emulsions and emulsified cakes were washed with an excess amount of toluene until clear toluene was observed, which indicates the asphaltenes that remained were those adsorbed on the oil-water interfaces. The water phase was evaporated in a vacuum oven (VWR symphony, No. 414004-578) at 90°C, leaving the isolated asphaltenes which were called Interfacially Active Asphaltenes (IAA). This interfacially active subfraction was

estimated at less than 10 wt% of the asphaltene fraction. The same procedure was applied to maltene to obtain its subfractions: Interfacially Active Maltene (IAM) and Remaining Maltene (RM).

### **3.2 Macroscopic Experiments: Jar tests**

#### **3.2.1 Materials**

The main materials for the jar tests were solid particles as the dispersed phase and liquid solvents as the continuous phase. The tests were done in a 30 mm height scintillation vial with TFE septa caps (Chemglass Life Sciences, CG490801).

##### **3.2.1.1 Solid Particles**

The silica particles used in this study were 0.25- $\mu\text{m}$  silica particles (Fiber Optic Center Inc.); they were used in the following forms: untreated, surface-modified by bituminous materials and fractions (i.e. asphaltene, maltene, and their subfractions), and methylated to become hydrophobic (with trimethylchlorosilane). The resulting three major types of solids are called “pure”, “bituminous-treated” and “chemically-treated”.

- Pure Silica

Pure silica in the bulk package from Fiber Optic Center Inc. was directly used in the experiments without further purification.

- Bituminous-treated Silica

Silica particles would undergo special surface treatment to mimic the fine solids in oil sand ore, which have had extensive contact with bitumen. The surfaces of pure silica particles were coated with an irreversibly adsorbed layer of bituminous materials (refer to Section 3.1 for the procedures to obtain the bituminous materials) by a series of pre-treatment procedures as follows:

A diluted bitumen solution was prepared by adding bitumen with toluene at a 1:9 bitumen-to-toluene mass ratio, which resulted in a total volume of 750 mL dilbit solution. The bitumen sample was provided by Syncrude Canada Ltd., while the toluene was from Fisher Scientific at HPLC grade. The pure silica beads, with an amount of 25g (the solid to liquid ratio is about 1:30 g/mL), were dispersed in the diluted bitumen solution gradually to avoid uneven wetting (i.e. lumps with

uncoated silicas in the center). This was done by adding dilbit solution, in small successive amounts, to the silica beads to make a paste; the well-stirred paste was then topped up with the remaining dilbit solution. Next, the dispersion was stirred overnight (i.e. 24 hours) with a magnetic stirrer (Fisher Scientific, 11-610-49SH) to ensure sufficient time for the bituminous material to adsorb onto the particle surfaces.

The silica beads were washed with fresh toluene and centrifuged at 2000 g for 15 mins (Beckman, JA-10) until a distinctive layer was formed between solid materials and solid free supernatant. The “dirty” supernatant was removed, replaced with fresh toluene, and the new suspension was agitated in a sonicator. This washing process was repeated 4-5 times until the supernatant was clear. The supernatant was then removed for the last time, and the solids were laid on a petri dish and dried under the fume hood to remove all excess liquid. The collected solids, being in the irregular form of lumps, were ground manually by using a mortar and pestle. The final form of bituminous-treated silica beads appeared as greenish powders and were assumed to closely replicate the behaviour of fine particles in oil sand ores.

- Chemically-treated Silica

The chemically-treated silica underwent the same treatment processes as the bituminous type (i.e. same ratio and procedure), with trimethylchlorosilane (TMCS) as the coating material to allow methylation on the bead surfaces. The chemical-treated beads were still in white powder form but with hydrophobic properties. The physical appearances of the two treated silica were different, as evident in Figure 3.3.

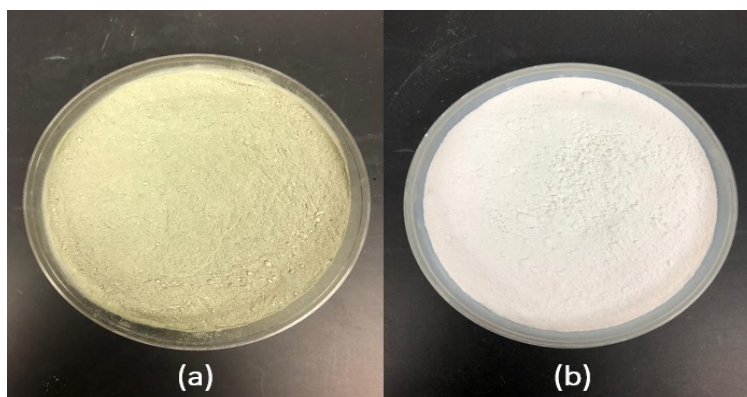


Figure 3.3 (a) Bituminous-treated silica appeared as greenish powder, and (b) chemically-treated with white colour.

### 3.2.1.2 Solvents

Both non-aqueous and aqueous solvents were used as the continuous phase to investigate the aggregation of silica particles in clean systems. The non-aqueous systems comprised toluene and *n*-heptane (both HPLC grade, Fischer Scientific) in order to mimic the hydrocarbon solvents in froth treatment (i.e a mix of aliphatic and aromatics components). Distilled water was used as the aqueous solvent (resembling, to some degree, oilsands tailings). In the preliminary experiments, pure *n*-heptane, toluene, and water were separately used as the continuous phase. As the next step, *n*-heptane and toluene were mixed to form non-aqueous liquids (called as 'heptol') in different volume fractions. The parameter  $\alpha$  was defined as the volume fraction of toluene (i.e.  $\alpha = 0$  is pure heptane, and  $\alpha = 1$  is pure toluene).

### 3.2.2 Sample Preparation for Jar Tests

The initial experiments to study the settling behavior of various silica particles were conducted in pure solvents — either aqueous or non-aqueous. As the experiments went further with more complex hydrocarbons, the solvent was prepared by mixing different volume ratios of *n*-heptane and toluene (or 'heptol'). The heptol composition was specified by its toluene volume fraction  $\alpha$ , which can range from  $\alpha = 0$  (pure heptane) to  $\alpha = 1$  (pure toluene). The dispersed particles (pure, bituminous-treated, or chemically-treated silica beads) were added to the solvent in a scintillation vial; the dispersion was then agitated in a sonicator for 5 minutes to ensure the perfect mixing. The steps were illustrated in Figure 3.4.

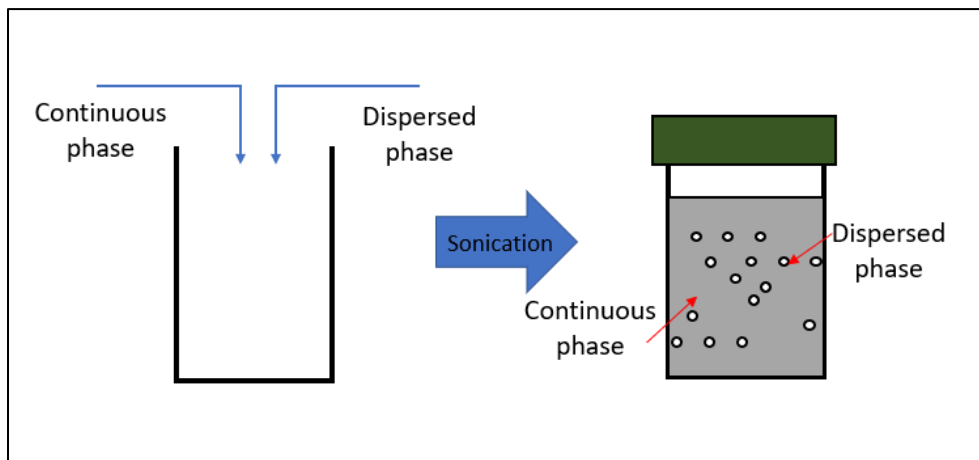


Figure 3.4. Jar test preparation procedures

### 3.2.3 Measurement of Settling Rate

The settling rate of particles can be considered an indicator of how fast the solids would interact, form flocs, and settle to the bottom of the vial. The main objective here was to study the behaviour of various types of solids in different solvents to understand more about the interactions between the solid particles and/or between the particles and the solvent.

A conventional method was used by monitoring the mudline (i.e. the distinctive transitional interface between the sludge and top clear liquid) to obtain the settling rate. This optical observation method worked perfectly in these systems as the transition line was sharp and liquids were transparent.

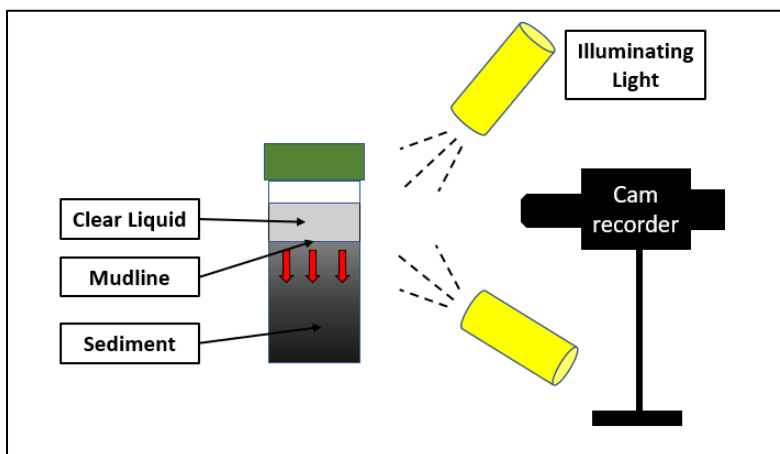


Figure 3.5. Measurement of settling rate by the optical method.

The visual observation for the batch settling test (as seen in Figure 3.5) was performed by using a closed scintillation vial to contain the dispersion (i.e. the subject for the gravity settling). The fine particles and solvent were initially mixed and sonicated to ensure the particles were dispersed perfectly in the liquid and to break up any aggregated lumps. At the instant that sonication ceased, the vials were quickly transferred to a well-illuminated observation area to be monitored. The height of the mudline was mostly measured visually (with a ruler); the experiments were also recorded with a camera so that the process can be replayed and analyzed (especially for cases with high settling rates). The data would be simply plotted as the mudline height versus time in a settling chart.

It is instructive to first classify settling behaviours into two rough but widely distinct categories: rapid and slow. This is based on the time for the mudline to traverse the entire height of the liquid column (30 mm). Rapid settling was defined as settling times that were from seconds to 1 min, while slow settling would take hours to days. Of course, this rough, binary classification would not be applicable for intermediate settling times (e.g. those that last for tens of minutes). In cases of slow settling, it was also useful to compare the mudline settling rate (typically in mm/hour) to the Stokes settling velocity of individual particles.

### **3.3 Microscopic Analysis: Direct Force Measurement**

#### **3.3.1 Materials**

This set of experiments utilized the micropipette technique to study the adhesion between two micron-sized glass ‘spheres.’ These ‘spheres’ were actually the tips of a micropipette (described in Section 3.3.2) and a microcantilever (Section 3.3.3). Like the silica beads in jar tests, these tips could be treated with bituminous materials before experimentation in different solvent environments. The measurement of interparticle forces was monitored with an inverted microscope that was connected to a CCD camera and a computer.

#### **3.3.2 Preparation of Straight Micropipette**

Glass capillary tubes with outer and inner diameters of 1 mm and 0.7 mm (Kimble Glass Inc) were the basic material for making the micropipettes. The long glass tubes were cut into shorter lengths with a glasscutter before their ends were tapered. To taper the ends, a needle/pipette puller (David Kopf Instruments, model 720) was used to stretch the short capillary tubes along their axis by passing them in between a hot platinum ribbon as shown in Figure 3.6. The pulling force would separate the tube into two parts with a tapered end on each side. Subsequently, the sharp tapered end was melted into a spherical shape by bringing it close to a hot platinum wire that was mounted on a device called the ‘microforge’ (Figure 3.7). The rounded tip would function as an individual glass particle.

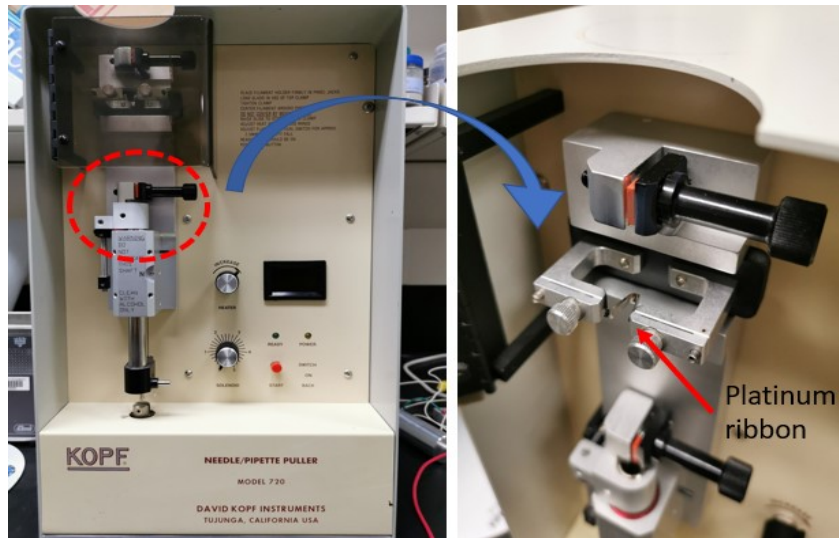


Figure 3.6. David Koff Instruments (Pipette puller). The magnified part shows the platinum ribbon where the pipette would be pulled into two parts with tapered ends.

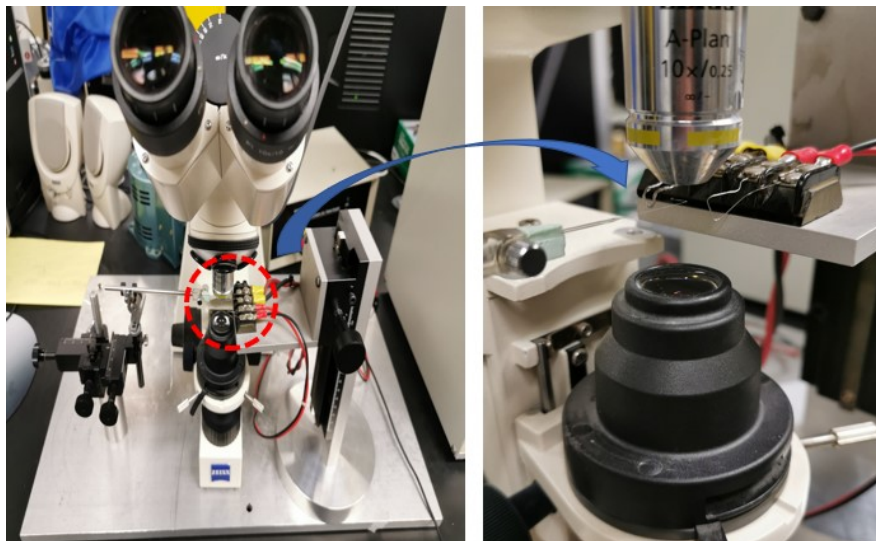


Figure 3.7. Forging and melting equipment associated with a 10x objective lens microscope to observe and control the process. The enlarged picture displays the thick platinum wire (for melting the tips) and a thread-like wire (for shaping the microcantilever).

### 3.3.3 Preparation of Microcantilever

The microcantilever was made from the straight micropipette, but with some modification on the shape to adopt a periscope-like configuration with two bends as shown in Figure 3.8. This resulted in a flexible cantilever that was sensitive to any external force that caused measurable deflection.



The first bend was made close ( $\pm 0.1$  mm) to the tip and the second was about 5 to 6 mm from the first bend. The second bend was the crucial part of determining the stiffness of the microcantilever (Moran et al., 1999). Each cantilever had a slightly different stiffness based on its shape and size; the stiffness is of course also a function of Young's modulus of the glass material. Calibration for each microcantilever (to obtain the stiffness) was made prior to force measurements.

The entire shape of the cantilever must be on a common plane. Those two bends were made using a homemade microforge device (Figure 3.7) that heated the glass material to a point where it was softened but not liquefied. Micromanipulators were then used to make the bends.

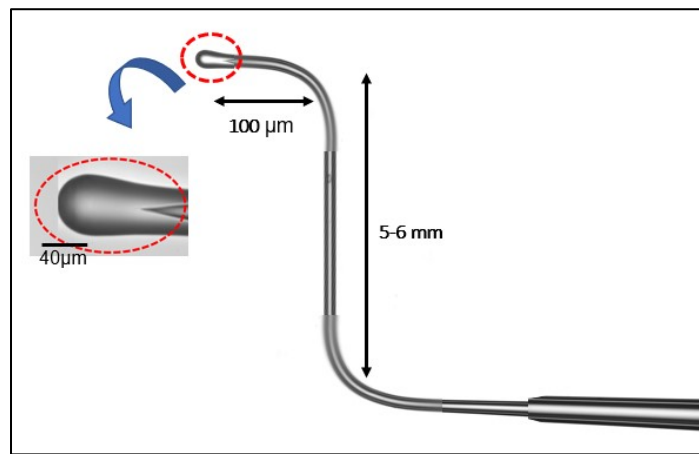


Figure 3.8. The Geometry of Microcantilever

### 3.3.4 Force Measurement by Microcantilever Technique

Adhesive forces between micron-sized particles could be detected with various methods. Here, the microcantilever technique was chosen due to its simplicity and ease of operation. This technique was initially introduced to determine the interfacial tension of individual emulsion droplets (Moran et al., 1999). The technique had also been used in oil sands research to measure interparticle forces (Fotovati, 2011; Jin et al., 2011).

The tips of both the micropipette and the microcantilever were spherically shaped (i.e. rounded in micron size with diameters roughly 30-40 μm) to mimic silica particles in settling tests. Furthermore, the surfaces of the tips were either coated with bituminous materials or left as clean glass (see Section 3.2.1.1). To coat the pipette tips, they were immersed in bituminous solutions diluted with toluene (in volume ratio 1:9) for 24 hours to enable enough time for the material to

adsorb onto the glass surfaces. Afterward, the tips were rinsed with an excess amount of toluene to remove any loose materials on the surfaces, leaving only a thin layer of bituminous material that was irreversibly adsorbed on the glass surfaces. In this study, the tips of the bitumen-coated micropipette and microcantilever (diameters of 30-40  $\mu\text{m}$ ) were assumed to have the same surface properties as the silica particles (diameters of 0.25  $\mu\text{m}$ ) used in the jar tests.

The setup of the microcantilever technique is illustrated in Figure 3.9. Force measurement experiments were conducted entirely in a small chamber (filled with the desired solvent) and observed with a microscope that was connected to a CCD camera and computer. The actual instrument is shown in Figure 3.10. The chamber was formed by two pieces of thin glass coverslips separated by a 1-mm gap; it was open on both sides to allow insertion of the micropipettes and filling of the solvent. The pipettes were mounted on micromanipulators capable of controlling motions with micron-scale accuracy. The cell was designed in a way to prevent evaporation of organic solvents so as to ensure an undisturbed environment for delicate force measurements. With only a 1-mm gap between the glass slides, the solvent could be retained in the chamber simply by capillary forces.

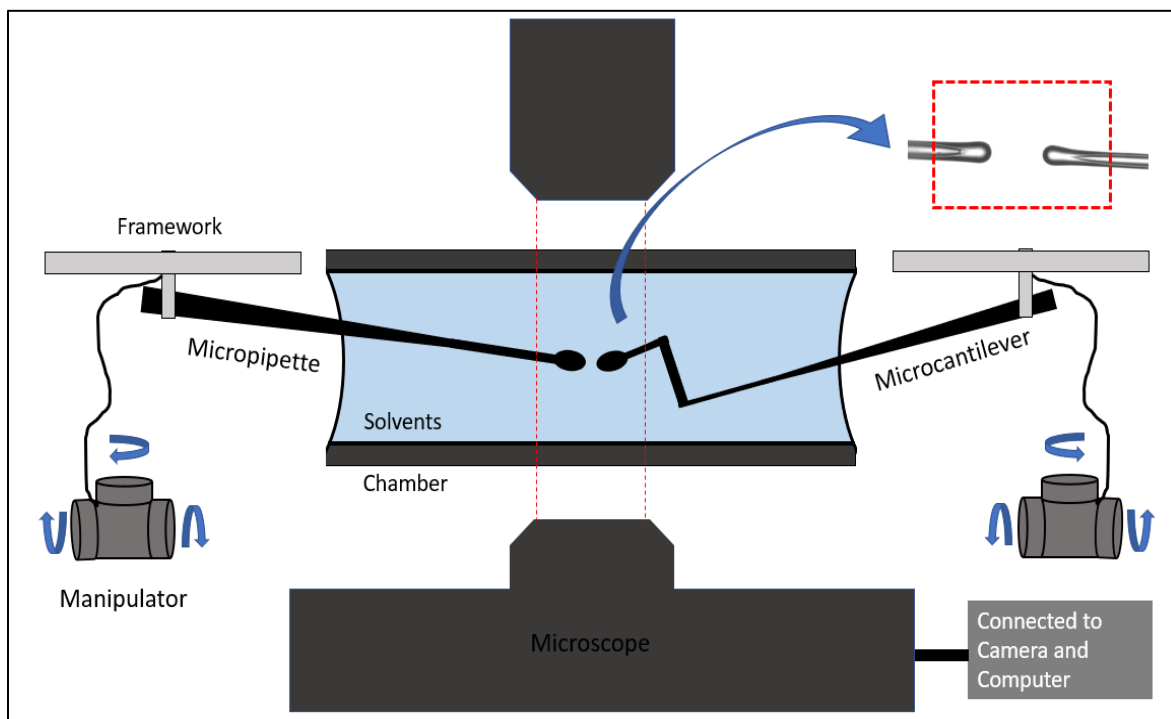


Figure 3.9. Configuration of the microcantilever technique to measure the inter-particle forces.

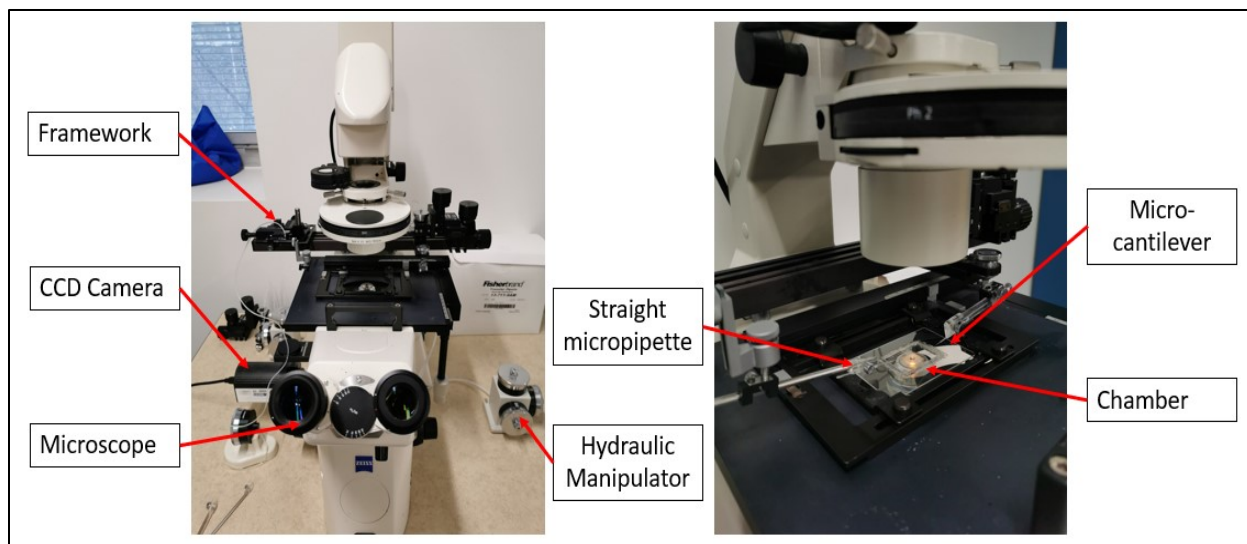


Figure 3.10. The force measurement instrument in real practice.

After pretreatment of the pipette tips, the straight micropipette was mounted on the left side of the chamber on a framework connected to a hydraulic manipulator (Narishige, MHW-3) that could control motions smoothly in 3D. The microcantilever was then positioned carefully in the middle of the 1-mm gap from the right side of the chamber (contrary to what was drawn in Figure 3.9, which was done for clarity, the actual orientation of the cantilever is horizontal). The microcantilever could also be precisely positioned with a manipulator. The entire front part of the microcantilever — including the tips, and first and second bends (the 5- or 6-mm arm) — must be completely immersed in the solvent medium to avoid intervention by irrelevant capillary forces.

With both the micropipette and the microcantilever in place, the solvent (*n*-heptane, toluene, or heptol with various volume fractions) was introduced into the chamber. The force-measuring sequences were explained in Figure 3.11. The microcantilever on the right (with only its tip shown in the image) was kept stationary for the entire experiment. The tip of the straight micropipette (on the left) was moved towards the microcantilever by the hydraulic manipulator. Both tips were gently brought into contact, then the straight pipette on the left was pulled back slowly. If an adhesive force existed between the two surfaces (and is adequately strong), the microcantilever would be deflected as the straight pipette was pulled back. The total deflection was determined as the microcantilever sprung back to its original point. The microcantilever behaved as a linear spring, so the maximum deflection  $\delta$  was expected to be directly proportional to the adhesive force  $F$ . Note that such a technique is incapable of quantifying repulsive forces, no matter how strong,

because it is not possible to determine nm-scale separations between the surfaces with this setup. If the cantilever shows no deflection, one may conclude that either the magnitude of the adhesive force is below the detection limit, or that there is repulsion between the surfaces.

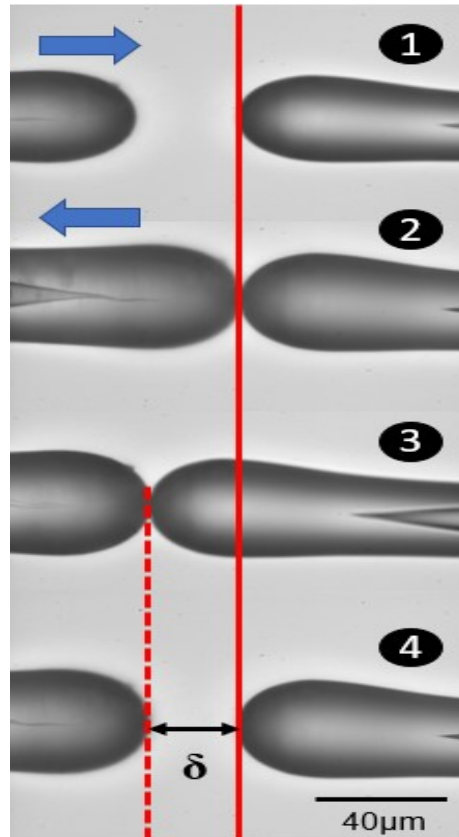


Figure 3.11 (1) The straight micropipette moved toward the stationary microcantilever on the right, (2) after the surfaces come into contact, the micropipette on the left was gently withdrawn back, (3) the microcantilever was deflected due to the adhesive force, (4) the microcantilever jumped back to the original position and the maximum deflection could be measured.

The entire experiment was monitored by a microscope with a 40× objective lens (Carl Zeiss Canada, Axiovert 200). The images were projected to a monitor and recorded by a CCD camera in video mode. Video imaging was recorded digitally for further analysis so that the deflections could be determined accurately.

The maximum deflection  $\delta$  could be converted to the adhesive forces,  $F$ , using the known cantilever stiffness  $K_b$  according to Hooke's law:

$$F = K_b \delta \quad (3.1)$$

The value of  $K_b$  (nN/ $\mu\text{m}$ ) was calculated using the linear beam theory, based on Young's modulus of borosilicate glass (approximately  $7 \times 10^{10}$  Pa) and the detailed geometry of the periscope-shaped cantilever. Its accuracy had been verified in previous studies Moran et al. (1999).

### 3.4 Scope of Experiments and Sample Size

The focus of this investigation was on the colloidal stability of the various solids (i.e. bitumen contaminated fines) in a clean system (pure solvent). It involved two main approaches: macroscopic (jar settling tests) and microscopic (direct forces measurement). The macroscopic work was performed in two stages, which we will call preliminary and heptol jar tests. The objective of the preliminary tests was to compare the settling behaviours of bitumen treated fines with the controls (pure silica that was hydrophilic and chemically-treated silica that behaved hydrophobically) in the oil phases (pure toluene and heptane) and the aqueous phase (water); the results can be summarized in a  $3 \times 3$  matrix.

For the next step, settling jar tests were conducted in heptol (i.e. mixture of *n*-heptane and toluene) as a model solvent that mimics real solvent in industrial practice (e.g naphtha or paraffinic diluent). The heptol solvent was prepared with increments of 10 vol% in toluene content, resulting in 11 different solvents in total. Regarding bitumen-modified solids, there were 7 types — corresponding to the 7 bitumen fractions shown in Figure 3.1.

The microscopic investigation spanned the same parameter space as that for the heptol jar tests: 7 types of solids in 11 solvents. The jar tests involved billions of particles, while force measurements involved only *two*. For clarity, the experimental parameters of this MSc study are summarized in Table 3.1.

Table 3.1 Sample Size for the Experiments

Type of Experiments	Type of Fines	Type of Solvents	No of Samples
Preliminary Jar Tests	Pure silica	Pure <i>n</i> -heptane	3×3 matrix (Total of 9 samples)
	Bitumen treated	Pure toluene	
	Chemical treated	Water	
Heptol Jar Tests and Direct Force Measurement	Bitumen treated	Heptol (mixture of <i>n</i> -heptane and toluene) Total of 11 different solvents in toluene content.	7 types of solids in 11 various solvents for 2 types of the experiment (total of 154 samples)
	Asphaltene treated		
	Maltene treated		
	Interfacially Active Asphaltene (IAA) treated		
	Remaining Asphaltene (RA) treated		
	Interfacially Active Maltene (IAM) treated		
	Remaining Maltene (RM) treated		

## 4. Results and Discussion

### 4.1 Preliminary Experiments: Colloidal Stability

Sedimentation of fine solids dispersed in either an aqueous or non-aqueous solvent could be a good indicator of colloidal stability. In this study, the solids used were the three type of 0.25- $\mu\text{m}$  silica, namely pure silica (with which were hydrophilic), bitumen treated silica (i.e coated by bituminous materials that form an adsorbed layer on the silica surface), and the chemically-treated silica (i.e. methylated with trichloromethyl silane or TMCS, rendering the surface hydrophobic). Each type of solids would be dispersed in different liquid media, namely, aqueous (i.e. water) and non-aqueous solvents (i.e. *n*-heptane or toluene) to analyze the settling behaviours.

Bitumen-modified silica can have distinctly different surface properties than pure silica due to the adsorbed outer layer (in particular, the chain length and surface groups of the adsorbed material). These types of solids may represent the troublesome fines in the oil sand ore, disrupting the extraction process and froth treatment. Comparing the settling behaviour of bitumen-treated silica to the controls, which were pure silica (hydrophilic) and chemically treated silica (hydrophobic), could provide insight into colloidal stability and the underlying mechanisms. Overall, we had three types of solids (i.e. pure silica, bitumen-treated, and chemically treated) dispersed in three types of pure solvents (i.e. *n*-heptane, toluene, and water), resulting in a 3 $\times$ 3 matrix of results.

The pre-treatment of silica and preparation of solvents were described in Section 3.2.1. The solids were added to a scintillation vial filled with pure solvent, then it was agitated in a sonicator for 5 minutes before the measuring process. The settling rate was measured visually by monitoring the height of the mudline using a ruler; the measurement continued until the mudline has reached the bottom of the vial (i.e. at a 30-mm depth). The settling behaviour was roughly classified into binary results: *rapid settling*, with the settling process lasting from seconds to minutes, and *slow settling*, which took up to hours or days. Rapid settling corresponded to colloiddally unstable systems, while slow settling meant that the system is stable. The batch settling curve (i.e. the plot of decreasing mudline height vs time) would only be recorded for stable systems and compared to the Stokes settling rate (i.e. the velocity of a single particle falling through an infinite fluid). Based on the literature review, the solid-to-liquid ratio in a dispersion system can be an important variable; thus, the volume fraction of the solids was fixed at a constant value of 0.003 for all experiments. Since all settling tests were done in pure solvents, the S:B (solvent-to-bitumen) ratio was not relevant.

### 4.1.1 Stable Systems

In this context, “stability” is meant in a colloidal sense. A colloidally stable dispersion implies that the particles do not aggregate and settle at a significant rate (Mondragon et al., 2012). In this case, with the given size of the primary particles, a stable system can take hours or even days to settle (i.e. in the slow setting regime). This phenomenon was a result of the net repulsive force between the particles, which prevented aggregation. As van der Waals attractive forces are always present between the particles (Liang et al., 2007), there must exist stronger repulsive forces that resulted in a net repulsion. This repulsive force would be further discussed in detail based on the different systems.

The settling rates of stable dispersions were compared to the Stokes settling velocity using Equation 4.1:

$$V_{\text{Stokes}} = \frac{2}{9} \frac{\Delta\rho g d^2}{\mu} \quad (4.1)$$

where the definitions of the parameters and their values are summarized in Table 4.1.

Table 4.1 Parameter for Stokes Velocity Calculation

Particle diameter	$d = 2.5 \times 10^{-7} m$
Density of water	$\rho_f = 997 kg/m^3$
Density of silica particle	$\rho_p = 2650 kg/m^3$
Viscosity of water	$\mu = 8.891 \times 10^{-4} Pa.s$
Gravity acceleration constant	$g = 9.81 m/s^2$
Density of toluene	$\rho_f = 862.1 kg/m^3$
Viscosity of toluene	$\mu = 5.2 \times 10^{-2} Pa.s$

$$V_{\text{Stokes,water}} = 6.33 \times 10^{-8} \frac{m}{s} = 0.2280 \frac{mm}{h}$$

$$V_{\text{Stokes,toluene}} = 1.17 \times 10^{-7} \frac{m}{s} = 0.3915 \frac{mm}{h}$$

Two additional concerns might interfere with the sedimentation of particles in pure solvents, namely Brownian motion and hindered settling. These effects must be considered (and ruled out)



before the experiments. Firstly, larger size particles (i.e. 2  $\mu\text{m}$  bitumen treated silica) were used in the sedimentation test in toluene and water; these particles were not expected to be in the range of influence of Brownian motions (1 to 100 nm). Since the settling velocity is quadratically related to particle diameter, the ratio between the settling rate of 2  $\mu\text{m}$  and 0.25  $\mu\text{m}$  is, according to Stokes law, 64 times. The experiments displayed a comparable result, suggesting that Brownian motions did not play a significant role in the settling process.

Hindered settling calculation based on Equation 4.2 was used to study its effect on the sedimentation system in this experiment. The value of  $K$ , the hydrodynamic volume factor (depends on the shape, material, and size of the particle), and  $n$ , the Richardson- Zaki index, were obtained from (Fouda & Capes, 1977) for similar systems. Here, it is estimated that  $K = 1.8$  (spherical glass beads) and  $n = 4.7$  (in the Stokes regime). We have also  $\alpha_p$ , the volume fraction of particles, having the value 0.003 (an experimental parameter). Using these parameters, one gets

$$V/V_{\text{Stokes}} = (1 - K\alpha_p)^n \approx 0.97 \quad (4.2)$$

This result shows that hindered settling is not expected to have a significant effect if the initial concentration of particles in the suspension was sufficiently low. Therefore, the settling rate of the particles in the present colloidal systems, in the absence of aggregation, is expected to be about the same as what is predicted based on Stoke's law.

#### 4.1.1.1 Pure Silica in Water

Pure silica ( $\text{SiO}_2$ ), with the natural structure of hydroxyl groups ( $-\text{OH}$ ) on the surfaces which form silanols ( $\text{Si}-\text{OH}$ ), causes a rapid reaction between the hydrophilic surface with atmospheric moisture (J. Yang et al., 2005). In an aqueous solution, the particles' surfaces would be readily charged due to the dissociation of the surface hydroxyl groups ( $-\text{OH}$ ). The ion distribution around and on the interface can lead to electric double layer (EDL) repulsion between these particles. This serves as a sufficiently strong repulsive force to prevent the aggregation between particles. Therefore, such particles are colloidally stable and would settle slowly; in fact, the EDL repulsion causes the particles to repel each other and settle at a rate that is slower than the settling rate of a single particle in the water, based on Stokes law. The settling curve for this system was shown in Figure 4.1, in which the straight line is the Stokes settling rate and the dots are the experimental values.

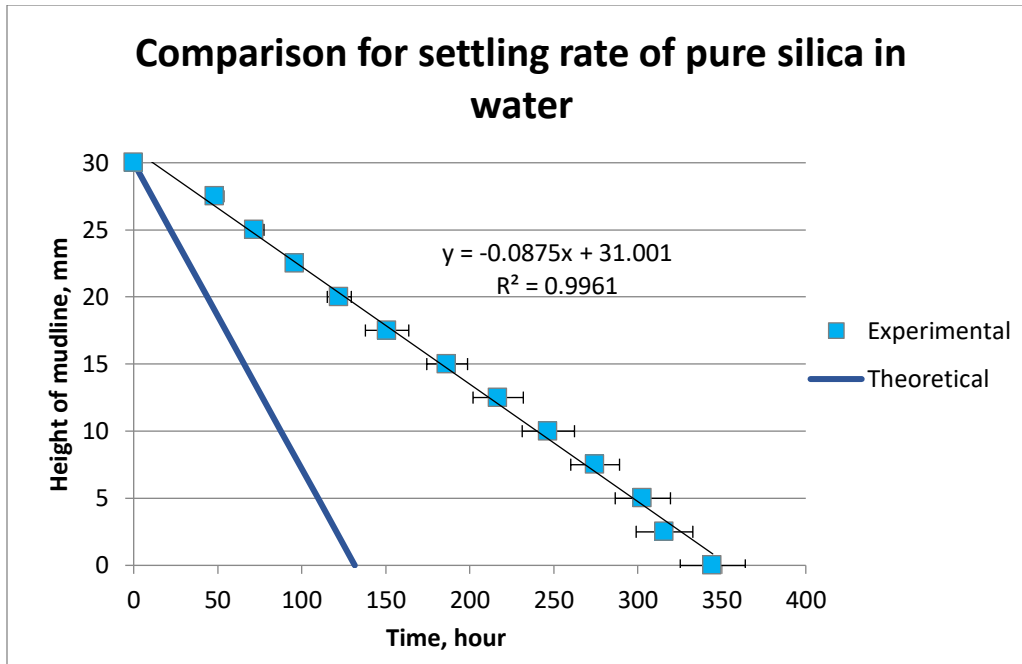


Figure 4.1. The settling rate of pure silica in water.

The settling of pure silica in water appears linear, which means the slope could be considered as the average settling velocity of the interface. Based on the experimental data, the settling rate for this system was

$$V = 0.0875 \frac{\text{mm}}{\text{h}}$$

The ratio between this settling rate to the Stokes velocity of silica in water is

$$\frac{V}{V_{\text{Stokes}}} = \frac{0.0875}{0.2280} = 0.38$$

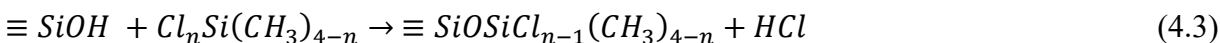
In terms of elapsed time, the entire sedimentation took up to 14.4 days to transverse 30 mm, compared to Stokes settling, which should require only 5.5 days.

As expected, silica in water was the most stable colloidal system in this experiment because EDL repulsion would dominate van der Waals attraction (Gelardi & Flatt, 2016). Another factor is due to the nature of the silica, which is hydrophilic (i.e. thermodynamically more favoured to interaction with water). Water would adsorb preferentially on the surface hydroxyls with simply several hydrogen bonds. This physical adsorption was interchangeably responsible for the chemical interaction with the surface groups (Hair, 1975).

#### 4.1.1.2 Hydrophobic Silica in Toluene

Hydrophobic silica was produced by methylating regular silica with trimethylchlorosilane (TMCS), which rendered the particles hydrophobic. Based on the thermodynamic concept, the interaction between a hydrophobic dispersed phase in a non-aqueous continuous phase was entropy-driven with low energy that favors dispersion (stability).

Modification of silica with different types of methyl-chlorosilanes would provide similar functional groups on the surface (Jal et al., 2004), but the reaction with trichloromethylsilane is unlikely due to the steric hindrance of the three surface hydroxyl groups. The adsorption for this chemical with the silanols on the surface of silica is given on Equation 4.3 (Gun'ko et al., 1993), with  $n=2$  for dimethyldichlorosilane (DMDS) and  $n=3$  for trichloromethylsilane (TMCS)



In the reactions shown in Figure 4.2, the Si-Cl on TMCS or DMDS was hydrolyzed by the water (i.e. replenished by the wet air) and chlorine ions would form hydrochloric acid with  $H^+$  from the silica surface. Therefore, methyl-chloro silane adsorbed on the silica in hydrogen bonds with the surface hydroxyl groups on the silica surface. The adsorption could occur in toluene under ambient conditions without catalyst (Chu & Seeger, 2015). The methyl chains on the surface of silica provided the hydrophobic behaviour.

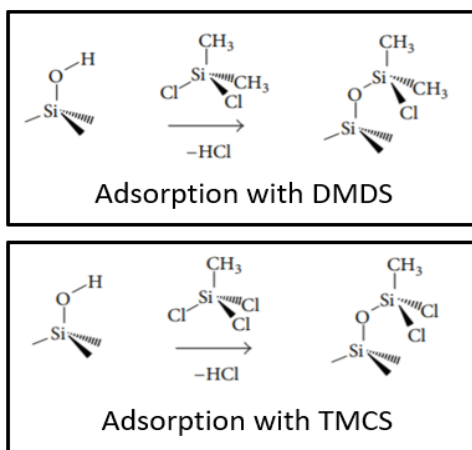


Figure 4.2. Adsorption of methyl-chloro silanes on the surface of silica (Grinerval et al., 2013).

In this study, TMCS was chosen over DMDS to avoid further polymerization of DMDS on the silica surface to form a long hydrocarbon chain when the chlorines were hydrolyzed. The long

hydrophobic chains might lead to a steric effect between particles to form a stable dispersion in the respective solvents, while the main purpose of this pre-treatment is to obtain the behaviour that is purely due to the interaction between hydrophobic particles in toluene (i.e. oil environment). The settling curve for this interaction was shown in Figure 4.3 with the comparison in theoretical value.

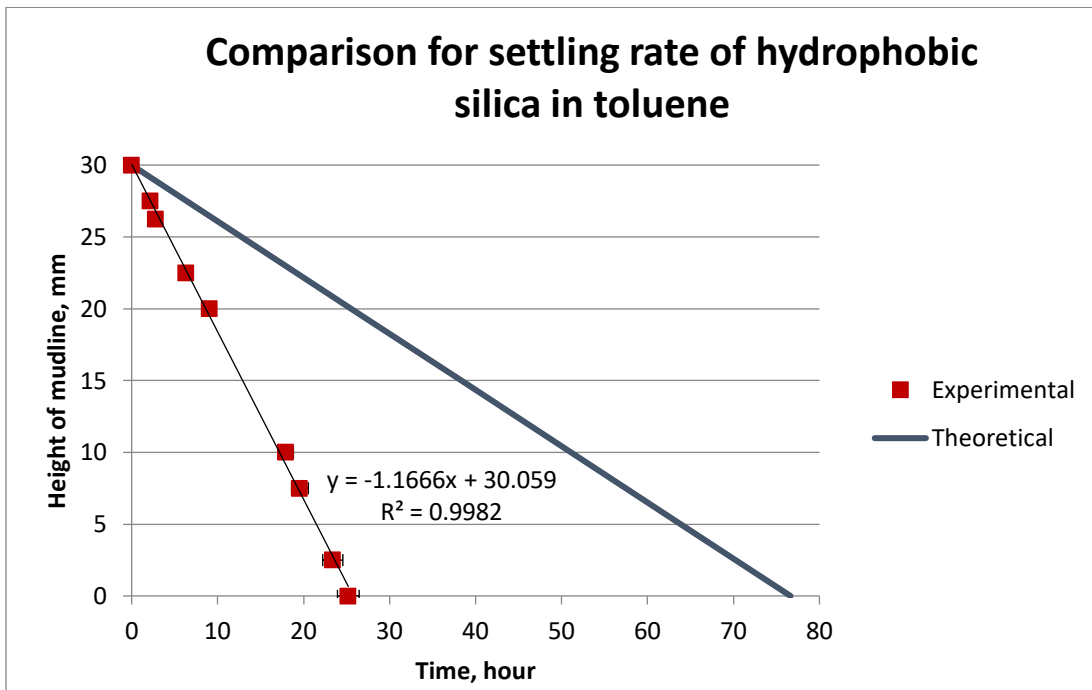


Figure 4.3. The settling rate of hydrophobic silica in toluene.

The slope for the settling rate of hydrophobic silica in toluene is linear, which means the gradient of the slope could be considered the average settling velocity of the interface. The settling rate for this system, based on experimental data, was

$$V = 1.1666 \frac{\text{mm}}{\text{h}}$$

The ratio between the settling rate to the Stokes velocity of hydrophobic silica in toluene is

$$\frac{V}{V_{\text{Stokes}}} = \frac{1.1666}{0.3915} = 2.98$$

In terms of elapsed time, the entire sedimentation took up to 1.1 days to transverse 30 mm, compared to free settling in the Stokes regime, which would have required 3.2 days in toluene.

This was the only case in which the experimental settling rate was faster than the Stokes velocity, indicating that the stability of the system was not as strong and may have involved some small degree of aggregation. The surfaces of hydrophobic silica particles had a smaller amount or absence of silanols, as they had been replaced with methyl chains from TMCS that resulted in weak hydrogen bonding interactions (responsible for aggregation) between particles (Yan et al., 2001). The suspension in toluene was postulated to be stabilized by the interaction of alkyl chains on the particle surfaces with the aromatic solvent (i.e. toluene), which was a CH –  $\pi$  bond (Brunner et al., 2014).

#### 4.1.1.3 Bitumen-treated Silica in Toluene

Bituminous materials (which we will assume for now as asphaltenes, until further experimental results with maltenes are discussed) were adsorbed irreversibly onto the surfaces of bitumen treated silica, providing surface behaviours that mimic those of the fines founds in oil sands processing (e.g. froth treatment and non-aqueous extraction). Asphaltenes are considered as complex macromolecules with long alkyl chains. Their adsorption on the surface, with either dense-packed or loose arrangement, could change the surface behaviour to hydrophobic. In a good non-polar solvent, in this case, toluene, the adsorbed bituminous materials on the particles would extend their chain-like molecules, as this conformation would maximize contact with the solvent.

Such interactions between the adsorbed molecules and hydrocarbon solvents with a high degree of aromaticity (e.g. toluene) were suggested previously by Fotovati (2011) and Jin et al. (2011) on the bitumen treated particles and Wang et al. (2010) on the asphaltene-treated beads and flat surfaces. They proposed that the asphaltenes adsorbed on the surface behaved like polymers in extending their structure into a good solvent, forming a “brush-like” structure around the particle. Now, the particles appeared to be swollen with a hydrophobic effect as shown in Figure 4.4 (left). When two particles approached each other, the adsorbed layer would serve as a steric barrier, resulting in repulsive forces between the particles that prevent aggregation by van der Waals attraction, as in Figure 4.4 (right). Therefore, the particles settle gradually as the net forces were dominated by repulsion, leading to the overall colloidal stability of such a system (i.e. bitumen-treated particles in toluene). The settling curve was plotted in Figure 4.5.

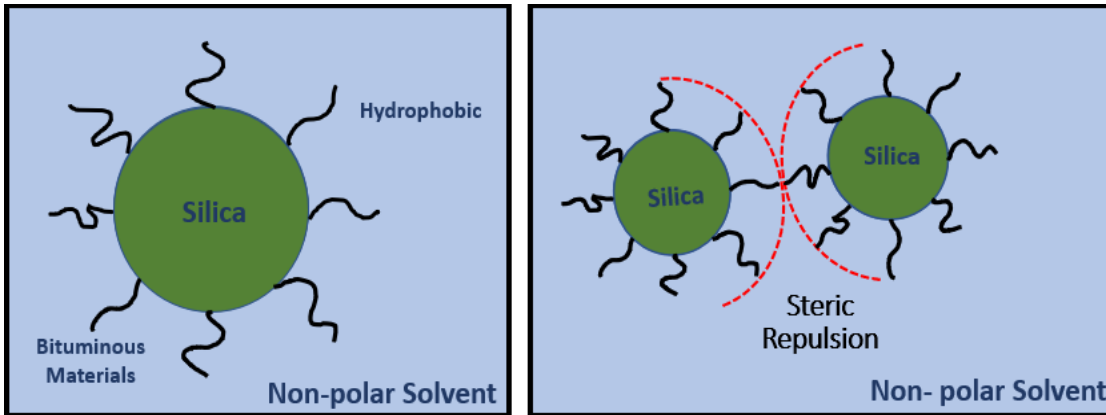


Figure 4.4. The interaction of bitumen treated silica in toluene (as a good solvent).

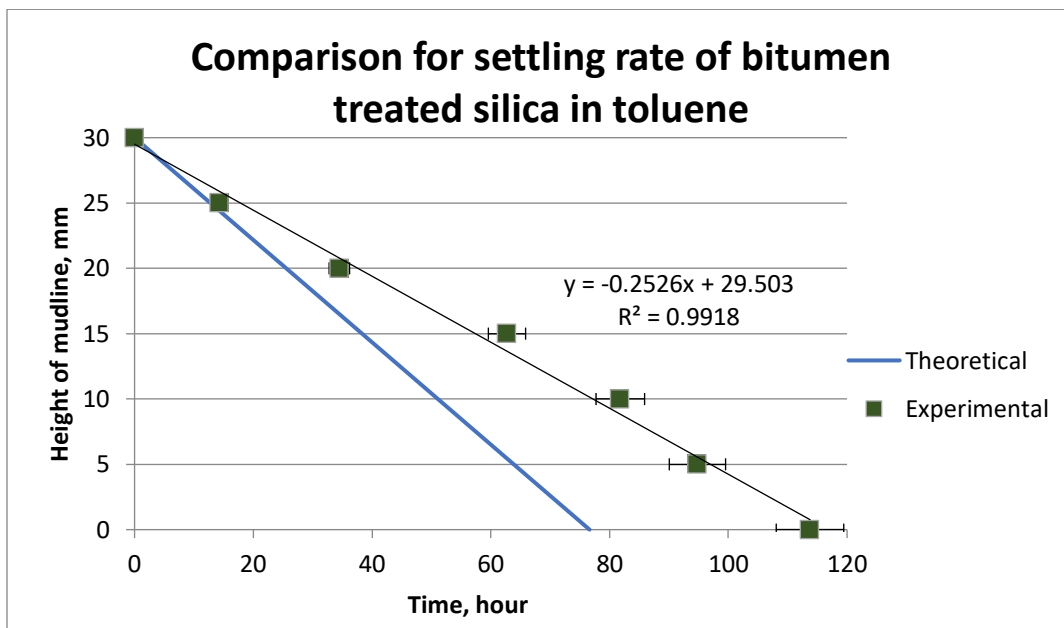


Figure 4.5. The settling rate of bitumen treated silica in toluene.

The slope for the settling rate of bitumen treated in toluene is constant, suggesting that the gradient of the slope could be considered as the average settling velocity. The settling rate for this system, based on experimental data, was

$$V = 0.2526 \frac{\text{mm}}{\text{h}}$$

The ratio of the settling rate to the Stokes velocity of the particles in toluene is

$$\frac{V}{V_{\text{Stokes}}} = \frac{0.2526}{0.3915} = 0.65$$

In terms of elapsed time, the entire sedimentation took up to 4.7 days to transverse 30 mm, compared to 3.2 days if the settling velocity were according to Stokes law. A lower settling rate was exhibited by this system compared to the hydrophobic silica in toluene, perhaps due to the difference in the stabilizing mechanisms. The interaction between alkyls themselves and the solvent was considered as weak interactions compared to steric repulsion between particles. These settling results also suggest that the EDL repulsion (in pure silica in water case) is stronger than the steric repulsion based on the sedimentation rate in the colloidal system (i.e. ratio to the Stokes velocity). However, the interactions might be complex and were affected by other factors.

#### 4.1.1.4 Bitumen-treated Silica in Water

Based on the hydrophobic nature of bituminous materials (due to the alkyl chains on asphaltenes or others), the bitumen-treated silica were predicted to be *unstable* in water, similar to the behaviours of other hydrophobic substances in aqueous media. However, the settling curve in Figure 4.6 suggested that this hypothesis could not be verified as the system was very stable, just slightly behind the silica-in-water system (i.e. the most stable case in this set of experiments). This system was a perfect reflection of the oil sands tailings case, where oil-contaminated fines are remarkably stable in water (i.e taking decades for the fine solids to settle in the ponds).

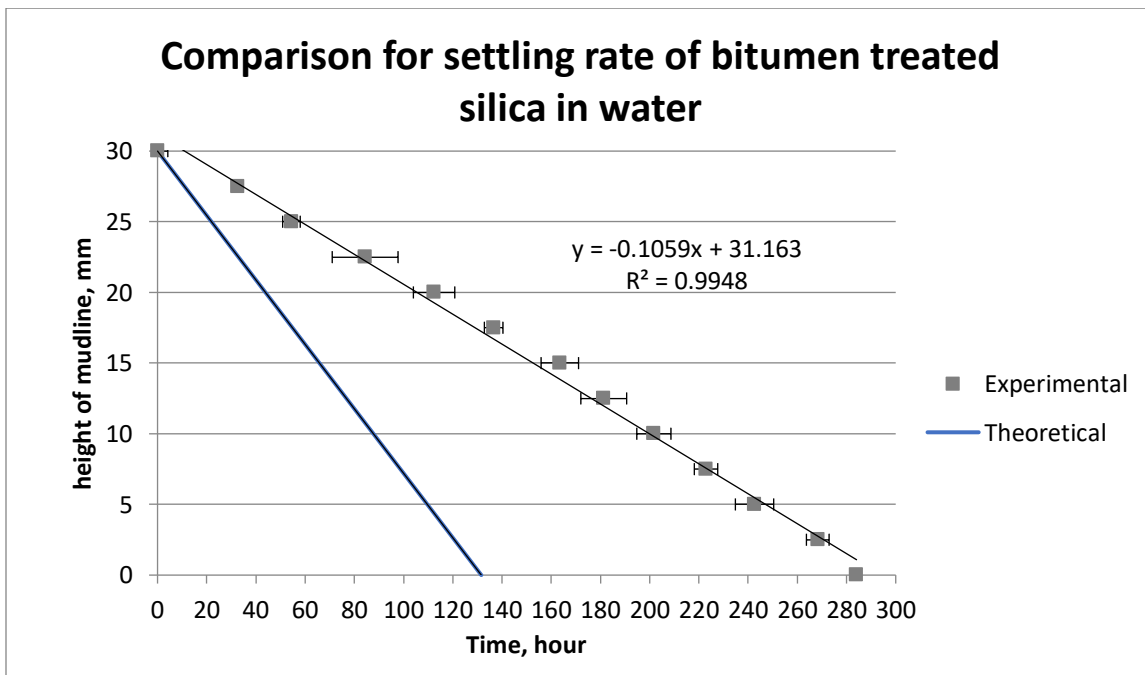


Figure 4.6. The settling rate of bitumen treated silica in water

The slope of the settling curve of bitumen-treated solids in water is constant, suggesting that the gradient of the slope could be considered as the average settling velocity of the interface. The settling rate for this system, based on experimental data, was

$$V = 0.1059 \frac{\text{mm}}{\text{h}}$$

The ratio between the settling rate to the Stokes velocity of the bitumen-treated solids in water is given by

$$\frac{V}{V_{\text{Stokes}}} = \frac{0.1059}{0.2280} = 0.46$$

In terms of elapsed time, the entire sedimentation took 11.8 days to transverse 30 mm, compared to 5.5 days if velocity were given by Stokes law.

The results from the settling curve Figure 4.6 suggest that the distribution of bituminous materials on the silica surface was F as displayed in Figure 4.7, leaving some surface areas that were not fully covered by the chains' network. This phenomenon was reflected especially in a poor solvent (the polar solvent, water) where the chains would collapse on the surface, causing the overall behaviour to be partially hydrophilic and hydrophobic. The hydrophilic portions were the parts of the surface that were left uncovered, with the same surface properties as those of clean silica. For the surface with adsorbed molecules, due to the poor quality of the solvent (water), the chains would effectively collapse, forming adsorbed layers that are perhaps no more than several nanometers in thickness, while the uncovered portions may still be capable of developing electric double layers forces that are longer ranged.

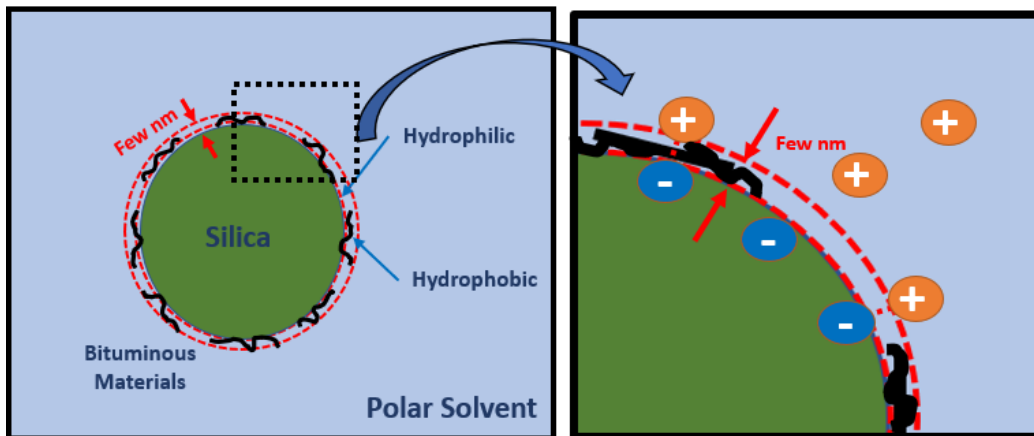


Figure 4.7 Collapsed molecules configuration on bitumen treated silica in water (as poor solvent)



The electric double layer (EDL) was formed by the charged surface and counterion layer, leading to a repulsive force when two particles come close to each other (refer to Figure. 4.8). This explanation is consistent with the results from the settling tests in which the apparent colloidal stability, in terms of the ratio  $V/V_{\text{Stokes}}$ , was more similar to pure silica in water (repulsion due to EDL repulsion) than the bitumen-treated particles in toluene (repulsion due to steric repulsion). The surface portions that were covered by collapsed bituminous materials might be able to supply the steric repulsion only when the coverage was thick enough. The combination of both repulsive forces is sometimes called the electro-steric repulsion (Fritz et al., 2002) by investigators in polymer science. If this is the case here, the EDL repulsion should dominate over the steric repulsion in greater magnitude or range as suggested by the slow settling rate results. However, the first suggestion — that EDL repulsion was responsible for the slow settling and overall stability — is more likely since the adsorbed materials would collapse into a thickness of only a few nanometers in a poor solvent; the chances of forming a steric barrier is very small (in fact, the attractive force was observed in the latter case by dispersing the bitumen-treated silica in heptane which was also poor solvent).

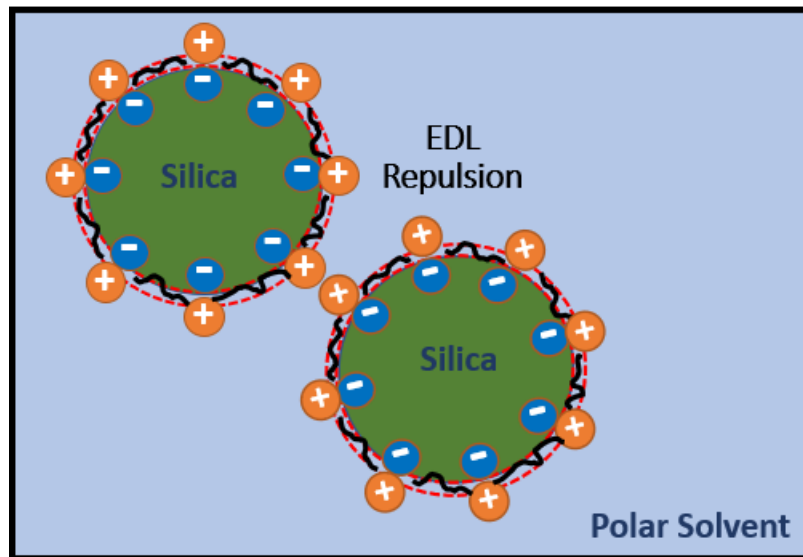


Figure 4.8. The interaction of bitumen treated silica in water.

Another interesting phenomenon was observed for bitumen-treated silica in water: some amount of solids in water tended to migrate to the air-water interface at the top (i.e. flotation) that was transported by the bubbles; the bubbles were formed during the agitation process and were

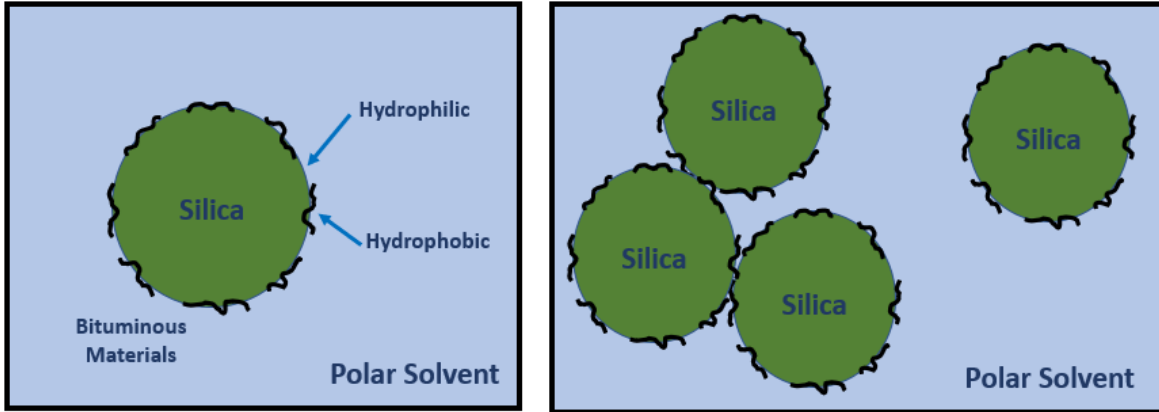
stabilized by the bitumen-treated solids, creating a “Pickering foam” (since neither surfactants nor macromolecules were added to the system, it is concluded that the solid particles were responsible for this stabilization). This phenomenon suggested that the surfaces of bitumen-treated particles were partially hydrophobic. The particles at the air-water interface would re-enter into the solution as the bubbles coalesced and burst in several hours.

#### **4.1.2 Unstable Systems**

These were colloidal dispersions whose particles were subjected to aggregation, followed by sedimentation over relatively short times. In all these cases, the sedimentation rates were in the rapid settling regime, with the total settling time (over a 30-mm distance) occurring in seconds to a minute. It is assumed that van der Waals forces were largely responsible for the observed aggregation. The detailed settling rates of these unstable systems will be further quantified in the next experiments, corresponding to the amount of the aromatics in the solvent.

##### **4.1.2.1 Bitumen-treated Silica in Heptane**

The case of bitumen-treated particles in toluene was discussed in Section 4.1.1.3, in which the system was stable. When the aromatic solvent (i.e. toluene) was substituted with a paraffinic one (i.e. heptane), the adsorbed bituminous material on the surface would collapse into a compacted structure (see Figure 4.9). Heptane is considered a “poor solvent” for bitumen and its fractions. The resulting thickness of the collapsed adsorbed layer was likely insufficient to create a steric barrier. Thus, steric repulsion was either absent or small compared to the effective van der Waals attractive forces as the particles approached one another. The dominating van der Waals interaction contributed to a net attractive force that facilitated the aggregation of particles to form larger aggregates, which led to rapid settling (an indicator of instability in the colloidal system). The van der Waals forces were expected to be weaker than for the case with pure silica as the surfaces were partially covered by bituminous materials of a certain thickness, which in turn could increase the separation between two particles. Also, EDL repulsion was absent in this non-aqueous system since ions are insoluble in such liquids.



4.9. The interaction of bitumen treated silica in heptane (as poor solvent).

#### 4.1.2.2 Pure Silica in Heptane and Toluene

The silanol (Si–OH) groups on the surfaces of silica were responsible for its hydrophilic behaviour. The interactions of a hydrophilic molecule (i.e. silanol) with water or other polar solvents were more thermodynamically favourable than its interaction with hydrocarbon or oil solvents. In non-aqueous solvents (e.g. heptane and toluene in this case), the hydrophilic molecules tend to stay with the same species in hydrogen bonding and aggregate to minimizing the surface contact. Van der Waals forces between particles were responsible for this aggregation (Liang et al., 2007), and the EDL repulsion that was able to neutralize the attraction was also absent in this system (i.e. generally applied for non-aqueous media; the detailed explanation was provided in the previous section: Bitumen treated Silica in Heptane).

The sedimentation rate for pure silica in heptane was higher than that in toluene, corresponding to the increased magnitude of aggregation due to higher attractive forces (i.e. van der Waals). This phenomenon could be approximately explained from the van der Waals calculation in term of energy (Equation 4.4) or force (Equation 4.5) by Derjaguin approximation for two identical particles (further derived from Equation 2.2):

$$E_{vdW} = -\frac{AR}{12D} \quad (4.4)$$

$$F_{vdW} = -\frac{d E_{vdW}}{dD} = -\frac{AR}{12D^2} \quad (4.5)$$

The force could be roughly estimated from the effective Hamaker constant between the asphaltene and hydrocarbon medium using Equation 4.6:

$$A_{\text{eff}} = \left( \sqrt{A_{\text{solid}}} - \sqrt{A_{\text{solvent}}} \right)^2 \quad (4.6)$$

The Hamaker constants of asphaltene, toluene, and heptane in air had been reported earlier; the values are summarized in Table 4.2:

Table 4.2 The List of Hamaker Constant with Respective References

Hamaker constant	References
$A_{\text{silica}} = 6.5 \times 10^{-20} \text{ J}$	(Senden & Drummond, 1995)
$A_{\text{heptane}} = 4.3 \times 10^{-20} \text{ J}$	(Hough & White, 1980)
$A_{\text{toluene}} = 5.4 \times 10^{-20} \text{ J}$	(J. H. Masliyah & Bhattacharjee, 2006)
$A_{\text{eff silica-heptane}} = 0.22 \times 10^{-20} \text{ J}$	Calculation based on Equation 4.6
$A_{\text{eff silica-toluene}} = 0.05 \times 10^{-20} \text{ J}$	Calculation based on Equation 4.6

This calculation provided a good correlation with the sedimentation rate for silica in heptane and toluene, wherein the higher settling rate in heptane was due to greater van der Waals forces, causing more effective aggregation. The details on the settling behaviour of these two systems would be further analyzed in the next section.

#### 4.1.2.3 Hydrophobic Silica in Heptane

Here, the initial expectation was that hydrophobic (i.e. methylated) particles would be stable in heptane, just as they were in toluene (see §4.1.1.2). However, what was observed was a completely reverse outcome, i.e. the hydrophobic particles were unstable in heptane.

Silanols were completely or partially removed during the methylation process and coated by TMCS with alkyl (i.e. methyl) chains, which were hydrophobic by nature. The absence of silanols on the surface of the particles caused a decreased effect of weak hydrogen bonding interaction among particles to aggregate and settle to the bottom. Even though the attractive forces that caused aggregation (i.e. van der Waals) were weaker, it is also noted that EDL and steric repulsion were completely absent. The weak net attractive force was reflected from the settling rate result, which was relatively slower than the other heptane systems, but still in a rapid settling zone. EDL

repulsion was absent in a non-aqueous solvent; at the same time, the short methyl chains from TMCS on the surfaces of the silica were not long enough to provide any steric barrier.

#### **4.1.2.4 Hydrophobic Silica in Water**

The hydrophobic (methylated) silica possessed the hydrophobicity because of reduced carbonyl and hydroxyl groups from the original silica surface (Huang et al., 2018); these were replaced by the methyl group (hydrophobic by nature) from TMCS. This system was observed with the tendency of nonpolar substances to aggregate and minimize contact with the aqueous solvent (i.e. thermodynamically unfavourable solvent) by staying at the interface. The aggregation between particles was due to van der Waals interaction, albeit weakly, as the hydroxyl functional groups (which contributed to hydrogen bonding between silica particles) were reduced totally or partially. Meanwhile, the tendency of the hydrophobic particles to stay together was an entropically driven effect that originated from the disruption of strong hydrogen bondings between molecules of water when a nonpolar solute was present (Silverstein, 1998). Both the hydrophobic effect and the van der Waals interaction contributed to the net result of a powerful tendency for hydrophobic particles to interact with the same species, but not water.

Hydrogen bonds were absent between a nonpolar molecule and water molecules; the water structure would be distorted locally as they are forced to form a cage-like structure (to allow H-bonding between water molecules) around the non-polar solute. The cage structure would restrict the motion of water molecules, thus the entropy of the system was decreased, leading to an energetically unfavourable condition (Schauperl et al., 2016).

#### **4.1.3 Summary for Preliminary Experiments**

Beginning from Section 4.1, the empirical results of preliminary experiments were discussed systematically. These preliminary experiments involved three types of particles and three types of solvent:

- Particles: Untreated silica, bitumen-treated silica, and hydrophobic (i.e. methylated) silica
- Solvent: Heptane, toluene, and water

For clarity, a summary of the empirical results is provided in Table 4.3.

Table 4.3 A Summary for Preliminary Experiments

Type of Solids	Solvent	Time to settle 30 mm in a vial	Settling Rate (mm/hour)	Ratio with Stokes velocity	Foam Formation	Mudline thickness
Silica Beads (untreated)	Heptane	30 to 50 secs	Unstable	N/A	-	sharp
	Toluene	60 to 80 secs	Unstable	N/A	-	sharp
	Water	14.4 days	0.09	0.38	-	1 mm
Bitumen Treated Beads	Heptane	50 to 70 secs	Unstable	N/A	-	sharp
	Toluene	4.7 days	0.25	0.65	-	1-2 mm
	Water	11.8 days	0.11	0.46	Yes (visible)	1 mm
Hydrophobic Beads*	Heptane	2 to 3 mins	Unstable	N/A	-	sharp
	Toluene	1.1 days	1.17	2.98	-	2-4 mm
	Water	N/A	Foaming	N/A	Yes	N/A

\* Chemically treated with trimethylchlorosilane (TMCS)

In pictorial summary of the empirical results in Table 4.3, along with some hypothesized mechanisms, is shown in Figure 4.10.

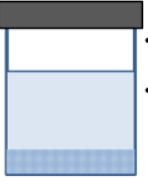

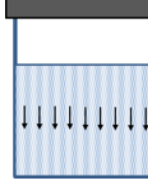

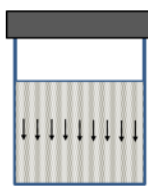
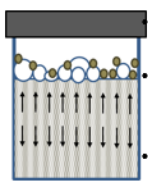

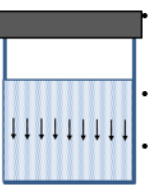
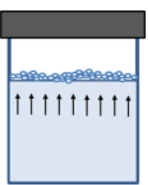
	Heptane	Toluene	Water
<b>Pure silica</b> (Hydrophilic)	 <ul style="list-style-type: none"> <li><b>Rapid Settling</b></li> <li>Absence of EDL repulsion</li> <li><b>Aggregation:</b> Silanol- silanol hydrogen bonding/ van der Waals</li> </ul> <p><b>Unstable</b></p>	 <ul style="list-style-type: none"> <li><b>Rapid Settling</b></li> <li>Absence of EDL repulsion</li> <li><b>Aggregation:</b> Silanol- silanol hydrogen bonding/ van der Waals</li> </ul> <p><b>Unstable</b></p>	 <ul style="list-style-type: none"> <li><b>Slow Settling</b></li> <li>Stabilized by EDL repulsion (dissociation of hydroxyls in water)</li> </ul> <p><b>Stable</b></p> $\frac{v}{V_{Stokes}} = 0.38$
<b>Bitumen treated</b> (Partially hydrophilic/hydrophobic)	 <ul style="list-style-type: none"> <li><b>Rapid Settling</b></li> <li>Absence of EDL Repulsion</li> <li>Absence of steric repulsion in poor solvent</li> <li><b>Aggregation:</b> van der Waals</li> </ul> <p><b>Unstable</b></p>	 <ul style="list-style-type: none"> <li><b>Slow Settling</b></li> <li>Not densely packed, but long chains are extending in solvent</li> <li>Stabilized by steric repulsion in good solvent</li> </ul> <p><b>Stable</b></p> $\frac{v}{V_{Stokes}} = 0.65$	 <ul style="list-style-type: none"> <li><b>Slow Settling</b></li> <li>Not densely packed, partially hydrophilic</li> <li>Absence of steric repulsion in poor solvent</li> <li>Stabilized by EDL repulsion</li> </ul> <p><b>Stable</b></p> $\frac{v}{V_{Stokes}} = 0.46$
<b>Chemical Treated</b> (Hydrophobic)	 <ul style="list-style-type: none"> <li><b>Rapid Settling</b></li> <li>Absence of EDL and steric repulsion (short chain)</li> <li><b>Aggregation:</b> weak van der Waals</li> </ul> <p><b>Unstable</b></p>	 <ul style="list-style-type: none"> <li><b>Slow Settling</b></li> <li>Weak van der Waals (absence or less silanol)</li> <li>Interaction between toluene and alkyl chain</li> <li>Interaction between alkyl chains</li> </ul> <p><b>Stable</b></p> $\frac{v}{V_{Stokes}} = 2.98$	 <ul style="list-style-type: none"> <li><b>Flotation</b></li> <li>Solids stay at interface (favorable)</li> <li>Entropic driven: disruption of hydrogen bonding</li> <li>Weak van der Waals and hydrophobic effect</li> </ul> <p><b>Unstable</b></p>

Figure 4.10. A 3 × 3 matrix for the dispersion of silica in various solvents system.

## 4.2 Macroscopic Analysis: Heptol Jar Tests

The preliminary experiments provided basic insights into the settling behaviors and underlying mechanisms for very simple dispersion systems. The stability of bitumen-modified fines in good solvent (aromatic) and instability in the poor solvent (aliphatic) was due to the interactions of adsorbed materials with the solvent molecules. In the oil sands industry, the proposed non-aqueous extraction process may utilize a solvent (e.g. naphtha) which is a mixture of aromatic and aliphatic components; however, the preliminary results focused only on solvents at the two ends (i.e. represented by toluene for aromatic and *n*-heptane for aliphatic). Starting in this section (§4.2), the experiments will go further with solvents that were prepared by mixing various volume ratios of *n*-heptane and toluene (or ‘heptol’). The adjustable variable for these jar tests was the degree of aromaticity (specifically, the volume fraction of toluene), denoted  $\alpha$ , which ranged from  $\alpha = 0$

(pure heptane) to  $\alpha = 1$  (pure toluene). Figure 4.11 shows a sequence of pictures of such jar tests; the numbers at the bottom, highlighted in blue, were the values of  $\alpha$ . All bottles at  $t = 0$  were well shaken and dispersed. Based on the preliminary results, heptane ( $\alpha = 0$ ) was considered a poor solvent and toluene ( $\alpha = 1$ ) was a good solvent for the adsorbed bituminous materials. Thus, the degree of aromaticity  $\alpha$  could be interpreted as a measure of the “quality of the solvent.”

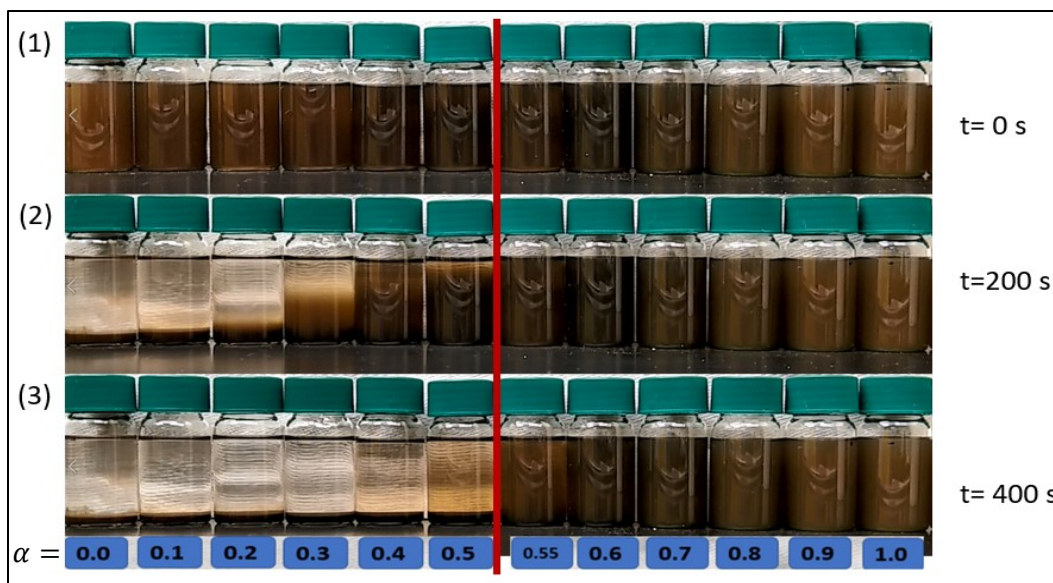


Figure 4.11. Bitumen-treated silica in heptol jar tests, as the example for the experimental procedure in general.

In addition to solids that were pre-treated with whole bitumen, pre-treatments were also made with bitumen subfractions (see section 3.1 and Figure 3.1 regarding the subfractions). The fractions (i.e. asphaltenes and maltenes) were based on the solubility factor and the sub-fractions on the adsorption at the oil-water interface (e.g. interfacially active and remaining). Fractionation is a sensible way of obtaining a greater understanding of the underlying mechanism of colloidal stability. For decades, asphaltene was believed to be the substance that was adsorbed on solid surfaces and prevented aggregation. The present jar tests will provide better insights by, for example, dispersing maltene-treated silica in heptol systems. The dispersed phase solids (i.e. those that underwent pre-treatment of various bituminous materials as explained in Section 3.2.1.1) were added to the heptol solvent with varied degrees of aromaticity in scintillation vials. Monitoring the mudlines, as shown in Figure 4.11, would reveal a wide range of settling rates. Batch settling curves (i.e. plots of decreasing height of mudline with respect to time) would only be given for the unstable systems.



### 4.2.1 Bitumen-treated Silica and Controls

Before presenting results with bitumen-treated silica, we first present results of the two types of ‘control’ particles, i.e. pure (untreated) silica and hydrophobic (methylated) silica. The curve for pure silica in heptol is seen in Figure 4.12.

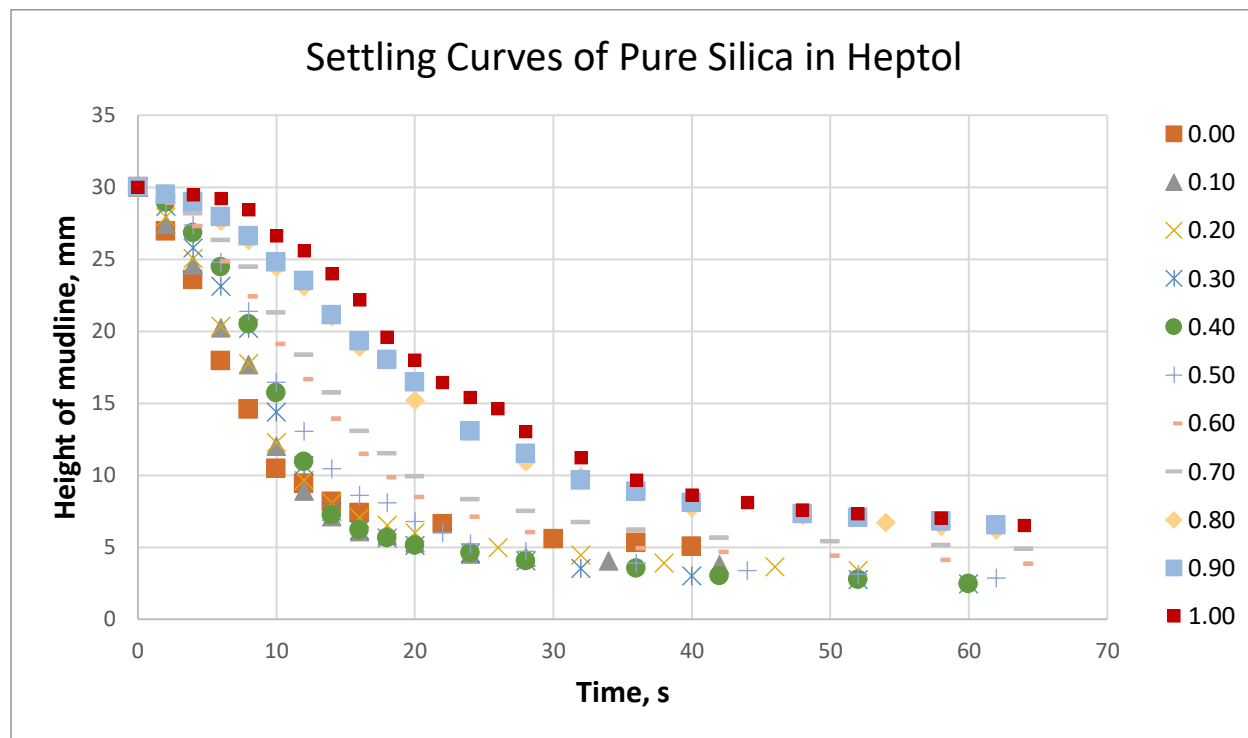


Figure 4.12. Settling curves of pure silica in heptol.

In all cases (i.e. for all values of  $\alpha$ ), sedimentation occurred over a duration of about a minute — suggesting rapid settling of pure silica in hydrocarbons. The differences between these curves may be due to slight variations in interparticle forces as the toluene content was changed.

The other ‘control case’ involved hydrophobic (i.e. methylated) silica in heptol; the results are displayed in Figure 4.12. Compared to the time scale in Figure 4.12, one may consider the sedimentations (except for the case with  $\alpha = 1.0$ ) to be ‘semi-rapid’: the dispersions were still unstable, but perhaps with weaker interparticle attractions. Note that the difference between the cases of  $\alpha = 0.95$  and  $\alpha = 1.00$ , with such small increment in the degree of aromaticity, was enormous: the settling time for the case with  $\alpha = 0.95$  was about 20 minutes, while it took 1.01 days in a heptol with  $\alpha = 1.0$  (pure toluene). The explanation for this dramatic difference is unclear and may be related to intramolecular interactions (e.g. aromatic delocalized  $\pi$  electrons, stacking, or methyl- $\pi$  interactions).

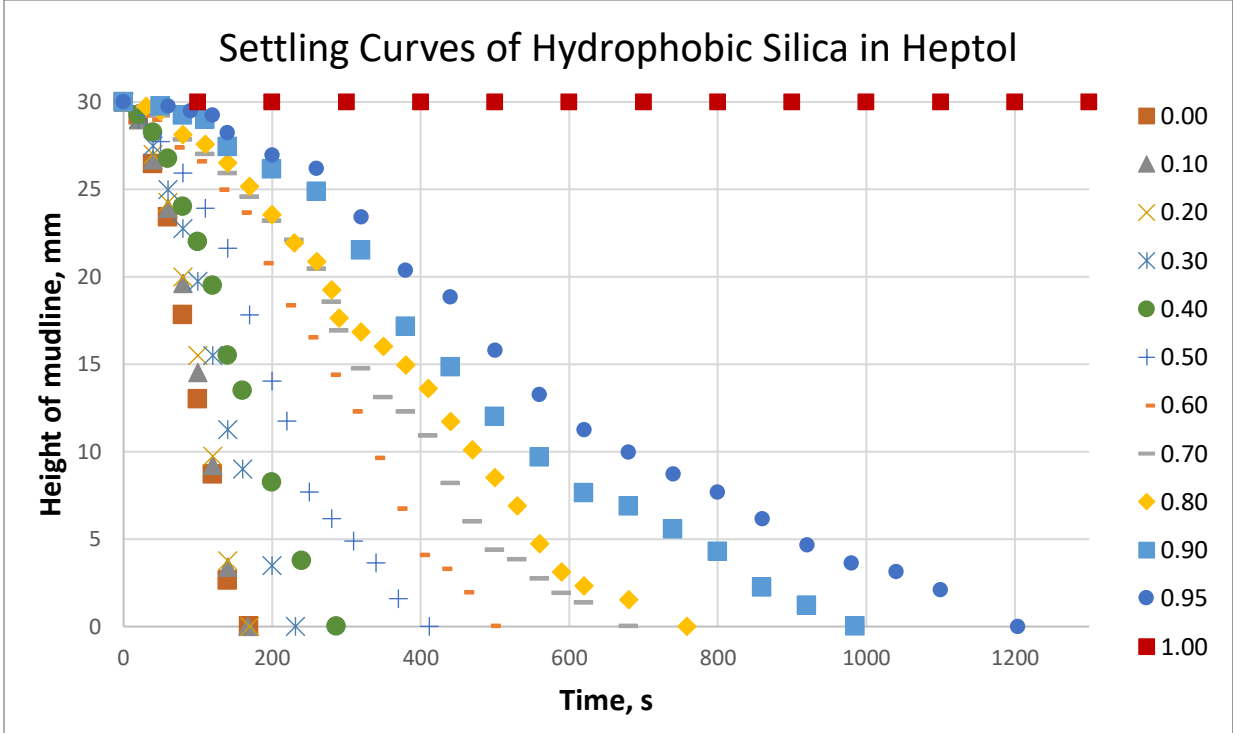


Figure 4.13. Settling curves of hydrophobic silica in heptol.

We now turn to the sedimentation of particles that were treated with various fractions of bitumen. Settling curves involving silica treated with whole bitumen are shown in Figure 4.14.

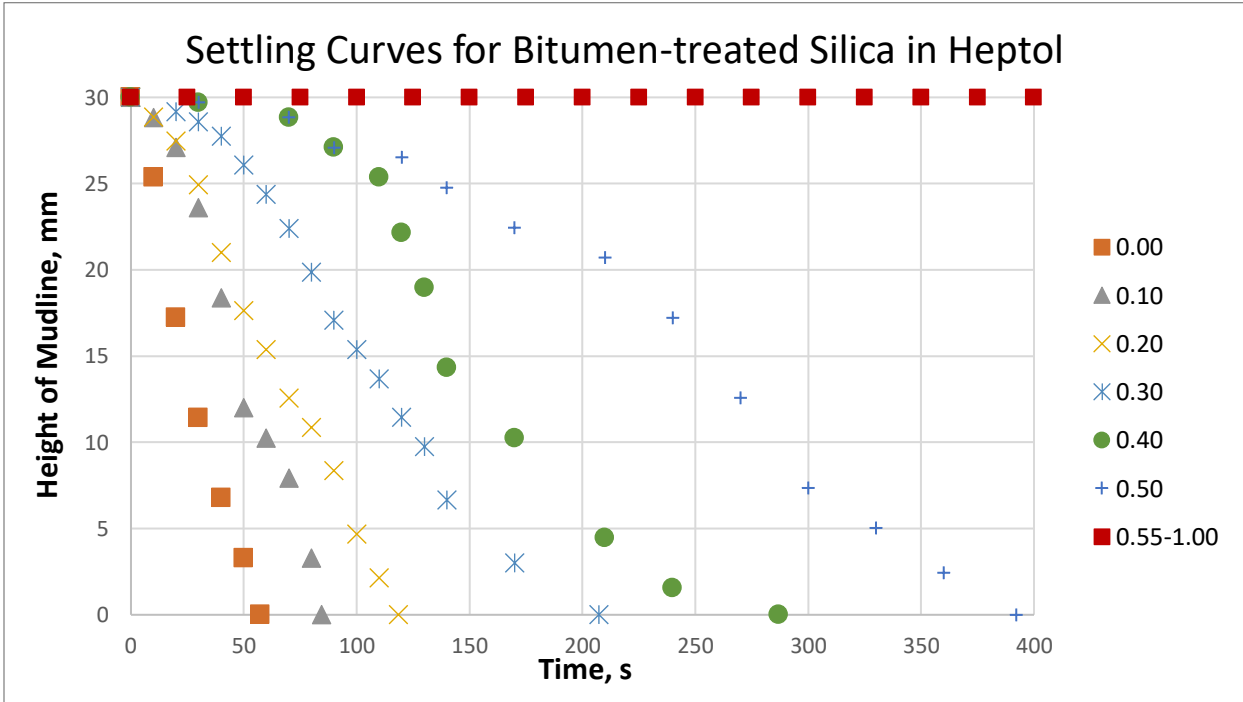


Figure 4.14. Settling curves of bitumen-treated silica in heptol.

Behaviours in the rapid settling regime for bitumen-treated silica in heptol can roughly be divided into two types: the linear trend for lower aromaticity, and the ‘general settling trend’ (i.e. shapes with an inflection point, from downward concavity to upward concavity) for aromaticities up to  $\alpha = 0.50$ . The linear trends corresponding to high contents of heptane were due to strong net attractive forces, with steric repulsion absent or limited in a lower quality solvent.

It is possible that the ‘general settling behaviour’ was due to weaker interparticle attractive forces. In such cases, the van der Waals forces, which contributed to a net attractive force, were weaker as the particles were partially hydrophilic/hydrophobic. At the same time, the adsorbed bituminous materials on particles created steric repulsion with the increasing magnitude as the ‘quality’ of solvent in heptol increased (i.e. steric repulsion was related to how far the adsorbed molecules extended into the solvent, and such an effect was the strongest in pure toluene).

At the same time as steric repulsion strengthens with increasing  $\alpha$ , the van der Waals attraction between particles is expected to decrease due to a change in the effective Hamaker constant (see Equation 4.6). The Hamaker constants of different materials are given in Table 4.4, assuming the bituminous materials adsorbed on the surface are asphaltenes. The Hamaker constant of heptol is assumed to be determined by volume averaging according to Equation 4.7:

$$A_{\text{heptol}} = (1 - \alpha)A_{\text{heptane}} + \alpha A_{\text{toluene}} \quad (4.7)$$

Table 4.4 Hamaker Constants for Various Materials

Hamaker constant	References
$A_{\text{asphaltene}} = 6.0 \times 10^{-20} \text{ J}$	(Fotland & Askvik, 2008)
$A_{\text{heptane}} = 4.3 \times 10^{-20} \text{ J}$	(Hough & White, 1980)
$A_{\text{toluene}} = 5.4 \times 10^{-20} \text{ J}$	(J. H. Masliyah & Bhattacharjee, 2006)

Based on these equations, the value of  $A_{\text{eff asphaltene-heptol}}$  is expected to decrease with increasing  $\alpha$  (toluene volume fraction), consistent with the weakening of van der Waals forces between particles.

The transition from rapid settling to slow settling occurred between  $\alpha = 0.50$  and  $\alpha = 0.55$ ; over this narrow range, there was a shift from net attractive force to net repulsive force as the value of

$\alpha$  increased. The net repulsive force was mainly a consequence of steric repulsion resulting from the brush-like bituminous materials on the surface of the silica.

We conclude this section with two additional findings that are noteworthy:

- If the solids content (which had been kept at 0.3% for all the jar tests) were increased to 0.6%, no shift in the transition range was observed; the only changes were increases in the settling rates.
- When the silica beads were replaced with bitumen-treated kaolinite clay particles, the transition from rapid to slow settling was seen in the same narrow interval of  $\alpha$  (between 0.5 and 0.55). This may not be surprising, as kaolinite clays and silica share similar surface properties.

#### **4.2.2 Silica Surface-Modified by Asphaltenes and Maltenes**

Asphaltenes, the complex higher-MW molecules in bitumen, are believed to preferentially adsorb onto the surfaces of silica during pre-treatment. Asphaltene molecules possess mainly polarizable aromatic ring systems with polar hetero-atomic functional groups (Clementz, 1976). When asphaltenes are removed from bitumen by a de-asphalting procedure (here, by precipitation using *n*-heptane), the fraction that remains soluble in heptane is referred to as maltenes. Compared to asphaltenes, the composition of maltenes is more similar to aliphatic hydrocarbons, and with a small fraction of aromatics. Therefore, maltenes generally have fewer polar functional groups, leading to less surface-active behaviours (Menon & Wasan, 1987). Settling curves for silica that were surface-modified by asphaltenes and maltenes (see protocol in §3.2.1.1) are presented in Figures 4.15 and 4.16.

The settling trends for both asphaltene and maltene particles are qualitatively similar to those for whole bitumen, which are linear for lower aromatics and exhibited ‘general settling trend’ (i.e. showing an inflection point) for higher values of  $\alpha$ . On closer examination, the distinctions between these three sets of data are (a) the transition from rapid to slow settling was shifted to the right (higher degree of aromaticity) for asphaltenes, and to the left for maltenes, when compared to bitumen, and (b) the times for full sedimentation, with the fastest case associated with maltenes.

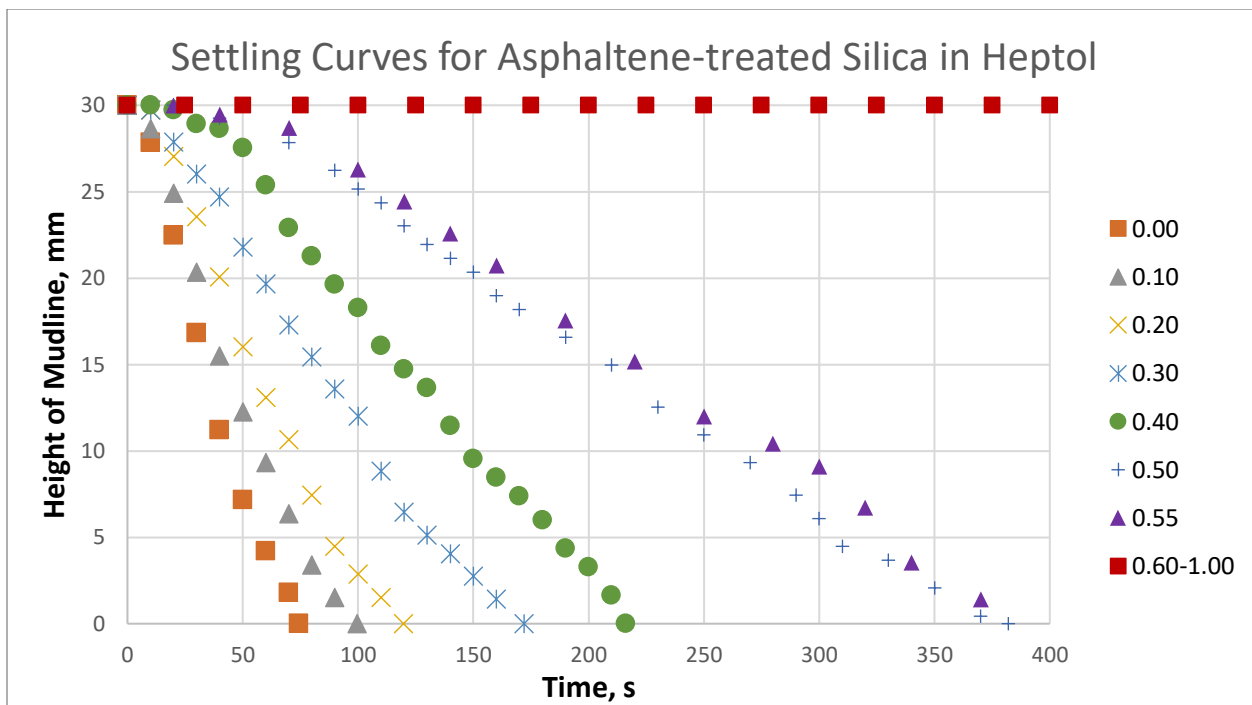


Figure 4.15. Settling curves for asphaltene-modified silica in heptol.

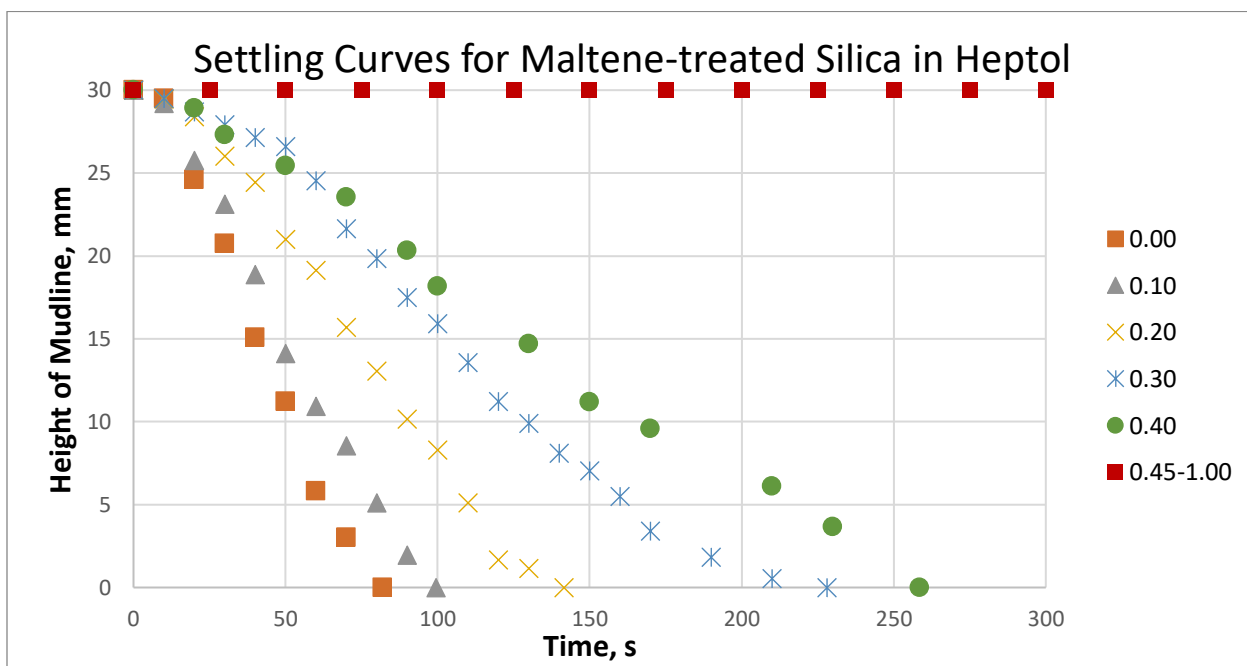


Figure 4.16. Settling curves for maltene-modified silica in heptol.

Interestingly, the transition (from rapid to slow settling) for asphaltene-modified silica shifted to the right compared to the case with whole bitumen. A shift to the right implies that a higher degree of aromaticity in the solvent is needed to ‘activate’ the steric repulsive forces. At present, we do

not have an explanation for such a phenomenon. Equally unexplained is the shift of the transition point to the left (implying less aromatics in the solvent) for the maltene-modified solids. One conclusion, however, is inescapable: one does not require asphaltene molecules at the solid surfaces to have a stable dispersion; maltenes alone can create enough interparticle repulsion to achieve colloidal stability.

#### 4.2.3 Silica Surface-Modified by Sub-fractions of Asphaltenes

The two sub-fractions of asphaltenes are ‘interfacially active asphaltenes’ (IAA) and ‘remaining asphaltenes’ (RA); the reader is referred to Figure 3.1 and the discussions in Section 3.1. Using identical procedures as before, silica beads were adsorbed (i.e. surface-modified) with IAA and RA. The resulting settling curves are shown in Figures 4.17 and 4.18. It is seen that these curves have very similar qualitative features as before. The one subtle difference, not captured in the plots, was that the ‘mudlines’ for these two types of particles became more diffuse when approaching the transition point from low  $\alpha$  values (typically the last two samples before the transition to slow settling). As evident from the settling curves, the transition from rapid to slow settling occurred between  $\alpha = 0.65$  and  $\alpha = 0.70$  for the IAA-modified solids, and between  $\alpha = 0.50$  and  $\alpha = 0.55$  for the RA-modified solids.

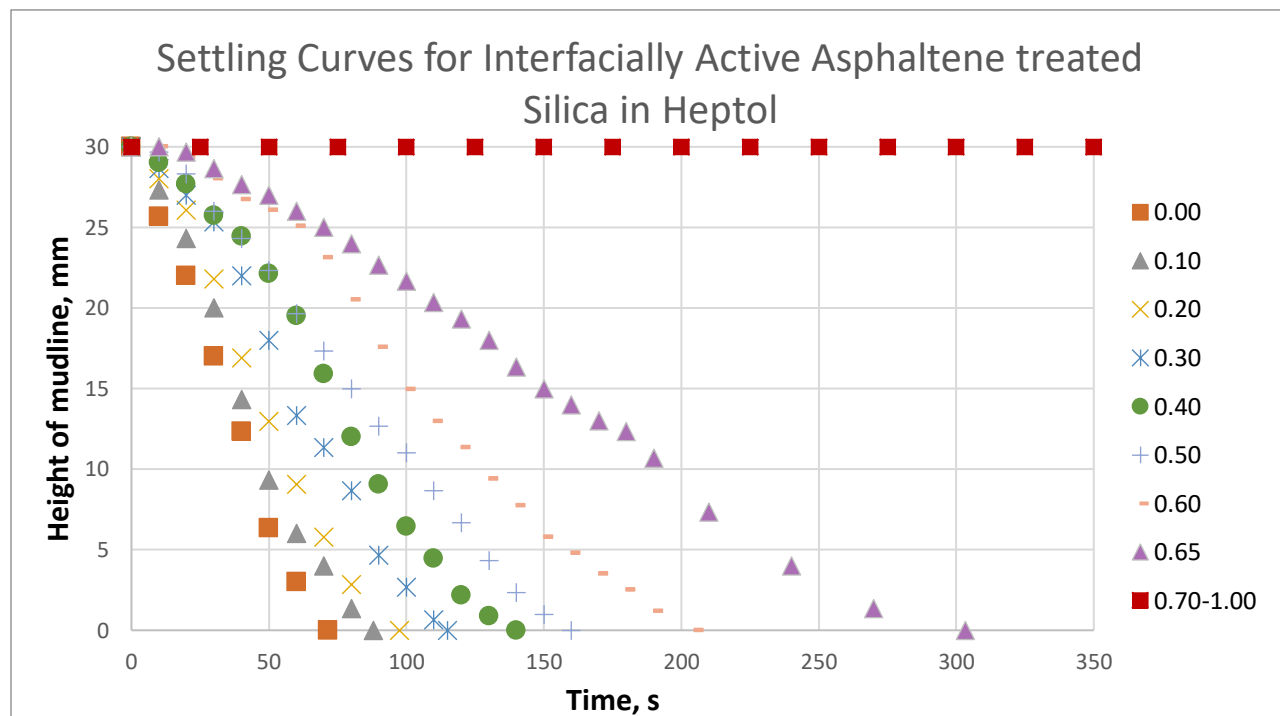


Figure 4.17. Settling curve for interfacially active asphaltene-treated silica in heptol.

The remaining asphaltenes comprised primarily about 98% of the total asphaltenes and are expected to behave more similarly to whole asphaltenes.

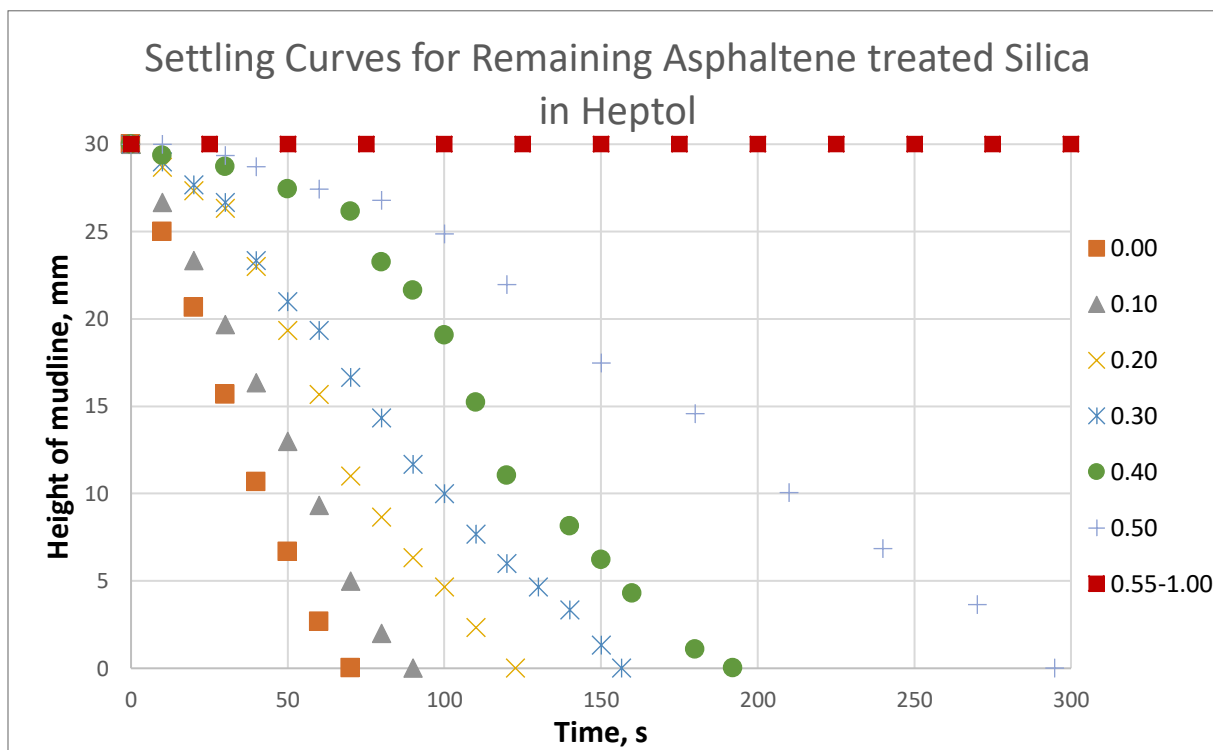


Figure 4.18. Settling curve for remaining asphaltene-treated silica in heptol.

#### 4.2.4 Silica Surface-Modified by Sub-fractions of Maltenes

The two sub-fractions of maltenes are ‘interfacially active maltenes’ (IAM) and ‘remaining maltenes’ (RM); the reader is referred to Figure 3.1 and the discussions in Section 3.1 (see also Menon & Wasan, 1987 and Qiao et al., 2017 for additional information). Using identical procedures as before, silica beads were adsorbed (i.e. surface-modified) with IAM and RM. The resulting settling curves are shown in Figures 4.19 and 4.20.

As seen, the sub-fractions of maltenes (especially the interfacially active component) had created distinctly different settling behaviours compared to that with whole maltenes. The settling curves of IAM-modified solids showed significant differences in transition range and settling times. This was also the first time that Type 1 settling (see §2.5.1) occurred for silica that was treated with bituminous materials. Overall, the settling times for IAM-treated silica were slower than for pure silica, with near-zero settling rates toward the end of sedimentation. As for pure silica systems, loose sediment beds were observed. However, a distinctive transition range (from rapid to slow

settling) was observed at somewhat high aromaticity — between  $\alpha = 0.75$  and  $\alpha = 0.80$ ; such a transition was absent for pure silica systems, as rapid settling was seen for all values of  $\alpha$  (see Figure 4.12). The shifting of the transition range to higher aromaticity may suggest that the interparticle forces (either van der Waals attraction or steric repulsion) were stronger. It is postulated that the more active surface groups in the IAM systems were related to hydroxyl ( $-OH$ ) groups. Further analyses on the chemical composition and surface morphology (e.g. using FTIR or SEM) should be made in order to prove this postulate since this sub-fraction was newly introduced.

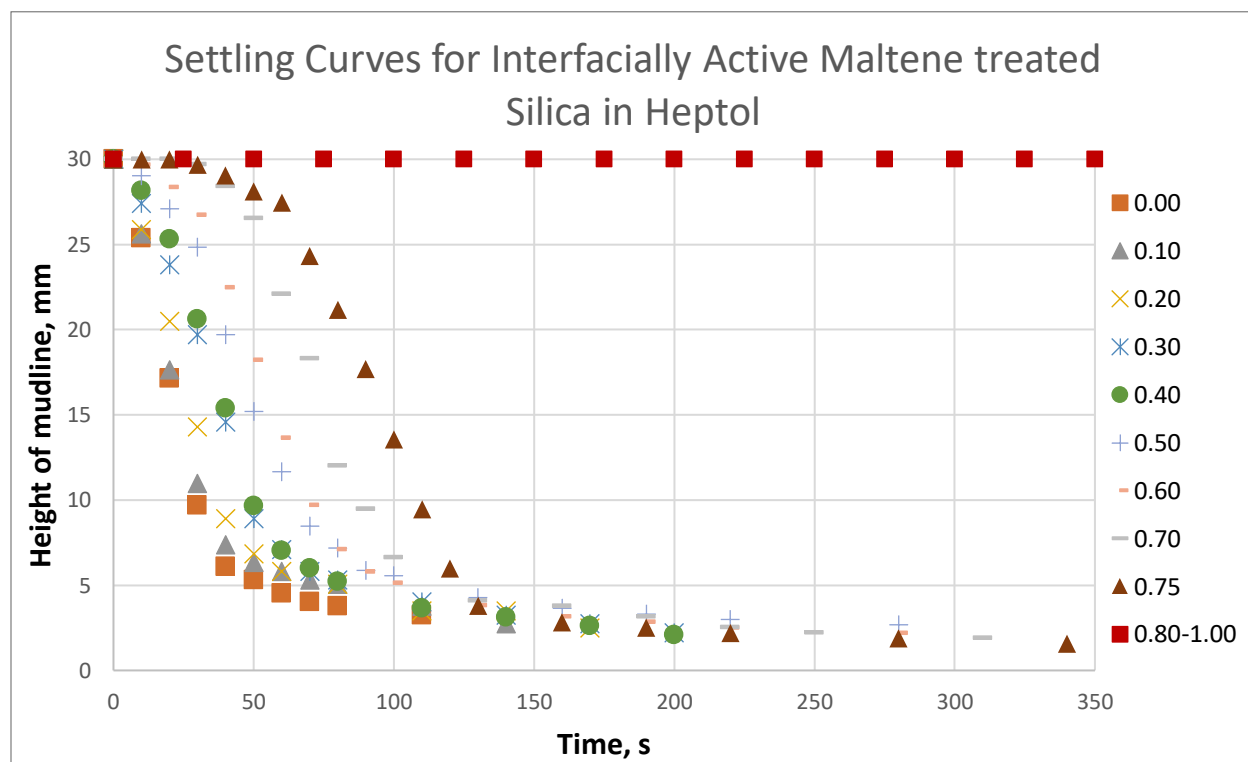


Figure 4.19. Settling curves for interfacially active maltene-treated silica in heptol.

In contrast, the RM-treated silica showed linear and general (i.e. with inflection point) trends, just as for the other bituminous material systems. The transition range for RM silica was at a lower degree of aromaticity (between  $\alpha = 0.35$  and  $\alpha = 0.40$ ) compared to the case for whole maltenes.



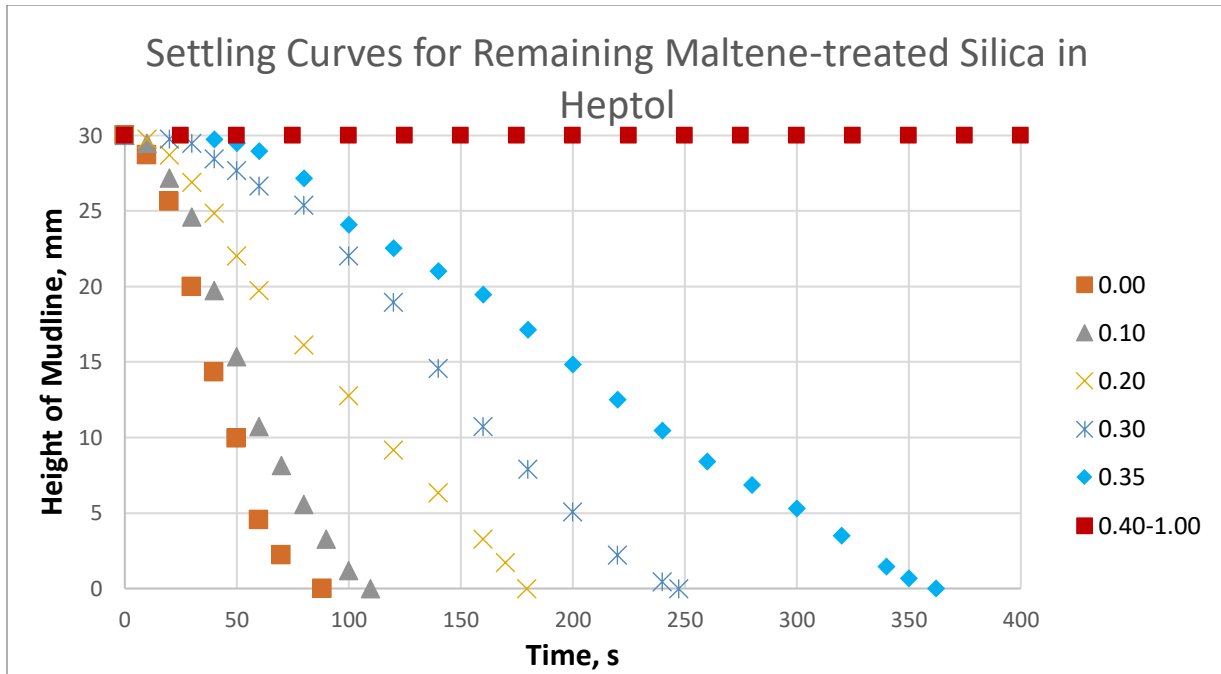


Figure 4.20. Settling curves for remaining maltene-treated silica in heptol.

#### 4.2.5 Summary for Heptol Jar Tests

Sedimentation curves in the rapid settling regime can be classified into three categories, as shown in Figure 4.21. First, Type 1 settling (A) is characterized by a sharp acceleration, followed by linear descent or directly into a deceleration trend. The second type of sedimentation, which we call general settling (B), begins with a delayed time at a constant rate before the acceleration and ends with a slowed-down rate. Lastly, a settling curve can be effectively linear from beginning to end (C). These different categories are likely created by specific interparticle forces, as well as the detailed dynamics of aggregation and floc breakup.

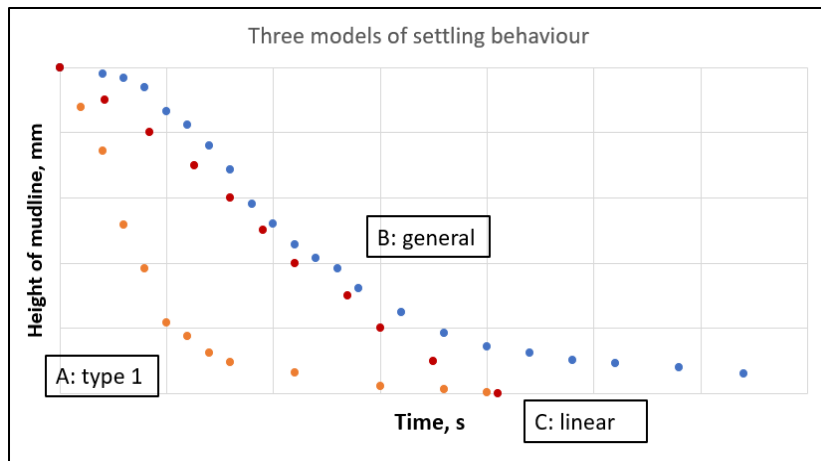


Figure 4.21. Three models of settling behaviours.

In general, for silica treated with bituminous materials, most settling curves at low aromaticities exhibited linear behaviours (perhaps due to the strong adhesive forces which led to rapid settling). As the value of  $\alpha$  increased, these linear features gradually turn into type B, especially when it got close to the transition point (perhaps as a result of the interparticle repulsions becoming more prominent). An exception to this was observed with IAM-treated silica, which exhibited general settling (B) at lower  $\alpha$  and type 1 settling (A) at higher  $\alpha$ ; this was more similar to the pure silica case. A summary of these experiments is presented in Table 4.5.

The transition ranges (from rapid to slow settling) for different types of bitumen fractions are summarized in Figure 4.22. A transition range could presumably be further narrowed down to a specific value of  $\alpha$ , at which point a sharp transition between rapid and slow settling occurred. However, in this study, the smallest increment of  $\alpha$  was 0.05. Nevertheless, the importance of  $\alpha$  (aromatic content in an organic solvent) has been amply demonstrated.

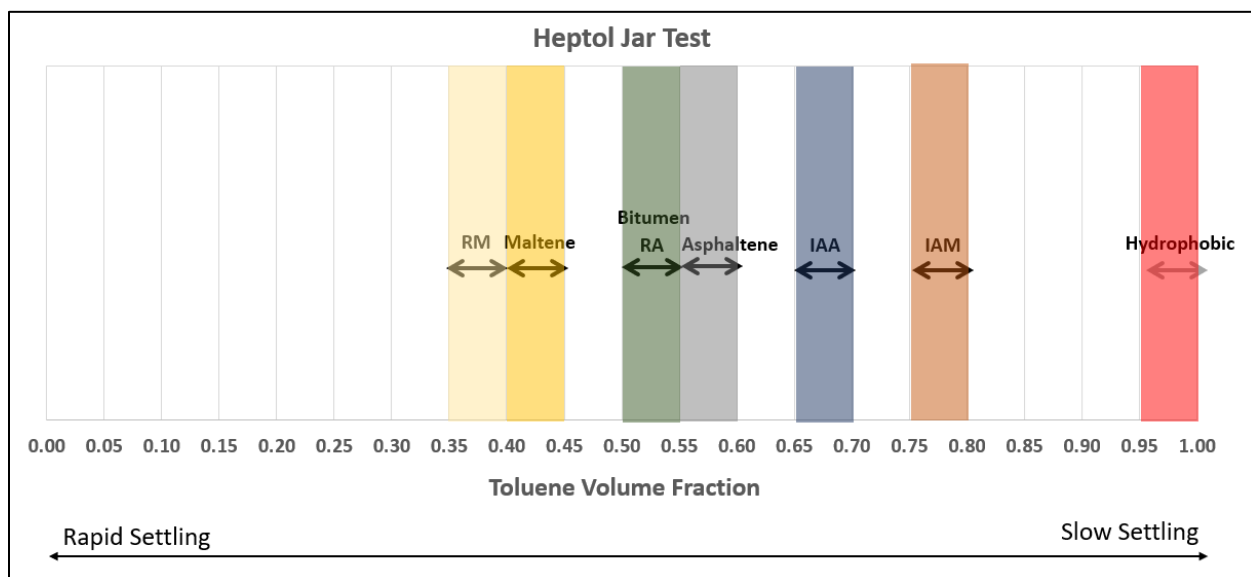


Figure 4.22. Transition ranges for various treated silica particles in heptol.

Table 4.5 Summary for Different Solids in Heptol Jar Tests

Type of solids	Transition range for Binary settling (in toluene vol%)	Settling Behaviour	Sediment bed	Time to reach 30 mm in heptane (second)	Time to reach 30 mm in toluene
Pure silica	-	General and type 1	loose	40 (reach 25mm)	mins
Chemical treated (hydrophobic)	0.95 - 1.00	Linear and general	compacted	169	days
Bitumen	0.50 - 0.55	Linear and general	compacted	57	days
Asphaltene	0.55 - 0.60	Linear and general	compacted	74	days
RA	0.50 - 0.55	Linear and general	compacted	70	days
IAA	0.65 - 0.70	Linear and general	compacted	72	days
Maltene	0.40 - 0.45	Linear and general	compacted	82	days
RM	0.35 - 0.40	Linear and general	compacted	88	days
IAM	0.75 - 0.80	General and type 1	loose	110 (reach 27mm)	days

### 4.3 Microscopic Analysis: Interparticle Forces Measurement

The colloidal stabilities of dispersions were clearly indicated through jar (i.e. macroscopic) tests. To further understand the underlying mechanisms, the role of interparticle forces (to be exact, the net attractive forces) will be examined as the next step.

Direct force measurements by the microcantilever technique were conducted between two glass tips with radii of curvature of approximately  $\sim 40\mu\text{m}$ . These rounded glass tips were subjected to the same surface pre-treatment, mimicking the interaction between two particles (as opposed to billions of particles in heptol jar tests). The overall net attractive force could be quantified based on the known stiffness of the microcantilever (calculated from beam theory) and the observed deflection. In such an experiment, a force was either (a) detectable, meaning that the force was attractive and sufficiently strong to cause micron-scale deflection, or (b) undetectable, suggesting that the adhesion was either very weak, or the net interparticle force was repulsive.

The results from these experiments are arranged in a plot with the adhesive force ( $\mu\text{N}$ ) on the vertical axis and the number of contacts on the horizontal axis. The ‘number of contacts’ represents the number of times adhesion between two pipette tips were measured *at the same contact locations*. This can offer insight into whether conditions at the particle surfaces are altered by physical contact. In addition, such information, on the ‘strength of re-flocculation,’ will be crucial to the numerical simulation of aggregation dynamics when flocs are allowed to repeatedly form and break up due to hydrodynamic shear.

#### 4.3.1 Pure Glass Surface and Bitumen-treated Surface

Experiments involving clean glass tips were first studied in *n*-heptane and toluene (the two ends of the ‘ $\alpha$  spectrum’); the results are shown in Figure 4.23. The first observation is that in both cases, there were appreciable adhesive forces, suggesting unstable dispersions with rapid settling. This is consistent with jar test results shown in Table 4.3. Note also that interparticle adhesion was slightly weaker in toluene (Figure 4.23), and that complete settling in jar tests took slightly longer in toluene (Table 4.3).

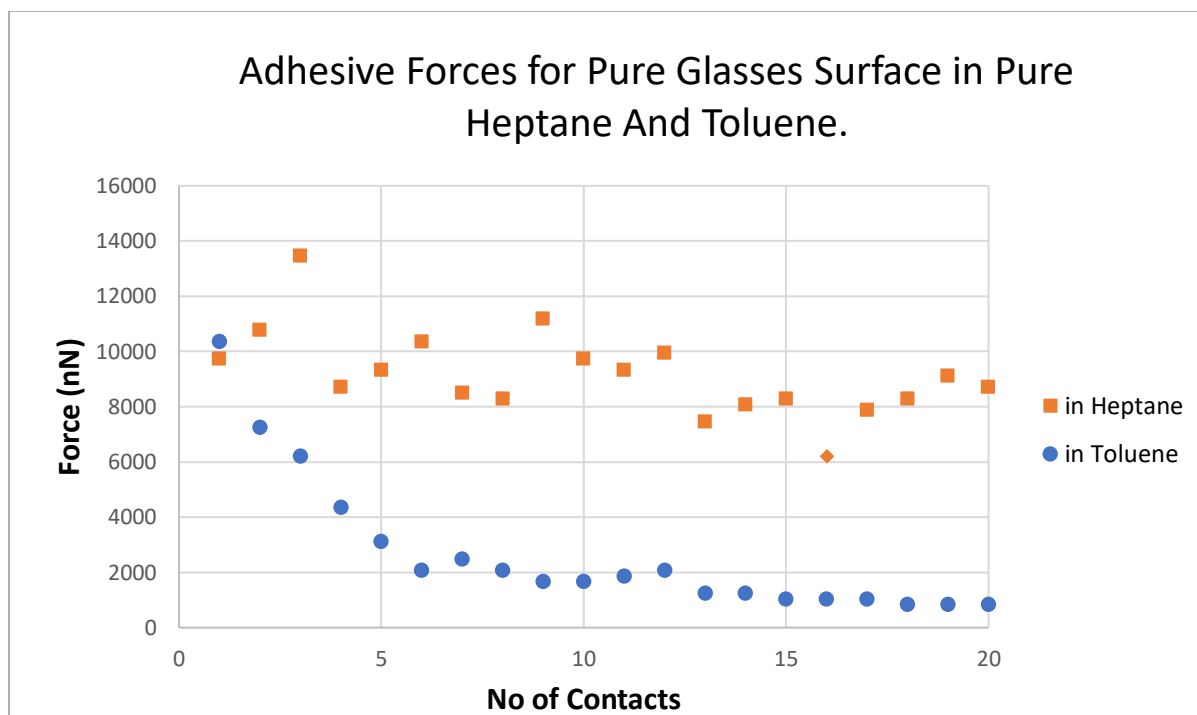


Figure 4.23. Adhesive forces for pure glasses surface in pure heptane and toluene.

From Figure 4.23, it is also interesting to see that interparticle adhesion in toluene appeared susceptible to a weakening effect upon repeated contacts. This implies an alteration of surface properties. Although the reason for this remains unclear, it was suggested that this was due to the physisorption of aromatic molecules (e.g. benzene, xylene, and toluene) on silica (Ncube et al., 2017). The interactions were attributed to hydrogen bonding between silanol on the surface of silica and delocalized  $\pi$  electrons of aromatics, with the adsorbed toluene laying flat on the silica surface (Parida et al., 2006). The weak adhesive forces measured after a number of contacts might be the  $\pi$ - $\pi$  interaction between toluene adsorbed silica particles.

In contrast to the case with toluene, adhesive forces in heptane, as shown in Figure 4.23, appeared to be quite insensitive to the number of contacts. Next, we remain focussed on heptane as the liquid medium and compare the adhesion between clean glass tips (using the same data from Figure 4.23) and those between bitumen-treated glass tips; the results are shown in Figure 4.24. It is seen that, for both types of pipette tips, adhesion did not weaken with repeated contacts. Also, as expected, the adhesion between ‘contaminated’ surfaces was weaker than that between clean surfaces. In both cases, the adhesive forces were sufficiently strong that one would expect unstable

dispersions; this was borne out by the jar tests in Table 4.3 (for clean surfaces) and in Figure 4.14 (for bitumen-treated surfaces).

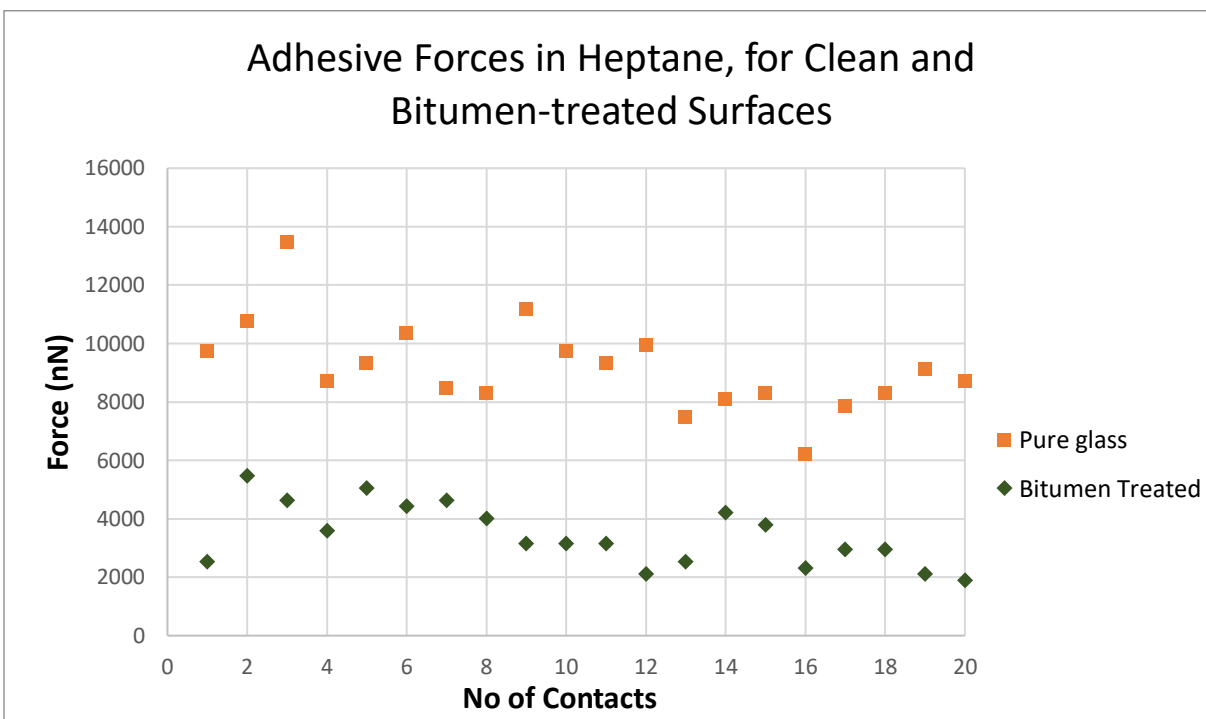


Figure 4.24. Adhesive forces in heptane, for clean and bitumen-treated surfaces.

We next focus on adhesion between bitumen-treated glass surfaces in heptols of different aromaticities (a specific case, with heptane as the medium, was already presented as green data points in Figure 4.24). The results are summarized in Figure 4.25. The important takeaway from these direct force measurements is that they correlate very well with macroscopic settling tests (cf. Figure 4.14): appreciable adhesive forces were detected from  $\alpha = 0$  (heptane) up to  $\alpha = 0.5$ , at which point there is, presumably, a transition from net attractive interparticle force to net repulsion. As seen earlier in Figure 4.14, the transition from rapid to slow settling occurred somewhere between  $\alpha = 0.50$  and  $\alpha = 0.55$ . However, Figure 4.25 shows that the shift of the interparticle force from net attraction to net repulsion happened between  $\alpha = 0.50$  and a value of  $\alpha$  that was *slightly larger* than 0.55. The reason, we believe, is the following:

At  $\alpha = 0.55$ , the microcantilever detected weak *adhesive* interparticle forces (of order 100 nN); nevertheless, jar tests showed that the corresponding dispersed system was stable. Here, it is proposed that for dispersion to become destabilized, the attractive (presumably van der Waals)

forces must overcome not only the repulsive colloidal forces but also the hydrodynamic repulsion between the moving (sinking) solids. This hydrodynamic hindrance is not considered a colloidal force; rather, it is a consequence of hydrodynamic lubrication (Kim & Zydney, 2004; Marshall & Li, 2014).

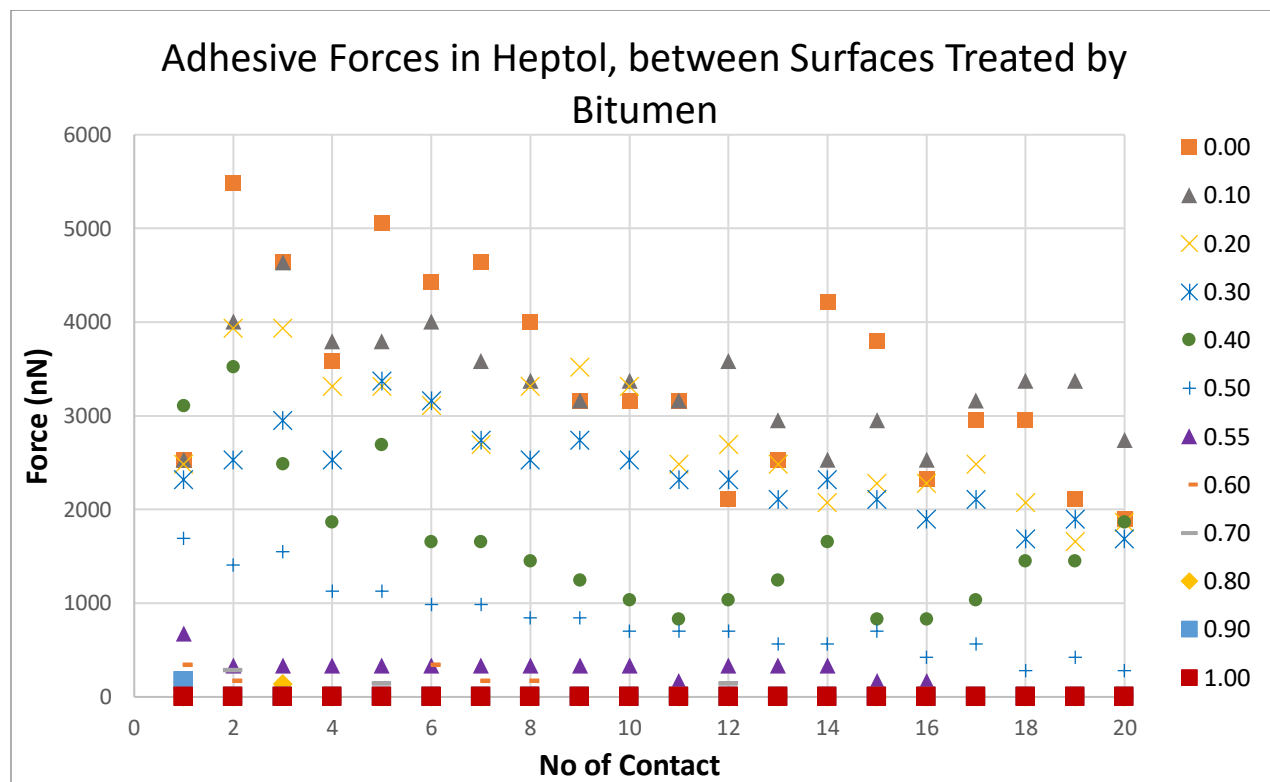


Figure 4.25 Adhesive forces in heptol, between surfaces treated by bitumen.

### 4.3.2 Glass Surfaces Adsorbed with Bitumen, Asphaltenes, and Maltenes

The next set of data is related to glass surfaces that were treated with bitumen, asphaltenes, and maltenes (bitumen data are taken from §4.3.1); adhesive forces between such surfaces were measured in heptane. The total number of contacts was increased (from 20 to 50) to provide additional information on how adhesion may change with repeated contacts. The measured forces are summarized in Figure 4.26. Two features are worth discussing:

- For surfaces coated with asphaltenes, the interparticle adhesion remained undiminished with repeated contacts. By contrast, adhesion between maltene-coated surfaces showed a steady decline, eventually to undetectable levels. We speculate that such a decline may not necessarily be with the number of contacts, but instead with time. Recall that the measurements in Figure

4.26 were made in heptane — a solvent in which maltenes are soluble but asphaltenes are not. As time progressed (with the increasing number of contacts), it is possible that the adsorbed maltenes on the solids surfaces would begin to swell and create a steric barrier that counteracted the attractive forces. Adsorbed asphaltenes, on the other hand, would remain in collapsed conformations in heptane.

- Very roughly speaking, Figure 4.26 suggests that interparticle adhesion was the strongest with asphaltenes, followed by bitumen, and was the weakest with maltenes. This may, with a certain amount of speculation, explain the shifts in transition points (from rapid to slow settling) in the earlier jar tests. Specifically, it is seen from Figure 4.22 that maltene-modified particles transitioned at the lowest value of  $\alpha$  (a measure of aromatic content in the solvent); bitumen-modified particles transitioned at a higher value of  $\alpha$ ; and asphaltene-modified particles required the highest amount of aromatics in the solvent for the transition. This is understandable if one considers toluene to be a solvent that promotes interparticle repulsion (by swelling adsorbed molecules into ‘brushes’ which in turn act as steric barriers). Thus, particles adsorbed with asphaltenes, which experienced the strongest adhesion, would require the highest amount of aromatics (i.e. the highest value of  $\alpha$ ) to acquire colloidal stability.

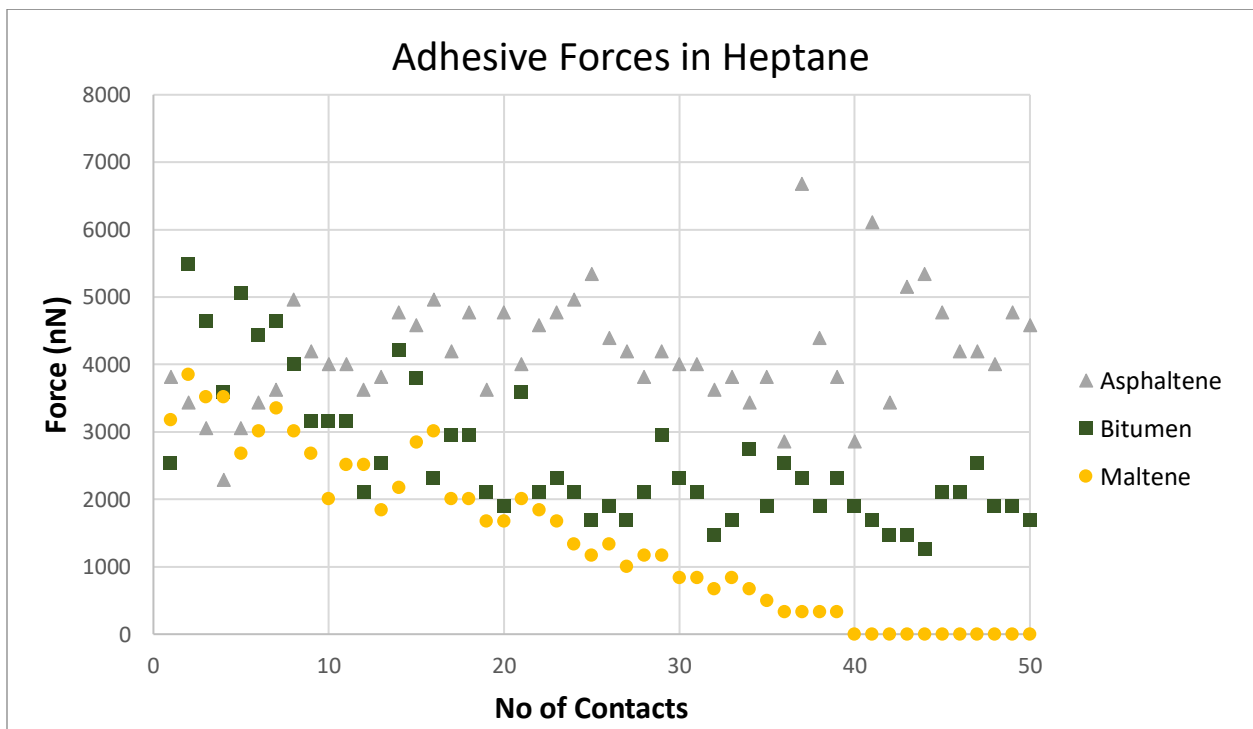


Figure 4.26. Adhesive forces in heptane, between surfaces treated by bitumen and its fractions.



Additional force measurements are presented in Figures 4.27 and 4.28, which separately show adhesion between asphaltene-coated surfaces and maltene-coated surfaces, respectively. Here, the liquid media were heptol solutions with  $\alpha$  ranging from 0 (heptane) to 1 (toluene).

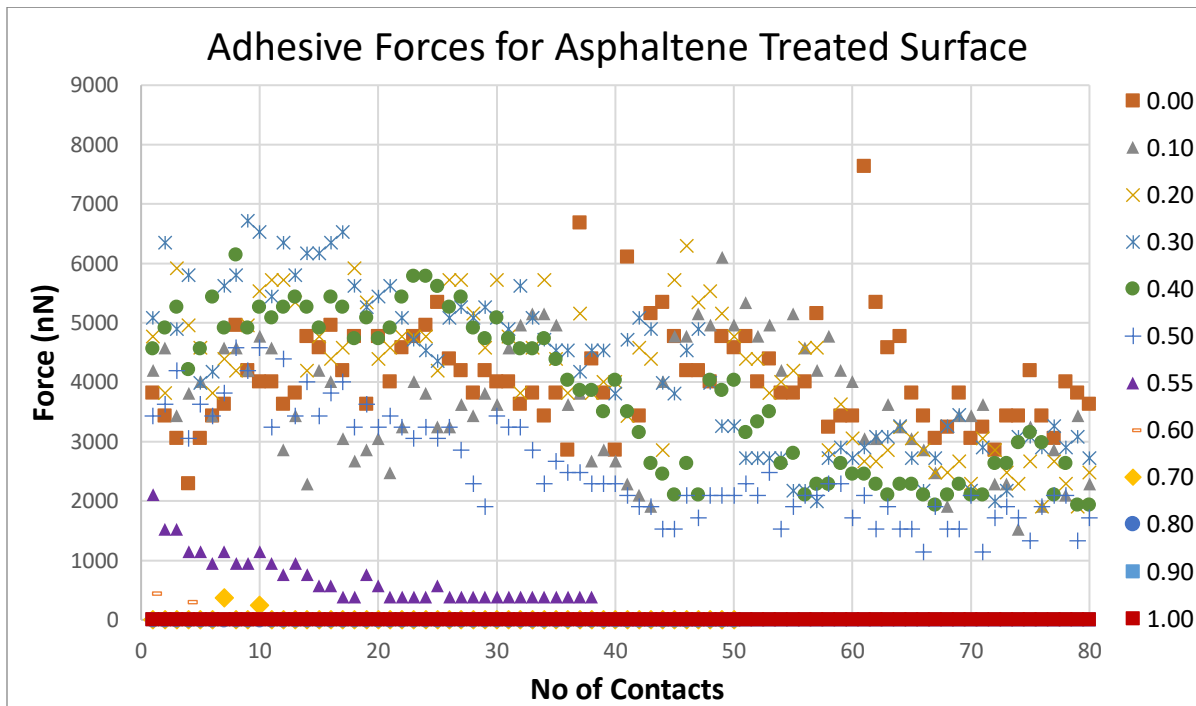


Figure 4.27. Adhesive forces for asphaltene treated surface in heptol.

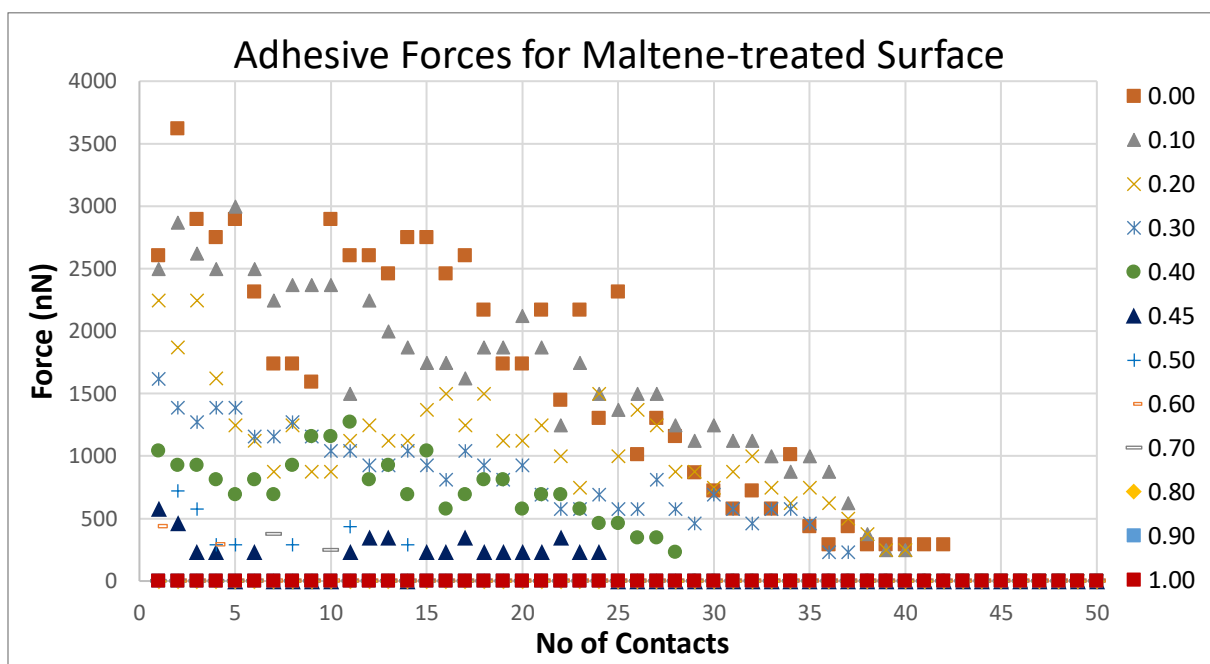


Figure 4.28. Adhesive forces for maltene treated surface in heptol.

### 4.3.3 Glass Surfaces Adsorbed with Sub-fractions of Asphaltenes and Maltenes

Lastly, we present data on adhesive forces between glass surfaces that were treated with the sub-fractions of asphaltenes and maltenes, namely, interfacially-active asphaltenes (IAA), remaining asphaltenes (RA), interfacially-active maltenes (IAM), and remaining maltenes (RM). The measurements were made in heptol with  $\alpha$  ranging from 0 (heptane) to 1 (toluene).

The measured forces are summarized in Figures 4.29 to 4.32. The amount of data is massive and somewhat difficult to interpret. One clear trend, however, is that the adhesive forces were strongest for low values of  $\alpha$ , and became undetectable at the opposite end. The other observation, which is more subtle but very significant, is the following: For all four sub-fractions, the diminishing of adhesive forces to near-zero values coincided exactly with the transition regimes (from rapid to slow settling) as summarized in Figure 4.22.

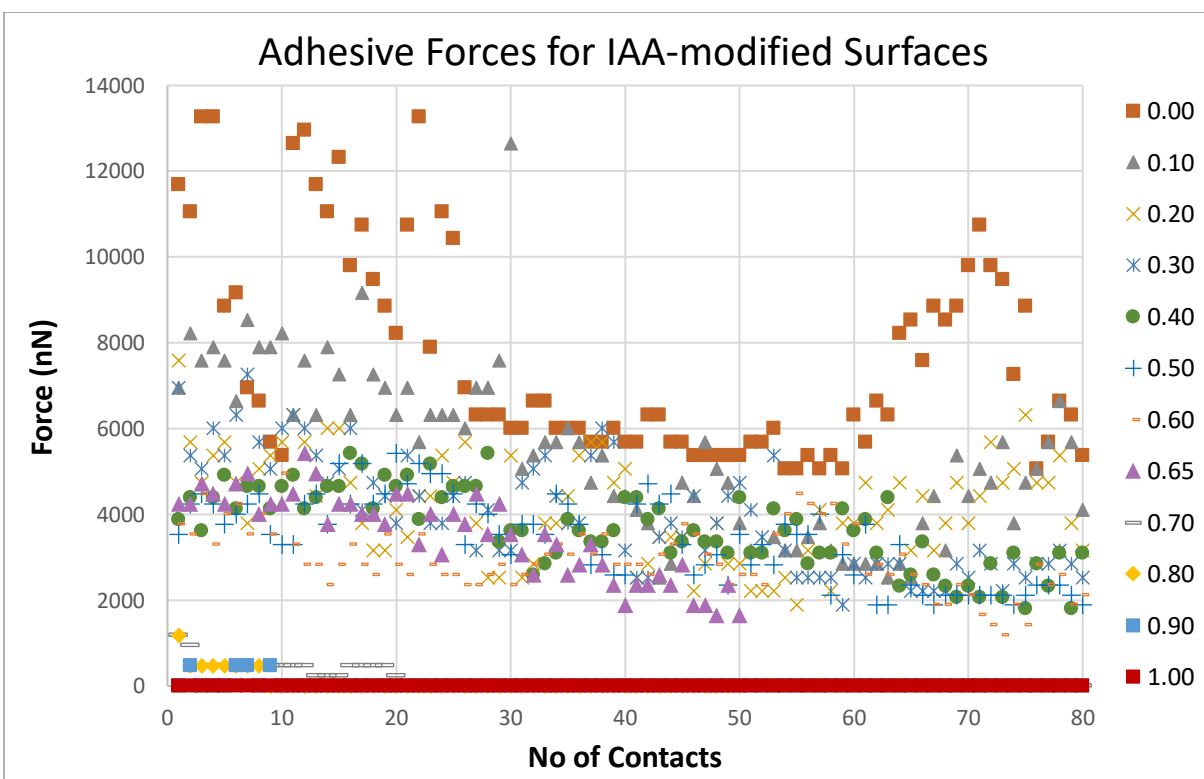


Figure 4.29. Adhesive forces for interfacially active asphaltene-treated surfaces in heptol.

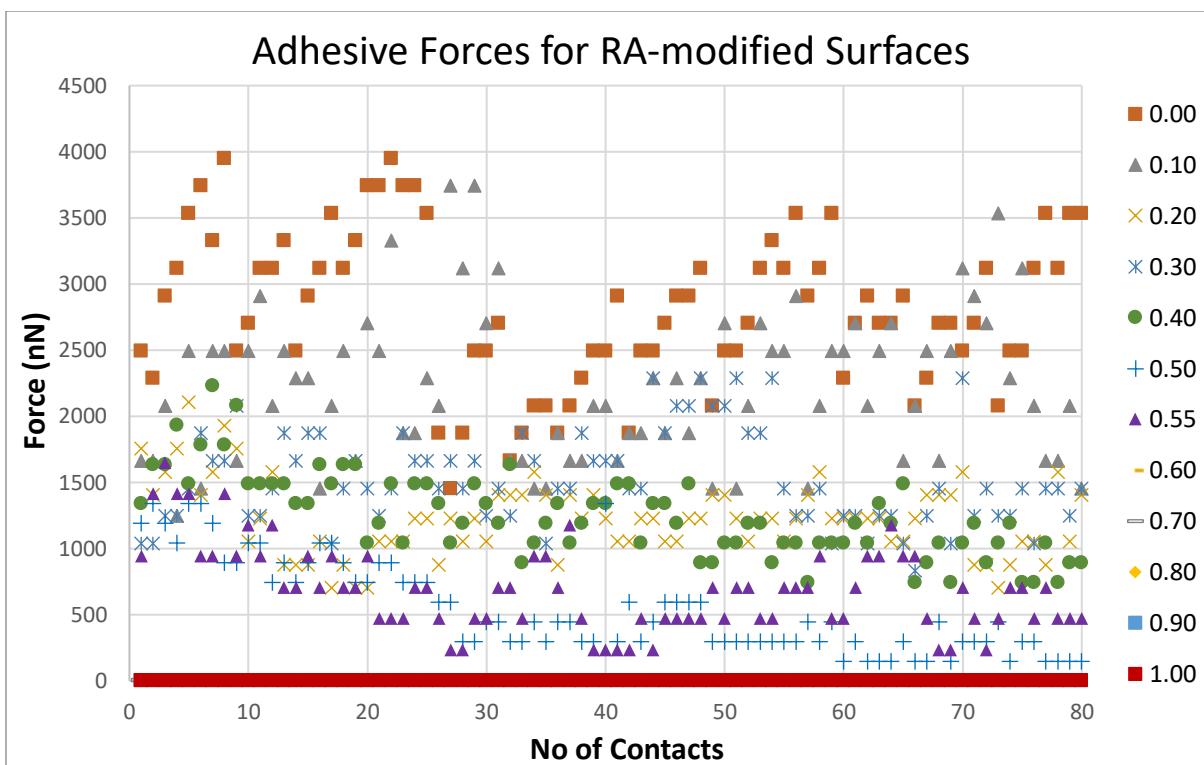


Figure 4.30. Adhesive forces for remaining asphaltene-treated surfaces in heptol.

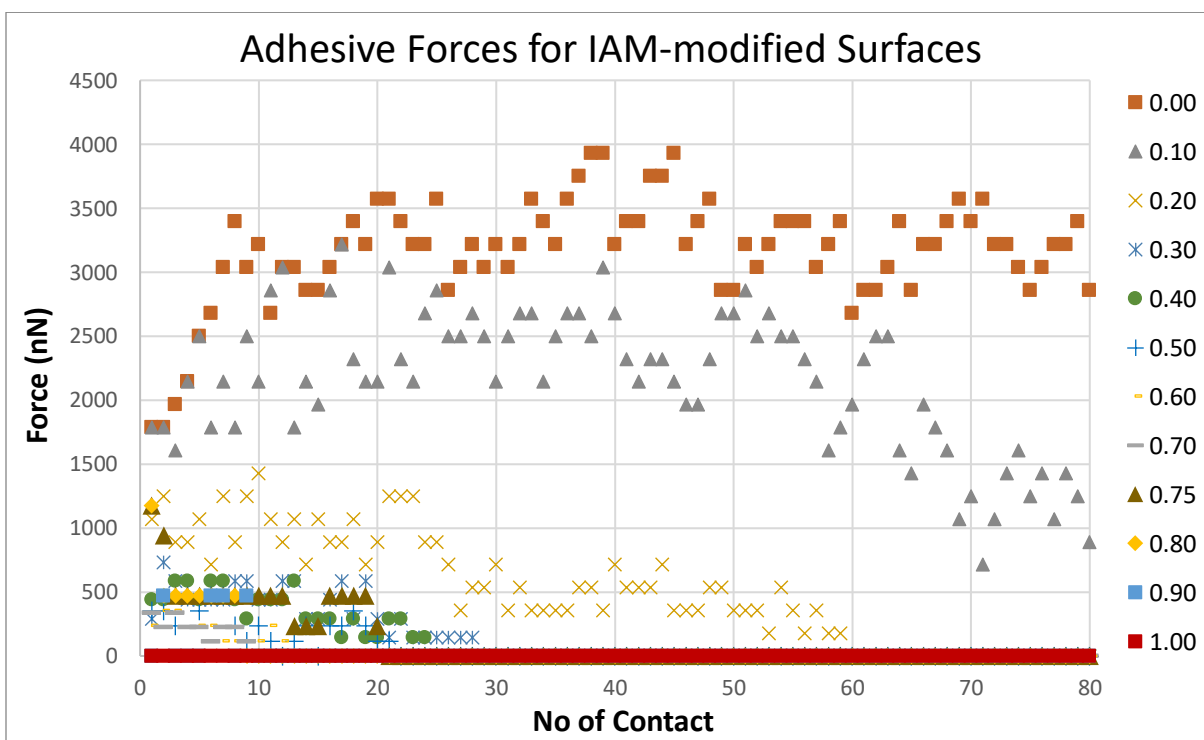


Figure 4.31. Adhesive forces for interfacially active maltene-treated surfaces in heptol.

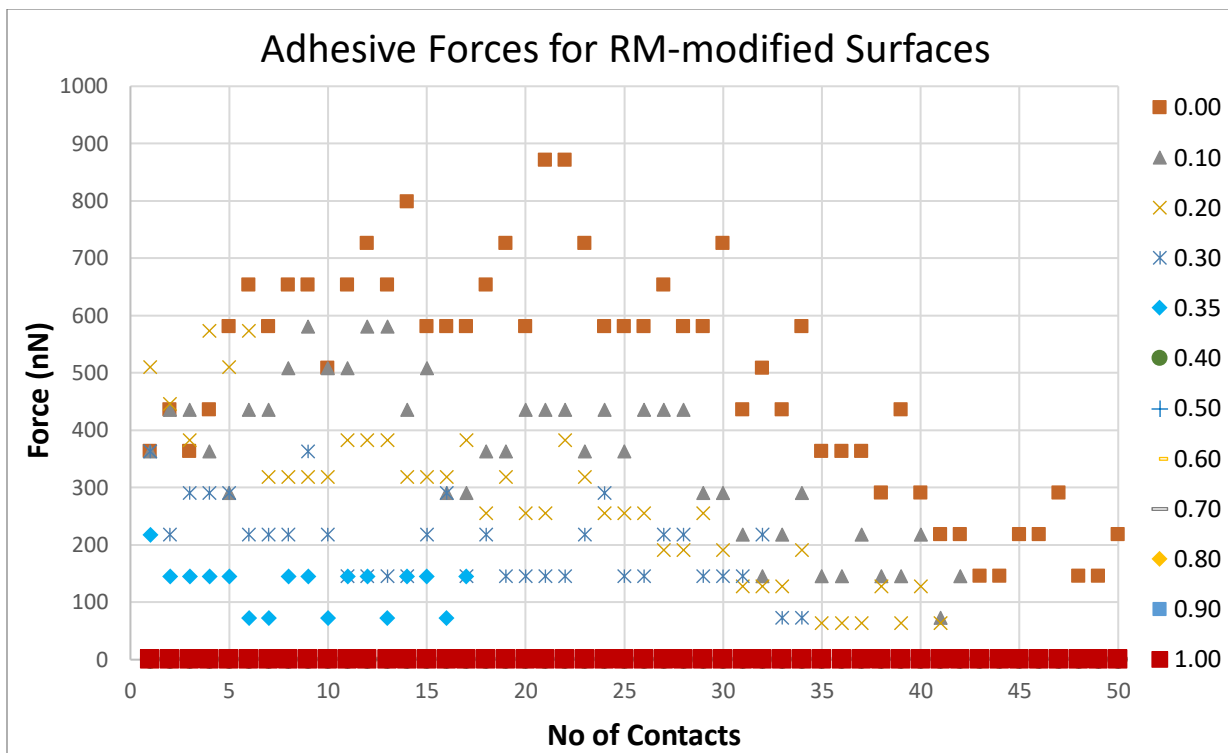


Figure 4.32. Adhesive forces for remaining maltene-treated surfaces in heptol.

## 5. Summary and Future Work

Environmental impact and economical feasibility are two issues that have plagued the water-based bitumen extraction technology in the oil sands industry. An alternative to water-based extraction, one that can operate at ambient temperatures, is the ‘solvent-based’ or ‘non-aqueous’ extraction (a technology that was first proposed decades ago). Although non-aqueous extraction does not suffer from the above-mentioned drawbacks of the water-based approach, it has its own challenges. One of the main challenges is the choice of an optimum solvent that could favour the removal of fine solids in the oil phase. This has served as the motivation for this study, which was an investigation into the best conditions under which dispersed fine solids could be separated and removed by gravity means. The surfaces of the fines are ‘contaminated’ through extended contact with bituminous materials, leading to a modification of the surface properties of the solids. Under certain conditions, these surface-modified solids can exist as a colloidally stable dispersion in an organic solvent. The purpose of this investigation is to identify the conditions — specifically, the aromatic content of the solvent phase — under which bitumen-contaminated solids can be destabilized (i.e. made to aggregate) in non-aqueous liquids. If the aromatic content of the solvent phase is the independent variable of this study, then the dependent variables, i.e. the observables, would be the settling rates of dispersions on the macroscopic scale, and the interparticle adhesive forces on the microscopic scale. This study would also provide insights into the underlying mechanisms behind the colloidal stability of non-aqueous solid dispersions.

As a preliminary study of colloidal stability, micron-sized fine solids with three distinct surface properties were dispersed in three different liquid media. The three surface properties were characterized as hydrophilic (untreated silica), hydrophobic (methylated silica), and bitumen-treated; the three liquids were water, *n*-heptane, and toluene.

For bitumen-treated silica in toluene, the bituminous materials that were adsorbed on the silica surfaces extended their chain-like molecules to maximize contact with the solvent, thus creating a steric barrier that prevented aggregation by van der Waals attractive forces; the result was a stable dispersion that was not amenable to gravity separation. In contrast, the chain-like molecules collapsed when in *n*-heptane (a poor solvent) and could not form the steric barriers that were present in the case for toluene. This led to the aggregation of the solids by van der Waals forces, which was manifested on the macroscopic scale as rapid settling.

A somewhat surprising result was that bitumen-treated silica remained as a stable dispersion in water — presumably a poor solvent for the adsorbed materials. It is surmised that the adsorbed materials may not fully cover the entire silica surface, leaving it partly hydrophobic and partly hydrophilic. When immersed in water, electric double layers could develop over the non-adsorbed portions of the particle surface and prevent aggregation. This phenomenon may be related to the remarkable stability of fine solids in tailings ponds.

Following the preliminary experiments that involved only three types of surface properties and three liquids, similar macroscopic (jar) tests were explained to include: (a) organic liquid mixtures with various proportions of toluene and *n*-heptane, and (b) silica surfaces that were adsorbed with different fractions and sub-fractions of bitumen. Sedimentation curves were plotted, and their rates were quantified. Different types of sedimentation characteristics were also discussed. Most importantly, it was discovered that as the aromatic content of the organic solvent was varied (increased), there was a rather abrupt transition from rapid settling to slow settling. The aromatic content at which this transition occurred depended on the type of material (fractions and sub-fractions of bitumen) that was adsorbed on the solid surface.

The transition from rapid to slow settling is presumably a direct result of the interparticle forces, with rapid settling corresponding to a net attractive force, and slow settling to a net repulsion. This hypothesis was largely confirmed by direct force measurements between two glass surfaces using the microcantilever technique. In particular, with regard to the aromatic content at which a transition would occur, there were remarkable agreements between macroscopic jar tests and microscopic force measurements (for all fractions and sub-fractions of bitumen). On the macroscopic scale, a transition occurs when the settling behaviour changed from rapid to slow; on the microscopic scale, it is when the adhesive force decreased precipitously from a significant magnitude to *near zero*. Here, it is necessary to clarify why the phrase “near-zero” is used. It was discovered that a colloidal dispersion could be stable on the macroscopic scale even if a small adhesive force existed between the individual particles. (Between two 40-micron particles, this “near-zero” force was of order 100 nN.) In this thesis, it is proposed that in order for a dispersion to be destabilized, the interparticle attractive force must overcome repulsive forces that are colloidal *and* hydrodynamic in origin (The hydrodynamic repulsion is created by fluid motion around the particles as they settle; such an effect is absent during microcantilever experiments).

Recommendations for future work are suggested based on aspects that were absent in this present investigation.

A measurement of settling rate as the function of water pH would provide a better understanding of the colloidal stability. Zeta potential of bitumen-modified silica, also as a function of pH would be a good insight for solid removal in the aqueous environment, complementing the comprehensive solution for oil sand tailings.

To study the settling behaviors in greater detail, the transition *range* in heptol jar tests could be further narrowed down to a transition *point* (the exact degree of aromaticity for the transition between rapid and slow settling). And the settling curves could be better characterized by fitting them to empirical equations.

Linear trends in settling curves (at higher degrees of aromaticity) are believed to be due to narrow size distributions. An analysis based on monitoring aggregate sizes during the sedimentation process could provide a better understanding of the flocculation dynamics.

Further analyses on the chemical composition and surface morphology of adsorbed materials (e.g. by FTIR and SEM) are strongly recommended to provide additional insights into the mechanisms of colloidal stability.

Instead of fractionating bitumen into asphaltenes and maltenes based on solubilities in solvents, it is perhaps worthwhile to consider fractionation by surface activity (e.g. adsorption onto oil-water or other solid-liquid interfaces). Further research on such fractions may provide better ideas on how best to tackle the current problems in the oil sands industry (e.g. removal of solids in tailing ponds and non-aqueous extraction, etc.).

## References

- Adams, J. J. (2014). Asphaltene Adsorption , a Literature Review. *Energy and Fuels*, 28, 2831–2856.
- Alberta Energy Regulator. (2015). ST98-2015: Alberta’s Energy Reserves 2014 and Supply/Demand Outlook 2015-2024. In *Alberta’s Energy Reserves 2014 and Supply/Demand Outlook*.
- ASTM D2007-93. (1993). *Standard Test Method for Characteristic Groups in Rubber Extender and Processing Oils by the Clay-Gel Adsorption Chromatographic Method*.
- BP Statistical Review. (2019). BP Statistical Review of World Energy Statistical Review of World. In *BP Statistical Review of World Energy*.
- Bratby, J. (2016). *Coagulation and Flocculation in Water and Wastewater Treatment* (3rd ed.). IWA.
- Bresme, F., & Oettel, M. (2007). Nanoparticles at fluid interfaces. *Journal of Physics Condensed Matter*, 19(41).
- Brunner, H., Tsuno, T., Balázs, G., & Bodensteiner, M. (2014). Methyl/phenyl attraction by CH/ $\pi$  interaction in 1,2-substitution patterns. *Journal of Organic Chemistry*, 79(23), 11454–11462.
- Buenrostro-Gonzalez, E., Lira-Galeana, C., Gil-Villegas, A., & Wu, J. (2004). Asphaltene precipitation in crude oils: Theory and experiments. *AIChE Journal*, 50(10), 2552–2570.
- Butt, H.-J., Graf, K., & Kappl, M. (2003). Surface Modification. In *Physics and chemistry of interfaces* (pp. 206–221). Wiley-VCH.
- CAPP. (2019). *2019 Crude Oil Forecast, Markets and Transportation*.
- Chu, Z., & Seeger, S. (2015). Robust superhydrophobic wood obtained by spraying silicone nanoparticles. *RSC Advances*, 5(28), 1–6.
- Clark, K. A. (1963). *The K.A. Clark Volume* (M. . Carrigy (ed.)). Research Council of Alberta.



- Clementz, D. M. (1976). Interaction of petroleum heavy ends with montmorillonite. *Clays and Clay Minerals*, 24(6), 312–319.
- Coe, H. ., & Clevenger, G. . (1916). Methods for Determining the Capacities of Slime-settling Tanks. *Trans. AIME*, 55, 356.
- Cormack, D. E., Kenchington, J. M., Phillips, C. R., & Leblanc, P. J. (1977). Parameters and mechanisms in the solvent extraction of mined athabasca oil sand. *The Canadian Journal of Chemical Engineering*, 55(5), 572–580.
- Cosultchi, A., Cordova, I., Valenzuela, M. A., Acosta, D. R., Bosch, P., & Mexicano, I. (2005). *Adsorption of Crude Oil on Na<sup>+</sup>-Montmorillonite*. 19(6), 1417–1424.
- Davies, R. (1968). The experimental study of the differential settling of particles in suspension at high concentrations. *Powder Technology*, 2(1), 43–51.
- Energy Information Agency. (2009). *International Energy Outlook*.
- Environment and Climate Change Canada. (2019). *National Inventory Report 1990–2017: Greenhouse Gas Sources and Sinks in Canada Canada's Submission To the United Nations Framework Convention on Climate Change*.
- Fan, T., & Buckley, J. S. (2002). Rapid and accurate SARA analysis of medium gravity crude oils. *Energy and Fuels*, 16(6), 1571–1575.
- Fan, T., Wang, J., & Buckley, J. S. (2002). Evaluating Crude Oils by SARA Analysis. *Proceedings - SPE Symposium on Improved Oil Recovery*, 883–889.
- Farnard, J. R., Meadus, F. W., & Sparks, B. D. (1985). Removal of Intractable Fine Solids From Bitumen. *Fuel Processing Technology*, 10(23546), 131–144.
- Fossen, M., Kallevik, H., Knudsen, K. D., & Sjöblom, J. (2007). Asphaltenes precipitated by a two-step precipitation procedure. 1. Interfacial Tension and Solvent Properties. *Energy and Fuels*, 21, 1030–1037.
- Fotland, P., & Askvik, K. M. (2008). Determination of Hamaker constants for asphaltenes in a mixture of pentane and benzene. *Colloids and Surfaces A: Physicochemical and Engineering Aspects*, 324(1–3), 22–27.

- Fotovati, M. (2011). *Aggregation and Sedimentation of Fine Solids in Non-Aqueous Media*. University of Alberta.
- Fouda, A. E., & Capes, C. E. (1977). Hydrodynamic particle volume and fluidized bed expansion. *The Canadian Journal of Chemical Engineering*, 55(4), 386–391.
- Fritz, G., Schadler, V., Willenbacher, N., & Wagner, N. J. (2002). Electrosteric stabilization of colloidal dispersions. *Langmuir*, 18, 6381–6390.
- Garmsiri, M. R., & Shirazi, H. H. A. (2012). A new approach to define batch settling curves for analyzing the sedimentation characteristics. *Journal of Mining and Environment*, 3(2), 103–111.
- Gelardi, G., & Flatt, R. J. (2016). Working mechanisms of water reducers and superplasticizers. In P.-C. Aïtcin & R. J. Flatt (Eds.), *Science and Technology of Concrete Admixtures* (pp. 257–278). Woodhead Publishing.
- Gosselin, P., Hruday, S. E., Naeth, M. A., Plourde, A., Therrien, R., Van Der Kraak, G., & Zhenghe, X. (2010). *Environmental and Health Impacts of Canada 's Oil Sands Industry*.
- Gray, M., Xu, Z., & Masliyah, J. (2009). *Physics in the oil sands of Alberta*. 31.
- Gregory, J. (2009). Monitoring particle aggregation processes. *Advances in Colloid and Interface Science*, 147–148, 109–123.
- Grinerval, E., Basset, J.-M., & Lefebvre, F. (2013). A Novel Approach to Prepare Well-Defined Silica-Supported Polyoxometalate Species by Reaction with a Chlorinated Support. *Journal of Inorganic Chemistry*, 2013(i), 1–8.
- Gun'ko, V. M., Voronin, E. F., Pakhlov, E. M., & Chuiko, A. A. (1993). Interactions of Chlorosilanes with a Silica Surface Catalyzed by Amines. *Langmuir*, 9(3), 716–722.
- Hair, M. L. (1975). Hydroxyl Groups on Silica Surface. *The Journal of Non-Crystalline Solids*, 19, 299–309.
- Hogg, R. (2012). Bridging flocculation by polymers. *KONA Powder and Particle Journal*, 30(30), 3–14.

- Hooshiar, A., Uhlik, P., Liu, Q., Etsell, T. H., & Ivey, D. G. (2012). Clay minerals in nonaqueous extraction of bitumen from Alberta oil sands: Part 1. Nonaqueous extraction procedure. *Fuel Processing Technology*, *94*(1), 80–85.
- Hough, D. B., & White, L. R. (1980). The calculation of hamaker constants from liftshitz theory with applications to wetting phenomena. *Advances in Colloid and Interface Science*, *14*(1), 3–41.
- Huang, W., Xu, J., Tang, B., Wang, H., Tan, X., & Lv, A. (2018). Adsorption performance of hydrophobically modified silica gel for the vapors of n-hexane and water. *Adsorption Science and Technology*, *36*(3–4), 888–903.
- Hupka, J., Miller, J. D., & Drelich, J. (2004). Water-Based Bitumen Recovery from Diluent-Conditioned Oil Sands Development of Bitumen Separation/Recovery Process for Utah Oil Sands. *The Canadian Journal of Chemical Engineering*, *82*(August), 978–985.
- Israelachvili, J. . (2011). *Intermolecular and Surface Forces* (Third). Academic Press.
- Israelachvili, J., Min, Y., Akbulut, M., Alig, A., Carver, G., Greene, W., Kristiansen, K., Meyer, E., Pesika, N., Rosenberg, K., & Zeng, H. (2010). Recent advances in the surface forces apparatus (SFA) technique. *Reports on Progress in Physics*, *73*(3).
- Jal, P. K., Patel, S., & Mishra, B. K. (2004). Chemical modification of silica surface by immobilization of functional groups for extractive concentration of metal ions. *Talanta*, *62*, 1005–1028.
- Jewell, D. M., Weber, J. H., Bunger, J. W., Plancher, H., & Latham, D. R. (1972). Ion-Exchange, Coordination, and Adsorption Chromatographic Separation of Heavy-End Petroleum Distillates. *Analytical Chemistry*, *44*(8), 1391–1395.
- Jiang, T., Hirasaki, G. J., Miller, C. A., & Ng, S. (2011). Wettability alteration of clay in solid-stabilized emulsions. *Energy and Fuels*, *25*(6), 2551–2558.
- Jin, Y., Liu, W., Liu, Q., & Yeung, A. (2011). Aggregation of silica particles in non-aqueous media. *Fuel*, *90*(8), 2592–2597.

- Kharrat, A. M., Zacharia, J., Cherian, V. J., & Anyatonwu, A. (2007). Issues with comparing SARA methodologies. *Energy and Fuels*, 21(6), 3618–3621.
- Kim, M. M., & Zydney, A. L. (2004). Effect of electrostatic, hydrodynamic, and Brownian forces on particle trajectories and sieving in normal flow filtration. *Journal of Colloid and Interface Science*, 269(2), 425–431.
- Kosior, D., Ngo, E., & Xu, Y. (2018). Aggregates in Paraffinic Froth Treatment : Settling Properties and Structure. *Energy and Fuels*.
- Lagaly, G. (1987). Water and Solvents on Surfaces Bristling with Alkyl Chains. In H. Kleeberg (Ed.), *Interactions of Water in Ionic and Nonionic Hydrates* (pp. 229–240). Springer.
- Lai, H., Fang, H., Huang, L., He, G., & Reible, D. (2018). A review on sediment bioflocculation: Dynamics, influencing factors and modeling. *Science of the Total Environment*, 642, 1184–1200.
- Liang, Y., Hilal, N., Langston, P., & Starov, V. (2007). Interaction forces between colloidal particles in liquid: Theory and experiment. *Advances in Colloid and Interface Science*, 134–135, 151–166.
- Lin, F., Stoyanov, S. R., & Xu, Y. (2017). Recent Advances in Non-Aqueous Extraction of Bitumen from Mineable Oil Sands : A Review. *Org. Process Res. Dev.*
- Long, Y., Dabros, T., & Hamza, H. (2002). Stability and settling characteristics of solvent-diluted bitumen emulsions. *Fuel*, 81(15), 1945–1952.
- López-Linares, F., Carbognani, L., Spencer, R. J., & Pereira-Almao, P. (2011). Adsorption studies in Athabasca core sample: Virgin and mild thermal cracked residua. *Energy and Fuels*, 25(8), 3657–3662.
- Masliyah, J. ., Czarnecki, J. A., & Xu, Z. (2011). *Handbook on Theory and Practice of Bitumen Recovery from Athabasca Oil Sands-Vol. 1: Theoretical Basis*. Kingsley.
- Masliyah, J. H., & Bhattacharjee, S. (2006). *Electrokinetic and Colloid Transport Phenomena*. John Wiley & Sons.

- Masliyah, J., Zhou, Z. J., Xu, Z., Czarnecki, J., & Hamza, H. (2004). *Understanding Water-Based Bitumen Extraction*. 82(August), 628–654.
- Menon, V. B., & Wasan, D. T. (1987). Adsorption of maltenes on sodium montmorillonite. *Colloids and Surfaces*, 25(2–4), 387–392.
- Michaels, A. S., & Bolger, J. C. (1962). Settling Rates and Sediment Volumes of Flocculated Kaolin Suspensions. *Industrial and Engineering Chemistry Research*, 1(1), 24–33.
- Mondragon, R., Julia, J. E., Barba, A., & Jarque, J. C. (2012). Characterization of silica-water nanofluids dispersed with an ultrasound probe: A study of their physical properties and stability. *Powder Technology*, 224, 138–146.
- Moran, K., Yeung, A., & Masliyah, J. (1999). Measuring interfacial tensions of micrometer-sized droplets: A novel micromechanical technique. *Langmuir*, 15(24), 8497–8504.
- Napper, D. H., & Netschey, A. (1971). Studies of the steric stabilization of colloidal particles. *Journal of Colloid And Interface Science*, 37(3), 528–535.
- Natarajan, A., Xie, J., Wang, S., Masliyah, J., Zeng, H., & Xu, Z. (2011). Understanding molecular interactions of asphaltenes in organic solvents using a surface force apparatus. *Journal of Physical Chemistry C*, 115(32), 16043–16051.
- Ncube, T., Suresh Kumar Reddy, K., Al Shoaibi, A., & Srinivasakannan, C. (2017). Benzene, Toluene, m-Xylene Adsorption on Silica-Based Adsorbents. *Energy and Fuels*, 31(2), 1882–1888.
- Nikakhtari, H., Vagi, L., Choi, P., Liu, Q., & Gray, M. R. (2013). Solvent screening for non-aqueous extraction of Alberta oil sands. *Canadian Journal of Chemical Engineering*, 91(6), 1153–1160.
- Oil Sands Discovery Center. (2016). *Facts about Alberta's oil sands and its industry*.
- Oil Sands Magazine. (2020a). *Froth Treatment Explained*. 2020 Oil Sands Magazine. <https://www.oilsandsmagazine.com/technical/mining/froth-treatment>
- Oil Sands Magazine. (2020b). *Oil Sands 101: Process Overview*. 2020 Oil Sands Magazine. <https://www.oilsandsmagazine.com/technical/oilsands-101>

- Oil Sands Magazine. (2020c). *Water Usage*. 2020 Oil Sands Magazine.  
<https://www.oilsandsmagazine.com/technical/environment/water-usage>
- Ortega-Vinuesa, J. L., Martín-Rodríguez, A., & Hidalgo-Álvarez, R. (1996). Colloidal stability of polymer colloids with different interfacial properties: Mechanisms. *Journal of Colloid and Interface Science*, *184*(1), 259–267.
- Parida, S. K., Dash, S., Patel, S., & Mishra, B. K. (2006). Adsorption of organic molecules on silica surface. *Advances in Colloid and Interface Science*, *121*(1–3), 77–110.
- Qiao, P. (2019). *Probing Challenges of Asphaltenes in Petroleum Production through Extended-SARA (E-SARA) Analysis*. University of Alberta.
- Qiao, P., Harbottle, D., Li, Z., Tang, Y., & Xu, Z. (2018). Interactions of Asphaltene Subfractions in Organic Media of Varying Aromaticity. *Energy and Fuels*, *32*(10), 10478–10485.
- Qiao, P., Harbottle, D., Tchoukov, P., Masliyah, J., Sjoblom, J., Liu, Q., & Xu, Z. (2017). Fractionation of Asphaltenes in Understanding Their Role in Petroleum Emulsion Stability and Fouling. *Energy and Fuels*, *31*(4), 3330–3337.
- Qiao, P., Harbottle, D., Tchoukov, P., Wang, X., & Xu, Z. (2017). Asphaltene Subfractions Responsible for Stabilizing Water-in-Crude Oil Emulsions. Part 3. Effect of Solvent Aromaticity. *Energy and Fuels*, *31*(9), 9179–9187.
- Rao, F., & Liu, Q. (2013). Froth Treatment in Athabasca Oil Sands Bitumen Recovery Process : A Review. *Energy and Fuels*, *27*, 7200–7207.
- Richardson, J. F., Harker, J. H., Backhurst, J. R., & Coulson, J. M. (2013). Sedimentation. In *Chemical Engineering Volume 2* (Fifth, Vol. 2, pp. 237–285). Butterworth-Heinemann.
- Richardson, J. F., & Zaki, W. N. (1954). The sedimentation of a suspension of uniform spheres under conditions of viscous flow. *Chemical Engineering Science*, *3*(2), 65–73.
- Schauperl, M., Podewitz, M., Waldner, B. J., & Liedl, K. R. (2016). Enthalpic and Entropic Contributions to Hydrophobicity. *Journal of Chemical Theory and Computation*, *12*(9), 4600–4610.

- Senden, T. J., & Drummond, C. J. (1995). Surface chemistry and tip-sample interactions in atomic force microscopy. *Colloids and Surfaces A: Physicochemical and Engineering Aspects*, 94(1), 29–51.
- Silverstein, T. P. (1998). The real reason why oil and water don't mix. *Journal of Chemical Education*, 75(1), 116–118.
- Sparks, B. D., Meadus, F. W., & Hoefele, E. O. (1988). Solvent extraction spherical agglomeration of oil sands. In *United State Patent*.
- Steinour, H. H. (1944). Rate of Sedimentation. *Industrial & Engineering Chemistry*, 36(9), 840–847.
- Subramanian, S., Sørland, G. H., Simon, S., Xu, Z., & Sjöblom, J. (2017). Asphaltene fractionation based on adsorption onto calcium carbonate: Part 2. Self-association and aggregation properties. *Colloids and Surfaces A: Physicochemical and Engineering Aspects*, 514, 79–90.
- Swenson, J., Smalley, M. V., & Hatharasinghe, H. L. M. (1998). Mechanism and strength of polymer bridging flocculation. *Physical Review Letters*, 81(26), 5840–5843.
- Tabor, D., & Winterton, R. H. . (1969). *Direct Measurement of Normal and Retarded Van Der Waals Forces*. 312(1511), 435–450.
- Tombácz, E., & Szekeres, M. (2006). Surface charge heterogeneity of kaolinite in aqueous suspension in comparison with montmorillonite. *Applied Clay Science*, 34(1–4), 105–124.
- Wang, S., Liu, J., Zhang, L., Masliyah, J., & Xu, Z. (2010). Interaction forces between asphaltene surfaces in organic solvents. *Langmuir*, 26(1), 183–190.
- Wang, S., Liu, J., Zhang, L., Xu, Z., & Masliyah, J. (2009). Colloidal interactions between asphaltene surfaces in toluene. *Langmuir*, 23, 862–869.
- Xu, Y. (2018). Asphaltene Precipitation in Paraffinic Froth Treatment: Effects of Solvent and Temperature. *Energy and Fuels*, 32(3), 2801–2810.
- Yan, N., Gray, M. R., & Masliyah, J. H. (2001). *On water-in-oil emulsions stabilized by fine solids*. 193, 97–107.

- Yang, F., Tchoukov, P., Dettman, H., Teklebrhan, R. B., Liu, L., Dabros, T., Czarnecki, J., Masliyah, J., & Xu, Z. (2015). Asphaltene Subfractions Responsible for Stabilizing Water-in-Crude Oil Emulsions. Part 2: Molecular Representations and Molecular Dynamics Simulations. *Energy and Fuels*, 29(8), 4783–4794.
- Yang, F., Tchoukov, P., Pensini, E., Dabros, T., Czarnecki, J., Masliyah, J., & Xu, Z. (2014). Asphaltene subfractions responsible for stabilizing water-in-crude oil emulsions. Part 1: Interfacial behaviors. *Energy and Fuels*, 28(11), 6897–6904.
- Yang, J., Meng, S., Xu, L., & Wang, E. G. (2005). Water adsorption on hydroxylated silica surfaces studied using the density functional theory. *Physical Review B - Condensed Matter and Materials Physics*, 71(3), 1–12.
- Yeung, A., Dabros, T., Masliyah, J., & Czarnecki, J. (2000). Micropipette: A new technique in emulsion research. *Colloids and Surfaces A: Physicochemical and Engineering Aspects*, 174(1–2), 169–181.
- Zhang, L., Shi, C., Lu, Q., Liu, Q., & Zeng, H. (2016). Probing Molecular Interactions of Asphaltenes in Heptol Using a Surface Forces Apparatus: Implications on Stability of Water-in-Oil Emulsions. *Langmuir*, 32(19), 4886–4895.